



NOAA Technical Memorandum NMFS-NWFSC-160

<https://doi.org/10.25923/e5rb-9f55>

Ecosystem Status Report of the California Current for 2019–20:

A Summary of Ecosystem Indicators Compiled by the California Current Integrated Ecosystem Assessment Team (CCIEA)

October 2020

U.S. DEPARTMENT OF COMMERCE

National Oceanic and Atmospheric Administration
National Marine Fisheries Service
Northwest Fisheries Science Center

NOAA Technical Memorandum Series NMFS-NWFSC

The Northwest Fisheries Science Center of NOAA's National Marine Fisheries Service uses the NOAA Technical Memorandum NMFS-NWFSC series to issue scientific and technical publications that have received thorough internal scientific review and editing. Reviews are transparent collegial reviews, not anonymous peer reviews. Documents within this series represent sound professional work and may be referenced in the formal scientific and technical literature.

The Northwest Fisheries Science Center's NOAA Technical Memorandum series continues the NMFS-F/NWC series established in 1970 by the Northwest and Alaska Fisheries Science Center, which subsequently was divided into the Northwest Fisheries Science Center and the Alaska Fisheries Science Center. The latter uses the NOAA Technical Memorandum NMFS-AFSC series.

NOAA Technical Memorandums NMFS-NWFSC are available from the NOAA Institutional Repository, <https://repository.library.noaa.gov>.

Any mention throughout this document of trade names or commercial companies is for identification purposes only and does not imply endorsement by the National Marine Fisheries Service, NOAA.

Cover image: School of northern anchovy. Photograph by M. Savoca, Stanford University.

Reference this document as follows:

Harvey, C. N. Garfield, G. Williams, N. Tolimieri, K. Andrews, K. Barnas, E. Bjorkstedt, S. Bograd, J. Borchert, C. Braby, R. Brodeur, B. Burke, J. Cope, A. Coyne, D. Demer, L. deWitt, J. Field, J. Fisher, P. Frey, T. Good, C. Grant, C. Greene, E. Hazen, D. Holland, M. Hunter, K. Jacobson, M. Jacox, J. Jahncke, C. Juhasz, I. Kaplan, S. Kasperski, S. Kim, D. Lawson, A. Leising, A. Manderson, N. Mantua, S. Melin, R. Miller, S. Moore, C. Morgan, B. Muhling, S. Munsch, K. Norman, J. Parrish, A. Phillips, R. Robertson, D. Rudnick, K. Sakuma, J. Samhuri, J. Santora, I. Schroeder, S. Siedlecki, K. Somers, B. Stanton, K. Stierhoff, W. Sydeman, A. Thompson, D. Trong, P. Warzybok, C. Whitmire, B. Wells, M. Williams, T. Williams, J. Zamon, S. Zeman, V. Zubkowsky-White, and J. Zwolinski. 2020. Ecosystem Status Report of the California Current for 2019–20: A Summary of Ecosystem Indicators Compiled by the California Current Integrated Ecosystem Assessment Team (CCIEA). U.S. Department of Commerce, NOAA Technical Memorandum NMFS-NWFSC-160.

<https://doi.org/10.25923/e5rb-9f55>



NOAA
FISHERIES

Ecosystem Status Report of the California Current for 2019–20: A Summary of Ecosystem Indicators Compiled by the California Current Integrated Ecosystem Assessment Team (CCIEA)

Chris Harvey, Newell (Toby) Garfield, Gregory Williams, Nick Tolimieri, Kelly Andrews, Katie Barnas, Eric Bjorkstedt, Steven Bograd, Jerry Borchert, Caren Braby, Richard Brodeur, Brian Burke, Jason Cope, Audrey Coyne, David Demer, Lynn deWitt, John Field, Jennifer Fisher, Peter Frey, Thomas Good, Christina Grant, Correigh Greene, Elliott Hazen, Daniel Holland, Matthew Hunter, Kym Jacobson, Michael Jacox, Jaime Jahncke, Christy Juhasz, Isaac Kaplan, Stephen Kasperski, Su Kim, Dan Lawson, Andrew Leising, Alex Manderson, Nate Mantua, Sharon Melin, Rebecca Miller, Stephanie Moore, Cheryl Morgan, Barbara Muhling, Stuart Munsch, Karma Norman, Julia Parrish, Amanda Phillips, Roxanne Robertson, Dan Rudnick, Keith Sakuma, Jameal Samhouri, Jarrod Santora, Isaac Schroeder, Samantha Siedlecki, Kayleigh Somers, Beckye Stanton, Kevin Stierhoff, William Sydeman, Andrew Thompson, Nick Tolimieri, Duy Trong, Pete Warzybok, Curt Whitmire, Brian Wells, Margaret Williams, Thomas Williams, Jeannette Zamon, Samantha Zeman, Vanessa Zubkousky-White, and Juan Zwolinski

<https://doi.org/10.25923/e5rb-9f55>

October 2020

Published by:

Northwest Fisheries Science Center
2725 Montlake Boulevard East
Seattle, Washington 98112

U.S. DEPARTMENT OF COMMERCE

National Oceanic and Atmospheric Administration
National Marine Fisheries Service
Northwest Fisheries Science Center

Contributors

California Current Integrated Ecosystem Assessment (CCIEA) Team

Corresponding authors

Dr. Chris Harvey	chris.harvey@noaa.gov
Dr. Newell (Toby) Garfield	toby.garfield@noaa.gov
Mr. Gregory Williams	greg.williams@noaa.gov
Dr. Nick Tolimieri	nick.tolimieri@noaa.gov

All contributors, by affiliation

NOAA Fisheries

Northwest Fisheries Science Center

Dr. Chris Harvey, Mr. Kelly Andrews, Ms. Katie Barnas, Dr. Richard Brodeur, Dr. Brian Burke, Dr. Jason Cope, Mr. Peter Frey, Dr. Thomas Good, Dr. Correigh Greene, Dr. Daniel Holland, Dr. Kym Jacobson, Dr. Isaac Kaplan, Ms. Su Kim, Dr. Stephanie Moore, Dr. Stuart Munsch,¹ Dr. Karma Norman, Dr. Jameal Samhour, Dr. Kayleigh Somers, Dr. Nick Tolimieri, Mr. Curt Whitmire, Ms. Margaret Williams,¹ and Dr. Jeannette Zamon

¹Ocean Associates, Inc.

Southwest Fisheries Science Center

Dr. Newell (Toby) Garfield, Dr. Eric Bjorkstedt, Dr. Steven Bograd, Dr. David Demer, Ms. Lynn deWitt, Dr. John Field, Dr. Elliott Hazen, Dr. Michael Jacox, Dr. Andrew Leising, Dr. Nate Mantua, Mr. Keith Sakuma, Dr. Jarrod Santora, Dr. Kevin Stierhoff, Dr. Andrew Thompson, Dr. Brian Wells, Dr. Thomas Williams, and Dr. Juan Zwolinski

Alaska Fisheries Science Center

Dr. Stephen Kasperski and Dr. Sharon Melin

West Coast Region

Mr. Dan Lawson

Pacific States Marine Fisheries Commission

Ms. Amanda Phillips and Mr. Gregory Williams

Cooperative Institute for Marine Ecosystems and Climate, Humboldt State University

Ms. Roxanne Robertson

Oregon State University

Ms. Jennifer Fisher, Ms. Cheryl Morgan, and Ms. Samantha Zeman

Scripps Institute of Oceanography

Dr. Dan Rudnick

Institute of Marine Sciences, University of California, Santa Cruz

Ms. Rebecca Miller, Dr. Barbara Muhling, and Dr. Isaac Schroeder

University of Connecticut

Dr. Samantha Siedlecki

University of Washington

Dr. Julia Parrish

Farallon Institute

Dr. William Sydeman

Point Blue Conservation Science

Dr. Jaime Jahncke and Mr. Pete Warzybok

California Department of Fish and Wildlife

Ms. Christy Juhasz

California Department of Public Health

Ms. Christina Grant, Mr. Duy Trong, and Ms. Vanessa Zubkousky-White

California Office of Environmental Health Hazard Assessment

Dr. Beckye Stanton

Oregon Department of Agriculture

Mr. Alex Manderson

Oregon Department of Fish and Wildlife

Dr. Caren Braby and Mr. Matthew Hunter

Washington Department of Health

Ms. Audrey Coyne and Mr. Jerry Borchert

Contents

List of Contributors.....	i
List of Figures.....	v
List of Tables.....	viii
Executive Summary.....	ix
1 Introduction.....	1
1.1 Ecosystem-Based Fisheries Management and Integrated Ecosystem Assessment.....	1
1.2 Notes on Interpreting Time-Series Figures.....	4
1.3 Sampling Locations.....	5
2 Climate and Ocean Drivers.....	7
2.1 Basin-Scale Indicators.....	7
2.2 Regional Upwelling Indices.....	14
2.3 Hypoxia and Ocean Acidification.....	17
3 Focal Components of Ecological Integrity.....	30
3.1 Northern Copepod Biomass Anomaly.....	30
3.2 Euphausiid Size off of Trinidad Head.....	31
3.3 Harmful Algal Blooms.....	31
3.4 Regional Forage Availability.....	33
3.4.1 Northern CCE.....	34
3.4.2 Central CCE.....	36
3.4.3 Southern CCE.....	38
3.4.4 Pyrosomes.....	39
3.5 Coastal Pelagic Species.....	40
3.6 Salmon.....	42
3.7 Groundfish Stock Abundance and Community Structure.....	47
3.8 Highly Migratory Species.....	48
3.9 Marine Mammals.....	49
3.9.1 Sea lion production.....	49
3.9.2 Whale entanglement.....	50

3.10	Seabirds.....	51
3.10.1	Seabird population productivity	51
3.10.2	Seabird diets.....	52
3.10.3	Seabird mortality	55
3.10.4	Seabird at-sea densities	57
4	Human Activities.....	59
4.1	Coastwide Landings by Major Fisheries	59
4.2	Bottom Trawl Contact with Seafloor	61
4.3	Aquaculture Production and Seafood Consumption	64
4.4	Nonfishing Human Activities	65
4.4.1	Commercial shipping.....	65
4.4.2	Oil and gas activity.....	66
4.4.3	Nutrient loading	66
5	Human Wellbeing.....	67
5.1	Social Vulnerability	67
5.2	Fishing Revenue Diversification.....	69
6	Synthesis.....	72
	List of References.....	74

Figures

Figure ES-1. Visual summary of the status and trends of key indicators in the California Current social–ecological system during 2019	xii
Figure 1. Loop diagram of the five progressive steps in iterations of the integrated ecosystem assessment process.....	2
Figure 2. Conceptual model of the California Current social–ecological system	3
Figure 3. a) Sample time-series plot, with indicator data relative to the long-term mean and ± 1.0 standard deviation of the full time series. b) Sample time-series plot with the indicator plotted relative to a threshold value. c) Sample quad plot where each point represents one normalized time series.....	5
Figure 4. Map of the California Current ecosystem and sampling areas	6
Figure 5. Monthly values of the Oceanic Niño Index, Pacific Decadal Oscillation, and the North Pacific Gyre Oscillation, 1981–2019	8
Figure 6. Sea surface temperature anomalies, 5-year means, and 5-year trends in winter and summer	9
Figure 7. Time–depth–temperature anomaly contours for nearshore hydrographic stations NH25 and CalCOFI 93.30	10
Figure 8. Area of North Pacific warm SST anomalies > 2.0 SD, 1982–2019.....	11
Figure 9. Standardized SSTa across the northeastern Pacific for a) May, b) Jul, and c) Sep 2019, and d) Jan 2020.....	12
Figure 10. Progression of standardized sea surface temperature anomalies in 2014–15, the time period when the 2013–16 large marine heatwave first expanded into California Current waters and intersected coastal waters	12
Figure 11. California Underwater Glider Network temperature anomalies at depths of 10 m and 50 m along CalCOFI line 90, extending from the coast to 500 km offshore, 2007–19	13
Figure 12. CUGN temperature indices on CalCOFI lines 67, 80, and 90 compared to the ONI.....	14
Figure 13. Daily 2019 values of Coastal Upwelling Transport Index and Biologically Effective Upwelling Transport Index, 1 Jan–31 Dec, relative to the 1988–2019 climatology ± 1.0 SD, at lats 33° , 39° , and 45° N.....	16
Figure 14. Mean winter and spring habitat compression index, 1980–2019	17
Figure 15. Areal extent of the HCI for the month of May, 1980–2019	18
Figure 16. Dissolved oxygen at 50 m depth off Newport, OR, through 2019	19
Figure 17. Annual maps of near-bottom DO levels during the months of Aug–Sep, 2015–19	19
Figure 18. DO at 150 m off San Diego, CA, through 2019	20
Figure 19. DO observations during the summer 2019 CalCOFI survey of the Southern CCE at 50 m, 150 m, and on the bottom of the hydrographic cast	20
Figure 20. Winter and summer aragonite saturation values at two stations off Newport, OR	21
Figure 21. Aragonite saturation vertical profiles for stations NH05 and NH25 off of Newport, OR.....	22

Figure 22. J-SCOPE forecasts of bottom DO, May–Sep 2019, averaged over all 3 ensemble members	23
Figure 23. J-SCOPE forecasts of bottom aragonite saturation state, Jan–Aug 2019, averaged over all 3 ensemble members	24
Figure 24. Anomalies of 1 April SWE in 5 CCE freshwater ecoregions through 2019.....	25
Figure 25. Mountain snowpack on 1 April 2020, at select monitoring sites relative to 1981–2010 median values	26
Figure 26. Mean maximum stream temperature in August measured at 466 USGS gages in 6 ecoregions, 1981–2019	27
Figure 27. Anomalies of the 7-day minimum streamflow measured at 213 gages in 6 ecoregions, 1981–2019	28
Figure 28. Anomalies of the 1-day maximum streamflow measured at 213 gages in 6 ecoregions, 1981–2019	28
Figure 29. Recent trend and average of maximum and minimum streamflow anomalies in 16 freshwater Chinook salmon ESUs in the CCE through 2019	29
Figure 30. Monthly northern and southern copepod biomass anomalies from Newport Hydrographic Line station NH05, 1996–2019	30
Figure 31. Mean krill carapace length off of Trinidad Head, CA, 2007–19.....	31
Figure 32. Monthly maximum domoic acid concentration in razor clams and Dungeness crab viscera through 2019 for WA, OR, NorCal, and Central CA.....	32
Figure 33. Multivariate analyses of forage dynamics in the Northern CCE through 2019.....	35
Figure 34. Spatiotemporal distributions of krill off of OR and WA, May–Jun 2011–19 (no 2012)	36
Figure 35. Multivariate analyses of forage dynamics in the Central CCE through 2019	37
Figure 36. Cluster analysis of key forage species in the Southern CCE through 2019	38
Figure 37. <i>Pyrosoma atlanticum</i> biomass during May–Jun in the CCE, 2013–19	39
Figure 38. Estimated and cumulative biomasses of the 5 most abundant coastal pelagic fish species in the CCE, 2008 and 2012–19, based on coastwide summer acoustic–trawl surveys	41
Figure 39. Acoustic proportions of coastal pelagic fish species in trawl clusters during 2017, 2018, and 2019.....	42
Figure 40. Recent trend and average of Chinook salmon escapement, with most systems updated through 2018	43
Figure 41. At-sea juvenile Chinook and coho salmon catch in Jun, 1998–2019, off WA and OR	44
Figure 42. Salmon returns versus the mean rank of ecosystem “stoplight” indicators from Table 1.....	45
Figure 43. Time series of observed and projected spring Chinook salmon adult counts and fall Chinook salmon adult counts, by out-migration year	46
Figure 44. Stock status of CCE groundfish.....	48
Figure 45. California sea lion pup counts, and estimated mean daily growth rate of female pups between 4–7 months of age, on San Miguel Island for the 1997–2019 cohorts	49

Figure 46. Confirmed numbers of whales reported as entangled in fishing gear and other sources along the U.S. West Coast, 2000–19	50
Figure 47. Standardized productivity anomalies for 5 seabird species breeding on Southeast Farallon Island through 2019	52
Figure 48. Rhinoceros auklet chick diets at Destruction Island, WA, through 2019	53
Figure 49. Common murre chick diets at Yaquina Head, OR, through 2019.....	53
Figure 50. SEFI seabird diets through 2019	54
Figure 51. Fork length of northern anchovy brought to rhinoceros auklet chicks at Año Nuevo Island, 1993–2019	55
Figure 52. Encounter rate of bird carcasses on WA, OR, and NorCal beaches through 2019.....	56
Figure 53. Encounter rate of bird carcasses on beaches in north-central California through 2019.....	57
Figure 54. At-sea density anomalies of 3 seabird species in spring–summer in 3 CCE regions through 2019	58
Figure 55. Annual landings of U.S. West Coast commercial and recreational fisheries, including total landings across all fisheries, 1981–2019.....	59
Figure 56. Annual revenue of U.S. West Coast commercial fisheries, 1981–2019.....	60
Figure 57. Distance trawled by federally managed groundfish bottom trawl fisheries across the entire CCE and within each ecoregion	62
Figure 58. Spatial representation of seafloor contact by bottom trawl gear from federal groundfish fisheries, calculated from annual distances trawled within each 2 × 2-km grid cell, 2002–18	63
Figure 59. Aquaculture production of shellfish and finfish in CCE waters, 1986–2018	64
Figure 60. Total and per-capita consumption of edible and nonedible fisheries products in the United States, 1962–2018.....	65
Figure 61. Distance transited by foreign commercial shipping vessels in the CCE, 1997–2018.....	65
Figure 62. Standardized index of the sum of oil and gas production from offshore wells in California, 1974–2018	66
Figure 63. Commercial fishing reliance and social vulnerability scores as of 2017, plotted for 25 communities from each of 5 CCE regions: WA, OR, NCC, CCC, and SCC.....	68
Figure 64. Commercial fisheries engagement and social vulnerability scores as of 2017, plotted for 25 communities from each of 5 CCE regions: WA, OR, NCC, CCC, and SCC	68
Figure 65. Trends in average diversification for U.S. West Coast and AK fishing vessels with over \$5K in average revenues and for vessels in the 2018 U.S. West Coast Fleet with over \$5K in average revenues, broken out by state, by average gross revenue class, and by vessel length class.....	70
Figure 66. Trends in commercial fishing vessel revenue diversification in major WA, OR, and CA ports, 1981–2018.....	71

Tables

Table 1. “Stoplight” table of basin-scale and local/regional conditions for smolt years 2016–19 and 2019 projected adult returns for coho and Chinook salmon that inhabit coastal OR and WA waters in their marine phase.....	44
Table 2. Table of conditions for naturally produced Central Valley fall Chinook salmon returning in 2020, from spawning years 2016–18	47

Executive Summary

This document is an expansion of the ecosystem status report (ESR) provided by the California Current Integrated Ecosystem Assessment Team (CCIEA Team) to the Pacific Fishery Management Council (PFMC) in March 2020 (Harvey et al. 2020). The CCIEA Team provides ESRs annually to PFMC, as one component of the overall CCIEA goal of providing quantitative, integrative science tools, products, and synthesis in support of a more holistic (ecosystem-based) approach to managing marine resources in the California Current.

The ESR features a suite of indicators codeveloped by the CCIEA Team and PFMC. The suite of indicators was initially identified in 2009, and has been refined and updated over the years to best capture the current state of the California Current ecosystem (CCE). The analyses in this document represent our best understanding of environmental, ecological, and socioeconomic conditions in this ecosystem roughly through late 2019 and early 2020. Because the time required to process data varies for different indicators, some of the resulting time series are slightly more up-to-date than others. The time series for some indicators (snowpack, sea lion reproduction and pup growth, seabirds, fishery landings, fishery revenue, and nonfishing human activities) have been updated since the March 2020 report to PFMC (Harvey et al. 2020).

The CCE was influenced by physical drivers in 2019 that likely continued to constrain system productivity in ways similar to 2013 through 2018. The system was strongly impacted by the major northeastern Pacific Ocean marine heat wave of 2013–16 (“the Blob”) and a major El Niño event of 2015–16. We considered late 2016 to 2018 to be “transitional” because many oceanographic indicators appeared to be shifting away from the highly unusual conditions—warm water temperatures, poor productivity across multiple trophic levels, widespread occurrence of warm-water or offshore species—of the marine heat wave and El Niño event. However, in 2018, another large marine heatwave occurred in the fall and lasted for several months, suggesting that the CCE remained subject to abnormal heating, and a mild El Niño also formed in late 2018. In 2019, many important climate and oceanographic drivers affected the CCE (Figure ES-1):

- The weak El Niño persisted into the late spring/early summer, although its warming effect on the CCE seemed mainly confined to California waters.
- The North Pacific Gyre Oscillation (NPGO) index indicates that the influx of subarctic waters into the northern part of the CCE was very weak. This finding is consistent with below-average productivity in the CCE.
- A new, major marine heatwave formed in the northeastern Pacific Ocean in May 2019, and over the next several months it came ashore along the northern and central portions of the U.S. West Coast before diminishing in fall and early winter. The 2019 heatwave was as large and intense at the sea surface as the 2013–16 Blob, though it did not persist as long.
- Subsurface measurements indicate a large amount of heat stored in the water column in much of the northeastern Pacific Ocean.
- The ribbon of cool, nutrient-rich upwelled water was compressed to a relatively narrow area along the coast, as it has been consistently since 2014.

- Widespread hypoxia occurred along the bottom of the continental shelf off of Washington and Oregon in the summer and early fall. Hypoxia of bottom waters is again forecast to occur in this region in 2020, along with conditions consistent with ocean acidification.

Ecological indicators in 2019 suggested that seasonal conditions in the CCE were average to above-average for some species but below-average for others. On the whole, most observations of below-average productivity occurred off Central and Northern California (Figure ES-1). Among the ecological metrics that indicated average or above-average CCE conditions were:

- The community of copepods (tiny free-swimming crustaceans near the base of the food web) off Newport, Oregon, were characterized by a cool-water, energy-rich assemblage in the late spring and early summer (although this community was present for a shorter period of time than is often observed).
- Northern anchovy (*Engraulis mordax*) abundances were among the highest ever observed in research surveys off Central and Southern California.
- Catch rates of juvenile Chinook salmon (*Oncorhynchus tshawytscha*) and coho salmon (*O. kisutch*) off of Washington and Oregon were very close to the long-term average in surveys conducted since the late 1990s.
- A number of biological and oceanographic indicators over the past several years suggested average Chinook salmon returns to the Columbia River basin in 2020.
- Abundance and growth rates of California sea lion (*Zalophus californianus*) pups at the San Miguel Island colony were above average, implying that adult female sea lions in that region had good feeding conditions, primarily related to abundant northern anchovy.
- All federally managed groundfish assessed in recent years have biomass estimates that are safely above the threshold for being declared “overfished,” and all but one were below the fishing mortality rate proxy for experiencing overfishing in their most-recent assessments.

However, other ecological indicators from 2019 suggested unfavorable conditions:

- Surveys that sample the upper 30–40 m of the water column in late spring found very few krill off of California and Oregon in 2019, suggesting that this valuable prey was not readily available to many predators.
- The same surveys also caught very low numbers of juvenile groundfish for the second straight year.
- Biological and oceanographic indicators in 2019 suggested below-average coho salmon returns to the Oregon coast in 2020.
- Indicators were consistent with below-average returns for the dominant age class of naturally produced (i.e., non-hatchery) Chinook salmon returning to the Sacramento and San Joaquin Rivers.
- Several types of seabird experienced poor fledgling production at a colony off of Central California, possibly related to lack of diversity in the forage community.
- Pyrosomes, free-swimming colonial gelatinous animals normally found in warmer waters further to the south, were highly abundant off of Central California.
- Reports of whale entanglements in fixed fishing gear in 2019 were above-average for the sixth consecutive year, although the number of reports was lower than in 2018.

- Domoic acid, a toxin produced by the phytoplankton *Pseudo-nitzschia*, exceeded action levels in Dungeness crabs (*Metacarcinus magister*) and razor clams (*Siliqua patula*) in Southern Oregon and some areas of Northern California, limiting fishery seasons in those areas.

This mix of above-average, average, and below-average patterns is a reminder that despite the large-scale physical drivers (e.g., the weak El Niño, the below-average NPGO, and the 2019 marine heatwave), species abundances and conditions may or may not directly reflect them, due to a range of other factors such as regional physical drivers (like upwelling) that can strongly affect local or regional conditions. Also, some species, particularly those with short life spans, respond relatively quickly to physical changes, while longer-lived species may respond with lag times of months to years, even after physical conditions and characteristics of the base of the food web have returned to average or above-average.

Economic and social indicators reflect recent declines in fishery landings, revenues, and the diversity of species that U.S. West Coast fisheries are landing (Figure ES-1). Fishery landings have been variable over the past five years, although they have declined since a recent peak in 2017. Much of the landings during these recent years can be attributed to strong catches of Pacific hake (*Merluccius productus*), which made up ~70% of estimated landings in 2019. However, commercial landings for many important target groups (coastal pelagic finfish species, most groundfish, highly migratory species, and salmon) are some of the lowest that have been seen over the past several decades, and recreational fishery landings have also been in decline since 2015. Total revenue from all U.S. West Coast commercial fisheries decreased 20% from 2018 to 2019, driven primarily by decreased landings revenue for crab and market squid (*Doryteuthis opalescens*). Very low diversification of catch revenues by commercial fishing vessels of all size and revenue classes continues in all three coastal states; in other words, on average, vessels are relying on relatively few species to provide the bulk of their revenues. We are working to understand how the reliance of coastal communities on commercial and recreational fishing relates to those communities' overall social wellbeing and vulnerability.

The sections that follow will go into greater detail about the status and trends of indicators summarized here; after a short [Introduction](#), we include sections related to [Climate and Ocean Drivers](#), the [Focal Components of Ecological Integrity](#), [Human Activities](#), and [Human Wellbeing](#), followed by a brief [Synthesis](#).

Figure ES-1 (overleaf). Visual summary of the status and trends of key indicators in the California Current social–ecological system during 2019. Graphic designed by S. Kim, NMFS/NWFSC.

2020 CCIEA Ecosystem Status Report Highlights

System Conditions 2019

- *Weak to neutral* El Niño conditions
- *Average to slightly positive* Pacific Decadal Oscillation (PDO)
- *Very weak* North Pacific circulation
- These conditions typically lead to *low productivity*

Large Marine Heatwave



- Emerged in mid 2019, similar in size and intensity to the 2013-2016 "Blob," but it *weakened* by December.
- Effects are still *unknown*

Whale Entanglement 2019

- *Above-average* reports of whale entanglements occurred for the 6th straight year
- However, reported entanglements *declined* from 2018

Average to Favorable Conditions 2019

Average or above-average productivity

The copepod community off Oregon was *high* in cool-water, lipid-rich species in summer

Anchovy densities continued to *increase* along most of the California coast

Juvenile Chinook and coho salmon catches off Oregon and Washington were *average*

Sea lion pup growth on San Miguel Island was *above average*

Unfavorable Conditions 2019

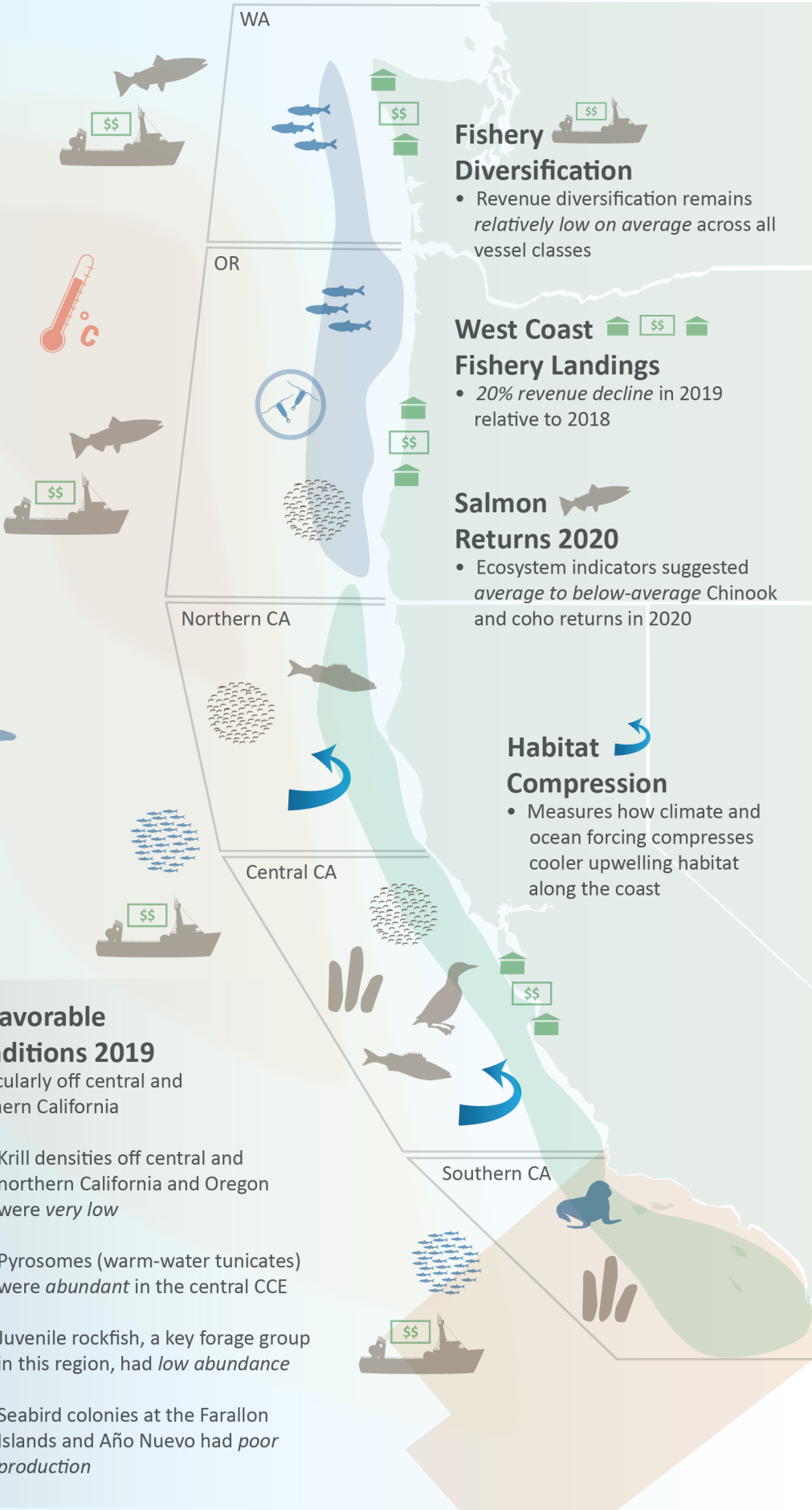
Particularly off central and northern California

Krill densities off central and northern California and Oregon were *very low*

Pyrosomes (warm-water tunicates) were *abundant* in the central CCE

Juvenile rockfish, a key forage group in this region, had *low abundance*

Seabird colonies at the Farallon Islands and Año Nuevo had *poor* production



Fishery Diversification

- Revenue diversification remains *relatively low on average* across all vessel classes

West Coast Fishery Landings

- *20% revenue decline* in 2019 relative to 2018

Salmon Returns 2020

- Ecosystem indicators suggested *average to below-average* Chinook and coho returns in 2020

Habitat Compression

- Measures how climate and ocean forcing compresses cooler upwelling habitat along the coast

1 Introduction

1.1 Ecosystem-Based Fisheries Management and Integrated Ecosystem Assessment

Ecosystem-based management of fisheries and other marine resources has emerged as a priority in the U.S. (EPAP 1999, Fluharty et al. 2006, McFadden and Barnes 2009, NOAA 2016) and elsewhere (Browman et al. 2004, Sainsbury et al. 2014, Walther and Möllmann 2014, Long et al. 2015). The NOAA National Marine Fisheries Service (NOAA Fisheries) defines ecosystem-based fisheries management (EBFM) as “a systematic approach to fisheries management in a geographically specified area that contributes to the resilience and sustainability of the ecosystem; recognizes the physical, biological, economic, and social interactions among the affected fishery-related components of the ecosystem, including humans; and seeks to optimize benefits among a diverse set of societal goals” (NOAA 2016). This definition encompasses interactions within and among fisheries, protected species, aquaculture, habitats, and human communities that depend upon fisheries and related ecosystem services. An EBFM approach is intended to improve upon traditional fishery management practices that primarily are focused on individual fished stocks.

Successful EBFM requires considerable effort and coordination due to the formidable amount of information required and uncertainty involved. In response, scientists throughout the world have developed many frameworks for organizing science and information in order to clarify and synthesize this overwhelming volume of data into science-based guidance for policymakers. NOAA Fisheries has adopted a framework called integrated ecosystem assessment (IEA; Levin et al. 2008, Levin et al. 2009), which can be summarized in five progressive steps (Figure 1):

1. Identifying and scoping ecosystem goals, objectives, targets, and threats.
2. Assessing ecosystem status and trends through the use of valid ecosystem indicators.
3. Assessing the risks of key threats and stressors to the ecosystem.
4. Analyzing management strategy alternatives and identifying potential tradeoffs.
5. Implementing selected actions, and monitoring and evaluating management success.

As shown in Figure 1, the IEA approach is iterative. Following the implementation of management actions, all other steps in the IEA loop must be revisited in order to ensure that a) evolving goals and objectives are clearly identified, b) monitoring plans and indicators are appropriate for the management objectives in mind, c) existing and emerging risks are properly prioritized, and d) management actions are objectively and regularly evaluated for success. Individual steps of the IEA process can also be iterative; for example, the suite of indicators in CCIEA reporting has evolved over the years as a result of emerging issues or at the request of management partners and stakeholders. The five steps of the IEA framework, plus its iterative nature, are very similar to and compatible with the core guiding principles of the NOAA EBFM Policy (NOAA 2016, Link 2017).

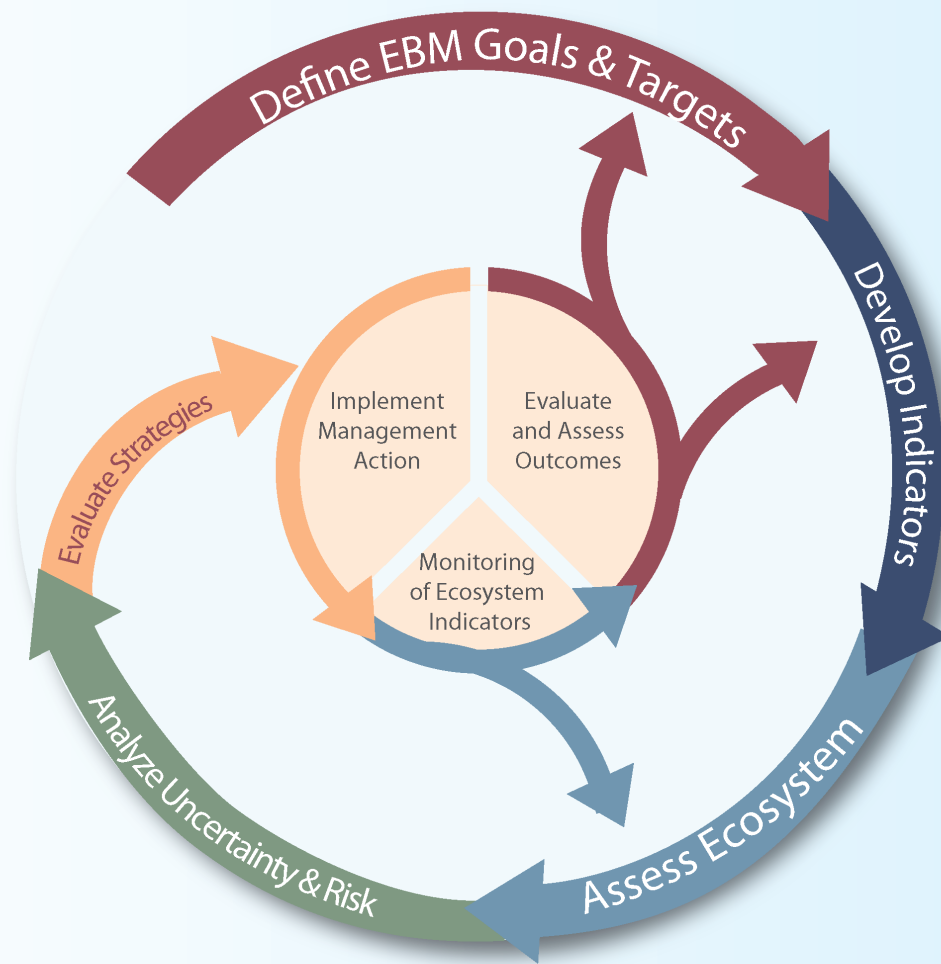


Figure 1. Loop diagram of the five progressive steps in iterations of the integrated ecosystem assessment (IEA) process. From Samhouri et al. (2014).

In 2009, NOAA line offices along the U.S. West Coast initiated the California Current Integrated Ecosystem Assessment (CCIEA). The CCIEA Team focuses on the California Current ecosystem (CCE) along the U.S. West Coast. In keeping with the principles of ecosystem-based management, the CCIEA team regards the CCE as a dynamic, interactive, social–ecological system with multiple levels of organization and diverse goals and endpoints that are both environmental and social in nature (Figure 2). The challenging task of assembling and interpreting information from this broad range of disciplines, locations, and time frames engages over 50 scientists from NOAA’s Northwest and Southwest Fisheries Science Centers and other NOAA offices, as well as colleagues from other agencies, academia, and nongovernmental entities. Information on CCIEA research efforts, tools, products, publications, partnerships, and points of contact is available on the [CCIEA website](http://www.integratedecosystemassessment.noaa.gov/regions/california-current-region/index.html).¹

¹ <http://www.integratedecosystemassessment.noaa.gov/regions/california-current-region/index.html>

Section 1.4 of the FEP outlined a reporting process wherein the CCIEA team provides PFMC with a yearly ecosystem status report (ESR) that describes the current status and trends of ecosystem attributes of the CCE. The purpose of the ESRs is to provide PFMC with a general sense of ecosystem conditions as context for decision-making. ESRs include information on a range of attributes, including climate and oceanographic drivers, status of key species groups, fisheries-related human activities, and human wellbeing in coastal communities. ESRs track ecosystem attributes through ecosystem indicators, most of which were derived through a rigorous indicator screening process developed by Kershner et al. (2011); details of specific CCIEA indicator screening exercises are documented elsewhere (Levin and Schwing 2011, Levin et al. 2013, Harvey et al. 2014).

Since 2012, the CCIEA Team has provided PFMC with eight ESRs, most recently in March 2020. The ESRs are available as online sections of [PFMC briefing books](#)⁴ for the meetings at which the CCIEA Team has presented the reports (November 2012, then annually in March 2014–20), and are also available on the [CCIEA website](#).⁵ The contents of ESRs have evolved over the years through cooperation between the CCIEA Team and PFMC and its advisory bodies, most notably through an [FEP initiative](#)⁶ begun in 2015 to refine the indicators in the ESR to better reflect PFMC’s needs. For example, PFMC has requested that the annual ESRs be confined to ~20 printed pages.

This technical memorandum is a companion document to the ESR delivered by the CCIEA Team to PFMC in March 2020 (Harvey et al. 2020), representing the status and trends of ecosystem indicators in the CCE through 2019 and, in some cases, early 2020. It is the fourth in an ongoing annual series of technical memorandums (beginning with Harvey et al. 2017) that provide a more thorough ESR of the CCE than the page limit allows us to present to PFMC. We will continue to provide the annual report to PFMC, and this technical memorandum series will largely be based on that report. However, as this series evolves, the technical memorandums will incorporate more indicators and analyses covering a broader range of ecosystem attributes. This is because the CCIEA Team looks to support other management partners in addition to PFMC, and our goal is for our annual ESR to feature information in support of ecosystem-based management (EBM) in other sectors and services in addition to fisheries (Slater et al. 2017). The technical memorandum format enables increased information content, contributions from a broader range of authors, and value to a wider range of audiences. It is our hope that an expanded ESR will lead to greater dialogue with potential partners and stakeholders; such dialogue and engagement is at the heart of the initial step of the IEA process (Figure 1), and is essential to every other step in all iterations as well.

1.2 Notes on Interpreting Time-Series Figures

Throughout this report, many data figures will follow one of two common formats, time-series plots or quad plots, both illustrated with sample data in Figure 3; see figure captions for details. Time-series plots generally contain a single dataset (Figures 3a and 3b), whereas

⁴ <https://www.pcouncil.org/category/briefing-book/>

⁵ <https://www.integratedecosystemassessment.noaa.gov/regions/california-current/cc-publications-reports>

⁶ <https://www.pcouncil.org/actions/initiative-2-coordinated-ecosystem-indicator-review/>

quad plots are used to summarize the recent averages and trends for multiple time series in a single panel, as when we have time series of multiple populations that we want to compare in a simplified visual manner (Figure 3c). Some time-series plots now show thresholds beyond which we expect substantial changes in response variables, such as when a physiological tolerance to a physical or chemical variable is exceeded (Figure 3b). Where possible, we include estimates of error or uncertainty in the data. Error estimates are defined in the figure legends and are usually standard deviations or standard errors.

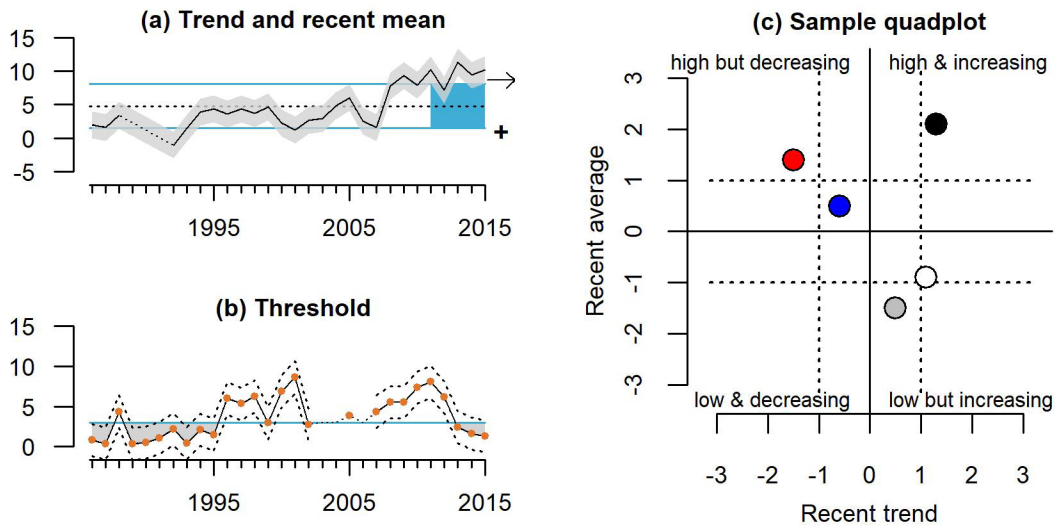


Figure 3. a) Sample time-series plot, with indicator data relative to the long-term mean (black dashed horizontal line) and ± 1.0 standard deviation (SD; solid blue lines) of the full time series. Dotted black line indicates missing data, and points (when included) indicate data. Arrow at the right indicates if the trend over the evaluation period (shaded blue) is positive (\nearrow), negative (\searrow), or neutral (\leftrightarrow). Symbol at the lower right indicates if the recent mean was greater than (+), less than (-), or within 1.0 SD of the long-term mean. When possible, times series indicate observation error (gray envelope), defined for each plot (e.g., SD, standard error, or 95% confidence intervals). b) Sample time-series plot with the indicator plotted relative to a threshold value (blue line). Dashed lines indicate upper and lower observation error, again defined for each plot. Dotted black line indicates missing data. c) Sample quad plot where each point represents one normalized time series. The position of a point indicates if the recent trend was increasing or decreasing over the evaluation period and whether the recent mean over the evaluation period was above or below the long-term mean. Dashed lines represent ± 1.0 SD of the full time series.

1.3 Sampling Locations

Figure 4a shows the major headlands that demarcate potential biogeographic boundaries, in particular Cape Mendocino and Point Conception. We generally consider the region north of Cape Mendocino to be the “Northern CCE,” the region between Cape Mendocino and Point Conception the “Central CCE,” and the region south of Point Conception the “Southern CCE.” Figure 4a also shows sampling locations for much of the regional climate and oceanographic data presented in this report. In particular, many of the physical and chemical oceanographic data are collected on the Newport Hydrographic Line off Oregon and the California Cooperative Oceanic Fisheries Investigations (CalCOFI) grid off central and southern California. Physical oceanography sampling is complemented by basin-scale observations and numerical models.

Freshwater habitats worldwide can be spatially grouped into “ecoregions” according to the designations of Abell et al. (2008). The freshwater ecoregions in the CCE are shown in Figure 4b, and are the basis by which we summarize freshwater habitat indicators relating to streamflow, stream water temperatures, and snowpack.

The map in Figure 4c represents field sampling from which most biological indicators are derived, including zooplankton, forage species, California sea lions, and seabirds. Zooplankton data are primarily reported from the Newport Hydrographic Line off Oregon and the Trinidad Head Hydrographic Line off northern California. The blue-, green-, and orange-shaded regions of coastal waters refer to the extent of major survey efforts that focus on forage species, juvenile salmon, and seabirds in shelf and slope habitats; in some cases, the surveys span both sides of the major zoogeographic boundaries of Cape Mendocino and Point Conception (especially the surveys represented by green shading), although the data we use in this report for those groups are mostly subsets drawn from areas that represent status and trends specific to the Northern, Central, and Southern regions. CPS surveys (Stierhoff et al. 2020) cover all of the colored regions in Figure 4c out to at least the 1,000-fathom (>1,800-m depth) isobath, up to 65 km from shore, while also extending to the northern end of Vancouver Island. Groundfish bottom trawl sampling and benthic dissolved oxygen sampling by the NOAA Fisheries West Coast Groundfish Bottom Trawl Survey (Keller et al. 2017) occurs in roughly the same area on the shelf and upper slope (depths of 55–1,280 m) as the blue- and green-shaded regions of Figure 4c.

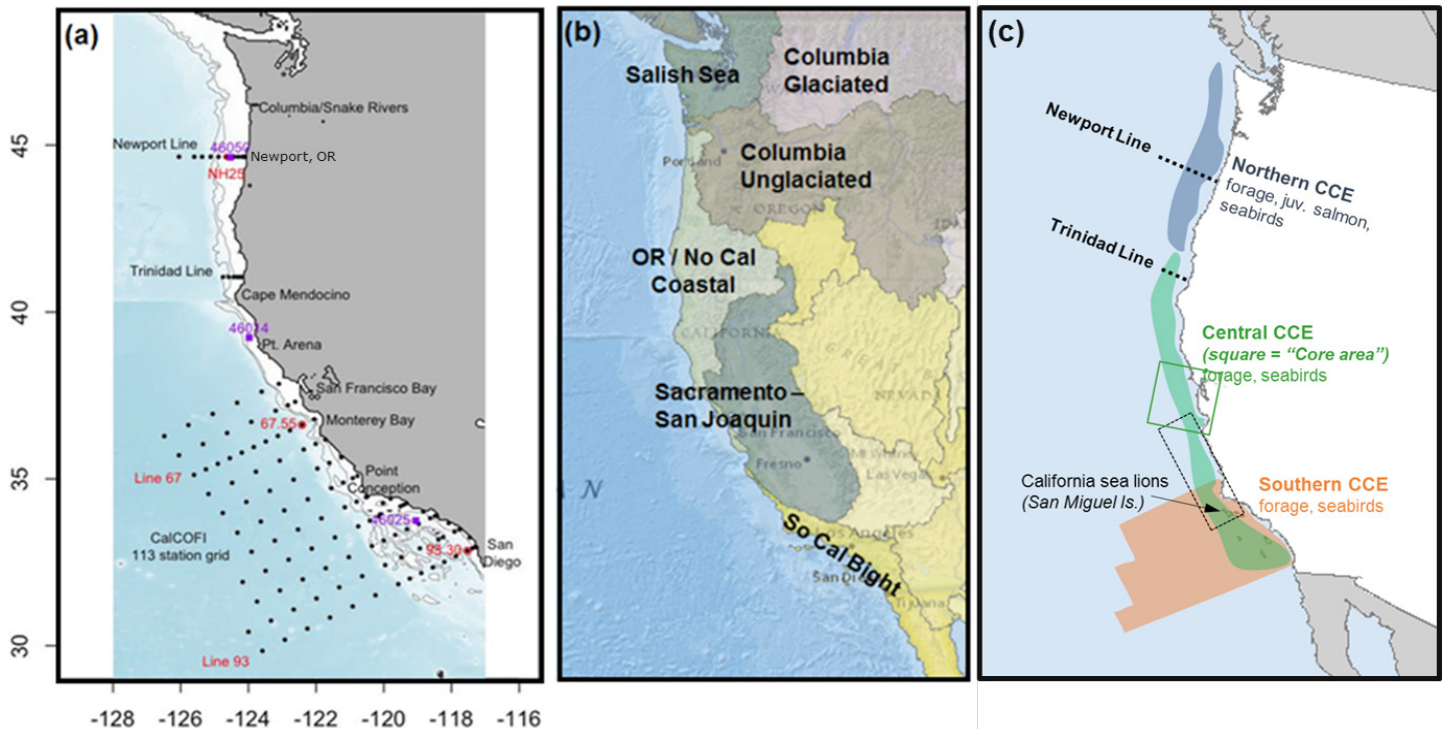


Figure 4. Map of the California Current ecosystem (CCE) and sampling areas: a) Key geographic features and oceanographic sampling locations. b) Freshwater ecoregions, where snowpack and freshwater indicators are measured. c) Biological sampling areas for zooplankton (Newport Hydrographic Line, Trinidad Line), pelagic forage, juvenile salmon, seabirds, and California sea lions. Solid box = core sampling area for forage in the central CCE. Dotted box approximates the foraging area for adult female California sea lions from the San Miguel colony.

2 Climate and Ocean Drivers

The northeastern Pacific Ocean experienced exceptional climate variability from 2013–19, reaching new extremes for many climate and oceanographic indicators during that period. As we describe in this section, this variability has affected many aspects of the CCE, including water and air temperature, winds, currents, mixing of ocean waters, water chemistry, and precipitation. The historically unprecedented North Pacific marine heat wave of 2013–16 and the strong El Niño event of 2015–16 gave way to cooler coastal waters, a succession of strong storms in the winter of 2016–17, and weak La Niña conditions by late 2017. By the end of 2018, mild El Niño conditions had returned, and the influx of cool, nutrient-rich subarctic water from the North Pacific Gyre had weakened to some of the lowest levels ever calculated. In addition, a short-lived marine heatwave occurred in the northeastern Pacific in the fall of 2018, though it remained more than 500 km offshore. The weak El Niño continued into mid-2019, as did the very weak influx of water from the North Pacific Gyre. A marine heatwave again occurred in the northeastern Pacific, lasting from roughly May 2019 to January 2020. This event was of similar size and had comparably positive sea surface temperature anomalies to the 2013–16 event, although it did not persist into the 2019–20 winter. Whereas the 2018 marine heatwave remained offshore, the 2019 marine heatwave briefly impacted the Northern California, Oregon, and Washington coasts. The large-scale climate and ocean indices observed in 2019 are generally consistent with periods of below-average productivity in the CCE. Superimposed on these large-scale climate and ocean drivers, regional indicators of upwelling, water chemistry, and stream conditions demonstrated their characteristically high spatiotemporal variability, resulting in patterns of local variation.

The following subsections provide in-depth descriptions of basin-scale, regional upwelling, hypoxia, ocean acidification, and hydrologic indicators of CCE climate and ocean variability.

2.1 Basin-Scale Indicators

The CCE is driven by atmosphere–ocean energy exchange that occurs on many temporal and spatial scales. To capture large-scale variability, the CCIEA Team tracks three indices: the status of the equatorial El Niño–Southern Oscillation (ENSO), described by the Oceanic Niño Index (ONI); the Pacific Decadal Oscillation (PDO); and the North Pacific Gyre Oscillation (NPGO). Positive ONI and PDO values and negative NPGO values usually denote conditions that lead to low CCE productivity, whereas negative ONI and PDO values and positive NPGO values are associated with periods of high CCE productivity.

ENSO events originate in the Pacific equatorial region and impact the CCE through atmospheric teleconnection and coastally trapped waves. Atmospheric impacts occur by modifying the jet stream and storm tracks, while coastally trapped waves change the nearshore thermocline and influence coastal currents that affect transport and distribution of equatorial and subequatorial waters (and species). The ONI is related to sea surface temperature (SST) in a region of the equatorial Pacific (lat 5°N–5°S, long 120–170°W), and is defined by a three-month running mean of sea surface temperature anomalies (SSTa) in that area. A positive ONI > 0.5°C for five consecutive months indicates El Niño conditions, which

usually means more storms to the south, weaker upwelling, and lower primary productivity in the CCE. A negative ONI $< -0.5^{\circ}\text{C}$ means La Niña conditions, which usually lead to higher productivity. The PDO is derived from the SSTa distribution in the northeastern Pacific Ocean, and often persists in “regimes” that last for many years. In positive PDO regimes, coastal SSTa in the Gulf of Alaska and the CCE tend to be warmer, while those in the North Pacific Subtropical Gyre tend to be cooler. Positive PDOs are associated with lower productivity in the CCE. The NPGO is a low-frequency variation of sea surface height, indicating variations in the circulation of the North Pacific Subtropical Gyre and the Alaskan Gyre, which in turn relate to the source waters for the CCE. Positive NPGO values are associated with increased equatorward flow, along with increased surface salinities, nutrients, and chlorophyll-*a*. Negative NPGOs are associated with decreases in such values, implying less subarctic source water and generally lower productivity.

In 2019, the ONI began at positive values indicative of the weak El Niño conditions that arose in 2018 (Figure 5, top). The ONI returned to neutral by June 2019. This El Niño was much weaker than the major El Niño of 2015–16; for example, the maximum ONI value in 2019 was 0.9° , compared to 2.6° during the 2015–16 El Niño. As of early June 2020, the [NOAA Climate Forecasting Center](#)⁷ had predicted a 65% chance of neutral ENSO conditions persisting through the summer of 2020. PDO values were neutral to slightly positive for most of the year, but exceeded one standard deviation (SD) above the long-term mean from April through June 2019 (Figure 5, middle). Overall, these neutral-to-weakly-positive PDO values were much lower than during the 2013–16 North Pacific marine heatwave. NPGO values, which had been highly variable but generally negative in recent years, decreased during 2018 to some of the lowest values estimated over the entirety of the time series, and these low values continued throughout most of 2019 (Figure 5, bottom). Collectively, the three basin-scale indices are consistent with below-average to average productivity in the CCE.

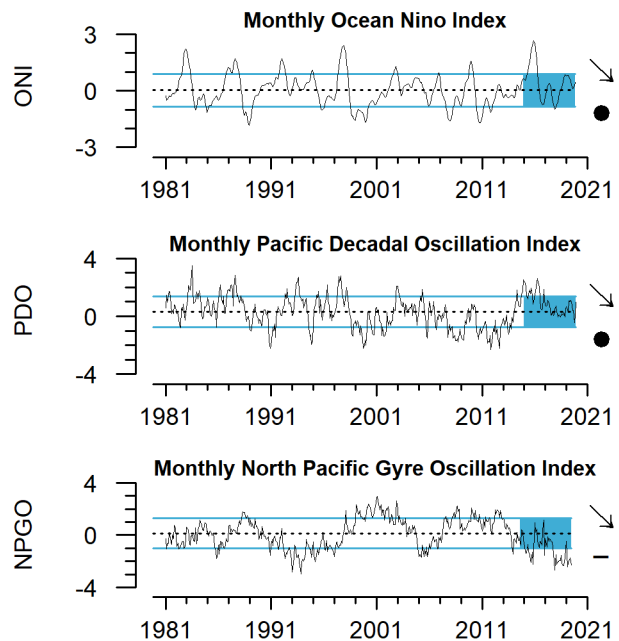


Figure 5. Monthly values of the Oceanic Niño Index (ONI), Pacific Decadal Oscillation (PDO), and the North Pacific Gyre Oscillation (NPGO), 1981–2019. Lines, colors, and symbols as in Fig 3a. ONI data from the [NOAA Climate Prediction Center](#).^{*} PDO data from N. Mantua, NMFS/SWFSC, derived from the University of Washington [Joint Institute for the Study of the Atmosphere and Ocean \(JISAO\)](#).[†] NPGO data from E. Di Lorenzo, [Georgia Institute of Technology](#).[‡]
^{*} <https://go.usa.gov/xG6NH>
[†] <http://research.jisao.washington.edu/pdo/>
[‡] <http://www.o3d.org/npgo/>

⁷ <https://go.usa.gov/xG6QU>

Seasonal SSTa values from 2019 reveal that CCE surface waters were warmer than average. In early 2019, SSTa values were above average for much of the North Pacific, including waters along the U.S. West Coast (Figure 6, upper left). SSTa values were even more strongly positive in the summer of 2019 (Figure 6, lower left), with three-month averages in many areas that were the greatest of the time series dating back to 1982 (denoted by \times es in Figure 6, lower left). Summertime SSTa values $>2^{\circ}\text{C}$ were common in many regions in 2019, including along the coast of central Oregon, along with a large patch of open ocean off the coast and several smaller patches to the northwest in the Gulf of Alaska. The warm SSTa values of 2019, along with the 2013–16 marine heatwave and 2015–16 El Niño event, collectively resulted in five-year mean SSTa values that were far above average in both winter and summer for a considerable portion of the northeastern Pacific, including waters along the U.S. West Coast (Figure 6, middle). The five-year trends for SSTa were strongly negative in nearly the entire region in winter (Figure 6, upper right), despite the relatively warm winter SSTa values in 2019; this negative trend reflects the overall cooling of the North Pacific following the extremely anomalous warm conditions during winter in 2015–16. Five-year trends in summer were mixed, with many regions showing positive trends (Figure 6, lower right) likely as a result of the very warm conditions in those areas during the summer of 2019 (Figure 6, lower left).

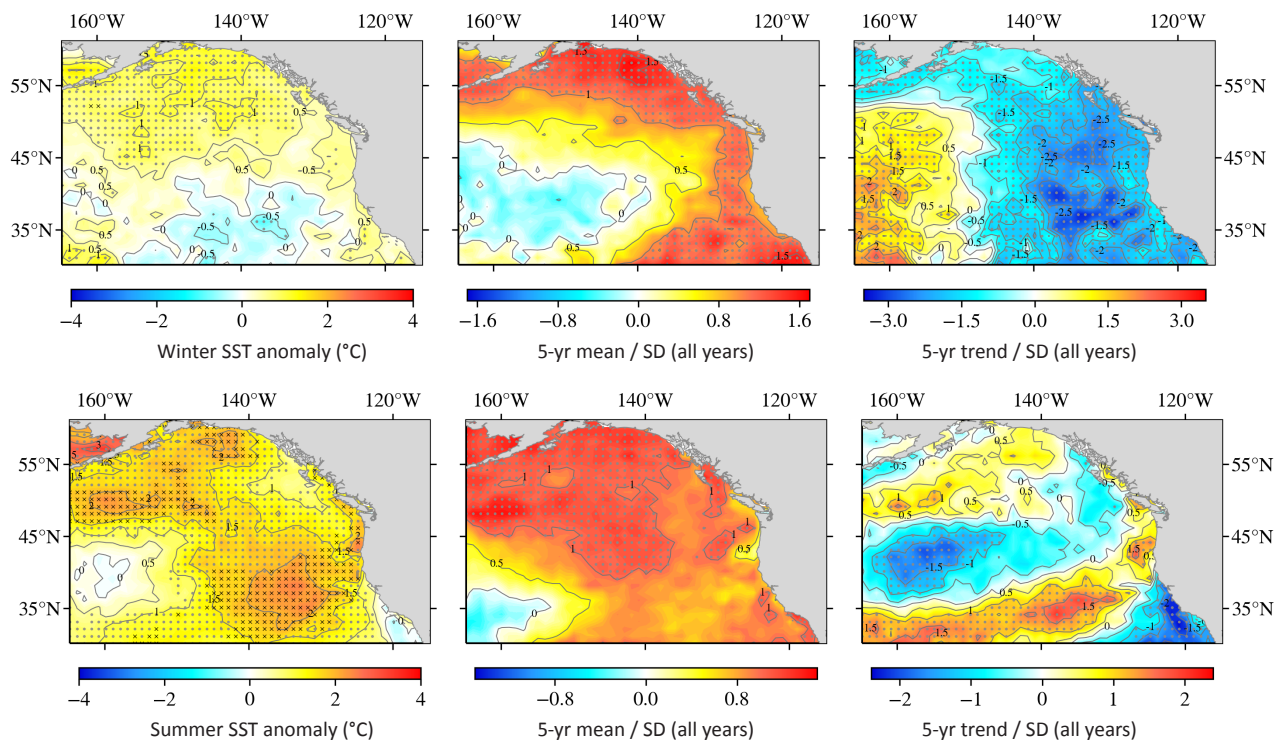


Figure 6. Sea surface temperature (SST) anomalies (2019, left), 5-year means (2015–19, middle), and 5-year trends (2015–19, right) in winter (Jan–Mar, top) and summer (Jul–Sep, bottom). The time series at each grid point began in 1982. Black circles mark cells where the anomaly was >1.0 SD above the long-term mean (left, middle) or where the trend was significant (right). Black \times es marks cells where the anomaly was the largest in the time series. For the SST 5-year means (middle) and trends (right), a given grid cell has been divided by the long-term SD, resulting in a map showing multiples of the long-term SD. SST maps are optimally interpolated remotely sensed temperatures (Reynolds et al. 2007), which can be downloaded using ERDDAP (<https://coastwatch.pfeg.noaa.gov/erddap/griddap/ncdcOisst21Agg.graph>).

Depth profiles of water temperatures in shelf waters off of Newport, Oregon and San Diego, California demonstrate the extent of recent warm and cool anomalies into the water column, as well as the spatial and temporal dynamics of those anomalies. Both areas of the coast experienced severe warming in the upper 50 m of the water column in 2014–15, associated with the marine heatwave at that time, and waters off San Diego experienced even deeper warming in 2015–16 associated with the major El Niño (Figure 7). Both areas were warm in the subsurface for much of 2017, while in 2018, waters off San Diego were cooler than average in much of the water column. In 2019, the water column over the continental shelf off Newport was warmer than average for most of the year, with extreme warming occurring above 50 m in the summer (Figure 7, top). This is consistent with the high positive SSTa values observed off central Oregon in the summer of 2019 (Figure 6, lower left). In contrast, CalCOFI station 93.30 off San Diego experienced warmth throughout the water column in the first half of 2019, particularly at depths from roughly 10 to 50 m (Figure 7, bottom), likely related to the weak El Niño that lasted through June 2019. After that, waters off San Diego were warm in the upper 10 m and then cooler than average for most of the water column. While these differences point to the distinct regional dynamics present at these two sites, it is nevertheless striking that both sites have been warmer than average throughout the water column for much of the time since 2014, implying substantial storage of heat in subsurface waters of the CCE. In future years, we will augment the spatial coverage of temperature-at-depth as collected by gliders and other survey platforms.

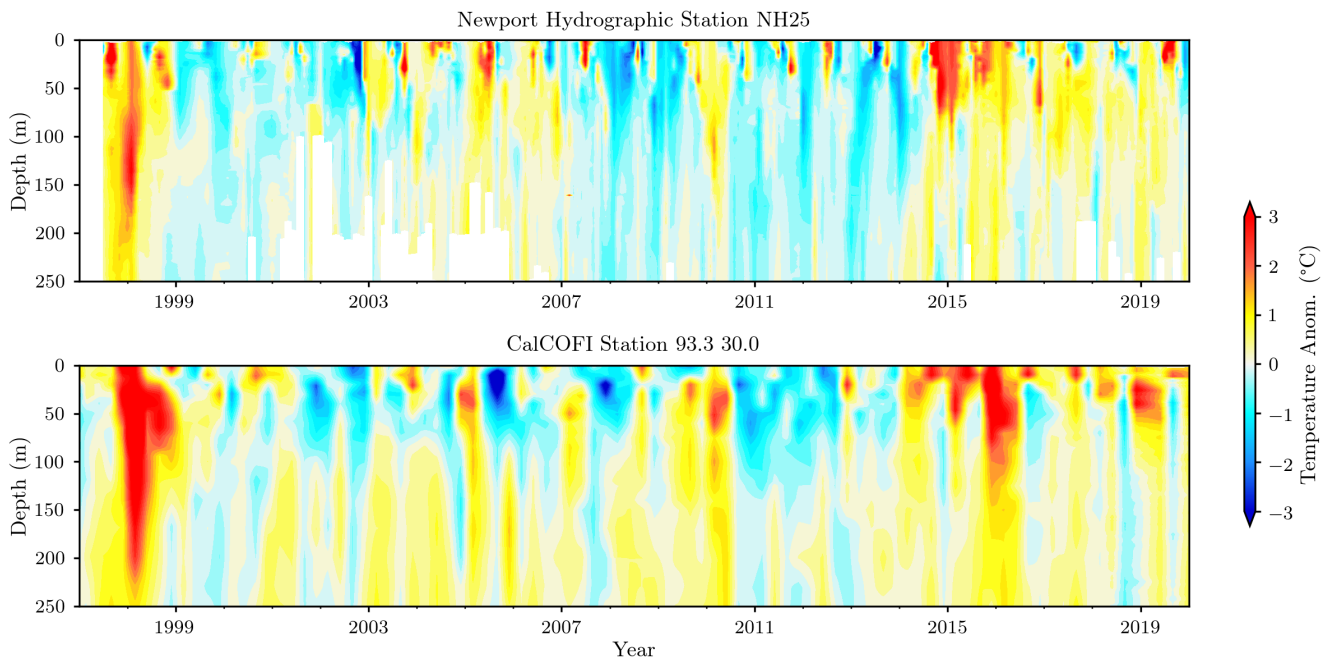


Figure 7. Time–depth–temperature anomaly contours for nearshore hydrographic stations NH25 (Jul 1997–Dec 2019) and CalCOFI 93.30 (Jan 1997–Nov 2019). For location of these stations, see Fig 4a. Newport Hydrographic (NH) line temperature data from J. Fisher, NMFS/NWFSC, OSU. CalCOFI data (<https://calcofi.org>) before Apr 2018 are from the bottle data database, while current data are from the final quality control conductivity–temperature–depth (CTD) database.

The surface warming anomalies described above and shown in Figures 6 and 7 coincided with the development of a new large marine heatwave in the northeastern Pacific Ocean in 2019. There is increased recognition that marine heatwaves can have immediate short-term impacts on the ecosystem and create short-term stock displacements (Jacox et al. 2020), similar to stock displacements that may occur with long-term climate warming. For these reasons, monitoring marine heatwaves and developing robust indices of these features are important for management. Based on an analysis of SSTa from 1982–2019, a marine heatwave has the potential to cause impacts in the CCE that are comparable to those from the 2013–16 event if the anomalous feature: 1) has statistically normalized SSTa >1.29 SD (90th percentile) of the long-term SSTa time series at a location; 2) is in the top 15% of area ($\sim 4.25 \times 10^5$ km²); 3) lasts for >5 days; and 4) comes within 500 km of the coast (Hobday et al. 2016, Leising in revision). Many such events have occurred in the North Pacific in recent decades, with some years experiencing multiple events, though none match the combined duration and intensity of the 2013–16 event (Figure 8). MHW-NEP19, the marine heatwave that formed in the northeast Pacific in 2019, exceeded all of these thresholds, and was similar to the 2013–16 marine heatwave in area (Figure 8) and intensity, although not in duration (see below). MHW-NEP19 was preceded by a fairly large heatwave during the fall of 2018, which also began to evolve during the middle of the year and continued until early December 2018, after which it was no longer expressed in SSTa values. Then, starting in May 2019, MHW-NEP19 developed rapidly and expanded in the offshore northeastern Pacific (Figure 9a). By July 2019, it had intersected with coastal Washington (Figure 9b). It reached its maximum area and intensity in August and September 2019 (Figure 9c), when it exceeded an area of 8×10^6 km² and an average temperature of 4°C above normal, rivaling the 2013–16 marine heatwave in area and intensity. At that time, the 2019 feature intersected the coast for all of Washington, Oregon, and Northern California (Figure 9c). After that, the feature receded from the coast and weakened, thus reducing its potential impacts on the coastal CCE. This continued until, by mid-January 2020, the feature no longer met the criteria for being a marine heatwave, although SST was still warmer than normal for a large offshore region of the northeastern Pacific (Figure 9d). Compared to the 2013–16 event, the 2019 marine heatwave did not penetrate as deeply into the water column.

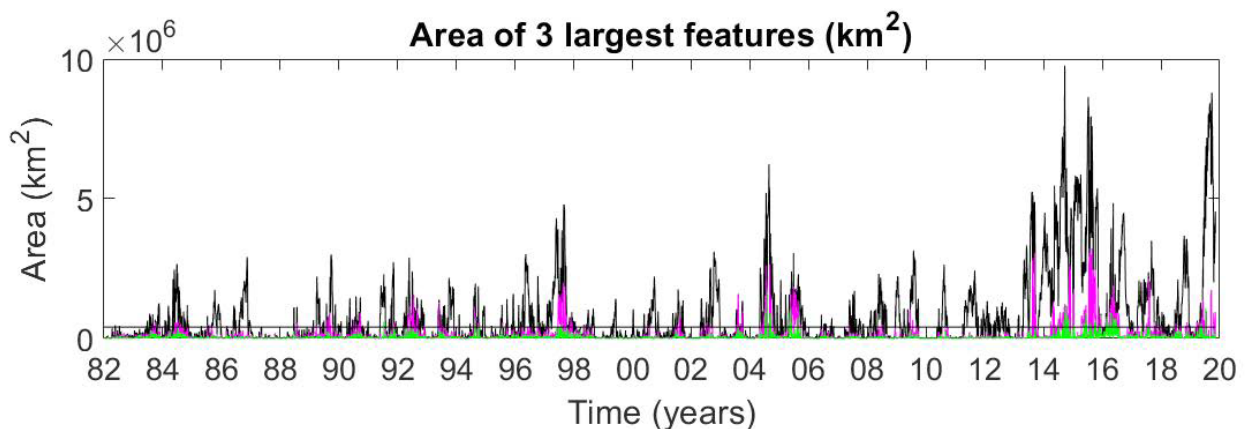


Figure 8. Area of North Pacific warm SST anomalies >2.0 SD from 1982–2019. Because multiple anomalies can be present, black is the largest anomaly, magenta is the second-largest, and green is the third-largest. The horizontal line represents 500,000 km², the area threshold for features likely to impact the coastal region of the CCE. Data courtesy of A. Leising, NMFS/SWFSC.

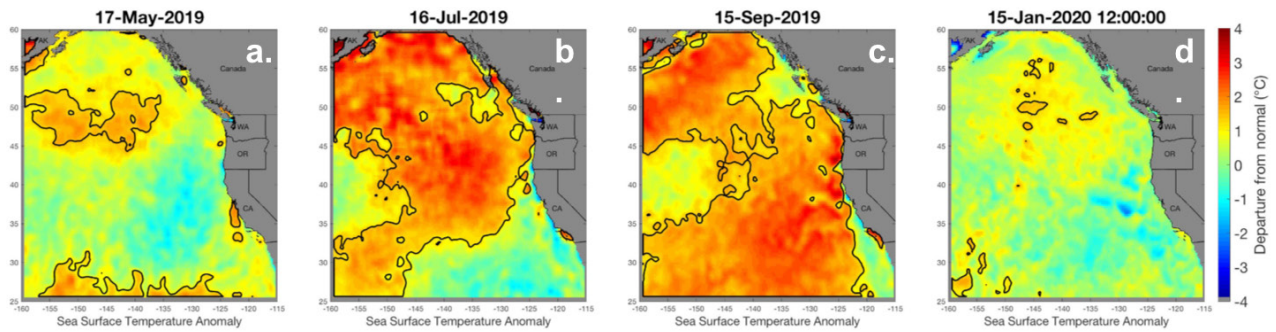


Figure 9. Standardized SSTa across the northeastern Pacific for a) May, b) Jul, and c) Sep 2019, and d) Jan 2020. Dark contours outline regions that meet the criteria of a marine heat wave (see text). The standardized SSTa is defined as SSTa divided by the SD of SSTa at each location calculated over 1982–2019, thus taking into account spatial variance in the normal fluctuation of SSTa. Plots were created by A. Leising, NMFS/SWFSC, using SST data from NOAA's optimum interpolation sea surface temperature analysis (OISST; <https://www.ncdc.noaa.gov/oisst>).

MHW-NEP19 had some similarities with, but also some important differences from, the 2013–16 event. The earlier marine heatwave began in the far-offshore region during mid-2013, grew and moved closer to the coast, and showed a slight recession during the winter of 2013–14. In 2014, it steadily gained strength through the spring and summer (Figure 10a–b) and reached a peak intensity that year during September (Figure 10c). The anomalous warming persisted into the winter of 2014–15 (Figure 10d). The 2019 event evolved much more rapidly to its maximum size, also peaked in September, but failed to persist through the winter (Figure 9). However, a significant pool of warmer-than-normal water remained in the far-offshore region.

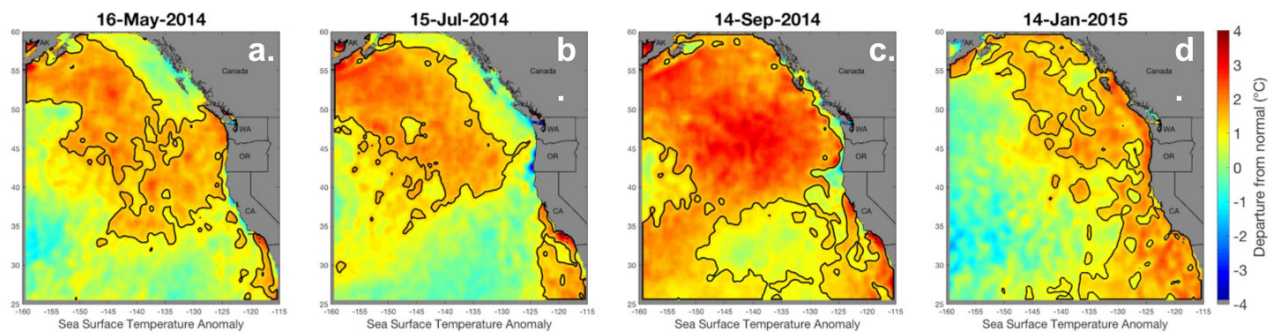


Figure 10. Progression of standardized sea surface temperature (SST) anomalies in 2014–15, the time period when the 2013–16 marine heatwave first expanded into California Current waters and intersected coastal waters. Dark contours outline regions that meet the criteria of a marine heat wave (see text). Compare with the progression of images for the 2019 marine heatwave shown in Fig 9. Plots were created by A. Leising, NMFS/SWFSC, using SST data from NOAA's optimum interpolation sea surface temperature analysis (OISST; <https://www.ncdc.noaa.gov/oisst>).

The above plots and analyses focus on sea surface temperatures. Subsurface temperature data from autonomous glider transects provide additional information. The northeastern Pacific Ocean has remained anomalously warm since the 2013–16 marine heatwave and 2015–16 El Niño (Figure 11). Time series of glider data along CalCOFI line 90 (off Dana Point in the Southern California Bight) at 10- and 50-m depths from the shore to a distance 500 km offshore illustrate the dramatic subsurface temperature change that occurred in 2014 and continued through the end of 2019.

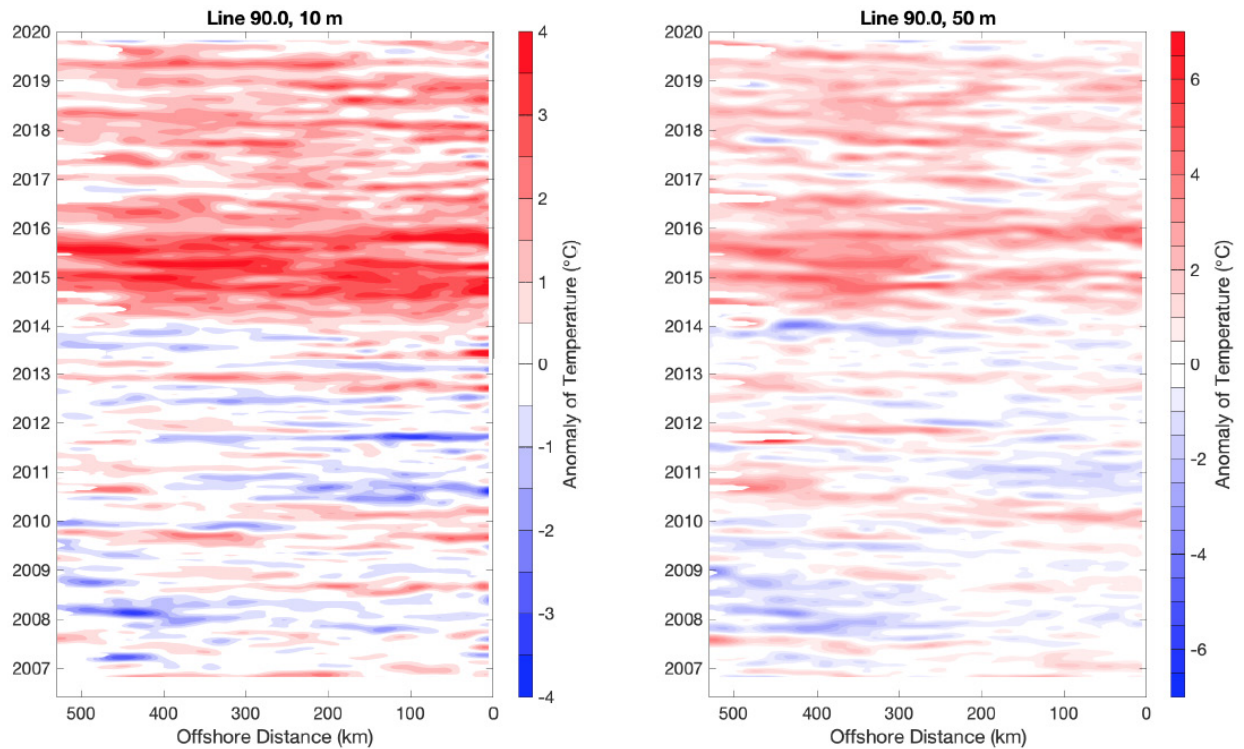


Figure 11. California Underwater Glider Network (CUGN) temperature anomalies at depths of 10 m (left) and 50 m (right) along CalCOFI line 90, extending from the coast to 500 km offshore, 2007–19. Data from CUGN are provided by D. Rudnick, Scripps Institute of Oceanography Instrument Development Group (DOI: 10.21238/S8SPRAY7292).

To compare the subsurface temperature data to the ONI, the temperature anomaly was computed for the 50-m depth along CalCOFI line 90.0 and at the 10-m depth for CalCOFI lines 67, 80, and 90, and averaged across the 200-km glider track extending from the coast (Rudnick et al. 2017). Prior to 2014, the subsurface temperature anomalies at both the 10- and 50-m depths tracked closely with the ONI index (Figure 12), consistent with the finding that the ENSO was the major source of variability in the CCE for the majority of this time series (Jacox et al. 2016). In 2014, the temperature indices on the three separate glider lines (CalCOFI line 67 off Monterey Bay, line 80 off Point Conception, and line 90 off Dana Point) show that the temperature increase began prior to the major 2015–16 El Niño, and did not return to tracking the ONI following the end of the El Niño in 2016. The glider trends increased with the mild 2018–19 El Niño, but still remained anomalously high. These data agree with the anomaly contours of CalCOFI line 93 in Figure 7, demonstrating that Southern and Central California have remained warm since the 2013–16 marine heatwave, and experienced some additional influence from the recent El Niño events.

Data from the glider surveys suggest further changes in the water column, in particular changes in subsurface salinity. A major salinity anomaly can be seen along CalCOFI line 90 at 10- and 50-m depths starting in 2018 (Harvey et al. 2020, Figure D.2.6). These represent some of the largest and most extensive positive anomalies of the available time series, and suggest that the Southern California Bight temperatures since 2018 may be due to the influx of warmer, saltier waters into the region.

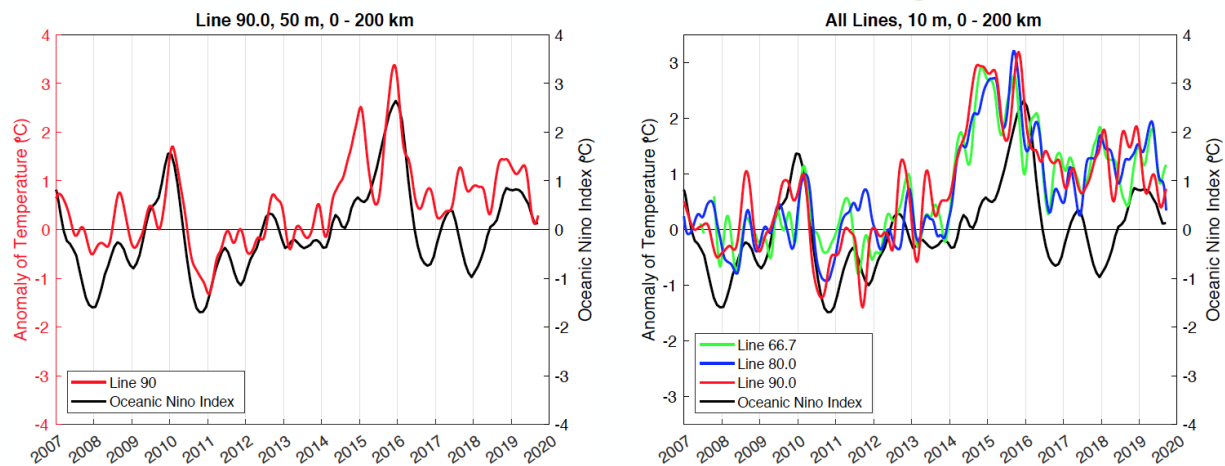


Figure 12. CUGN temperature indices on CalCOFI lines 67, 80, and 90 compared to the ONI. The indices are the temperature at the indicated depth averaged from the shore to 200 km offshore. ONI data are from the NOAA Climate Prediction Center. Data from CUGN are provided by D. Rudnick, Scripps Institute of Oceanography Instrument Development Group (DOI: 10.21238/S8SPRAY7292).

In summary, following the 2013–16 marine heat wave and the 2015–16 El Niño event, basin-scale temperatures moderated during 2017–18, with notable exceptions such as a very warm patch of water off Southern California in the summer of 2018 and the brief marine heatwave in the North Pacific in late 2018 (Figure 8). These events were followed by another substantial marine heatwave in 2019. Additionally, the weak El Niño of 2018–19 and the strongly negative NPGO of the past two years are indicative of poor conditions for overall system productivity in the CCE. In addition, there remains a large amount of stored heat in the North Pacific water column following the succession of marine heatwaves and El Niño events from 2013–20. We are therefore concerned that the system may be primed for another heatwave in 2020.

2.2 Regional Upwelling Indices

Seasonal cross-shore gradients in sea level pressure produce the northerly alongshore winds that drive coastal upwelling in the CCE. Upwelling is a physical process of moving cold, nutrient-rich water from deep in the ocean to the surface, which fuels the high seasonal primary production at the base of the CCE food web. The timing, strength, and duration of upwelling vary greatly in space and time. In previous ESR documents, we summarized upwelling timing and intensity using the well established Bakun Upwelling Index (BUI), estimated at three-degree latitudinal intervals along the coast. The BUI, derived from the U.S. Navy Fleet Numerical Meteorology and Oceanography Center’s sea level pressure product, provided information on the onset of upwelling-favorable winds (the “spring transition”), a general indication of the strength of upwelling, relaxation events, and the end of the upwelling season at a given location. However, the BUI does not take into consideration the underlying ocean structure (e.g., ocean stratification), which can have considerable influence on the nutrient content of the upwelled water. Nor does it consider the influence of ocean circulation, which can impact upwelling. Finally, assumptions of the BUI break down off of Central and Southern California due to features of coastal geography, leading to poor wind (and therefore upwelling) estimates there. Jacox et al. (2018) developed new estimates of coastal upwelling using ocean models to improve upon

the BUI by estimating the vertical transport in the Cumulative Upwelling Transport Index (CUTI) and nitrate flux in the Biologically Effective Upwelling Transport Index (BEUTI). These indices are derived from a CCE configuration of the Regional Ocean Modeling System (ROMS) model with data assimilation (Neveu et al. 2016). CUTI provides more accurate estimates of vertical transport of water, whereas BEUTI provides valuable additional information about the nature of the upwelled water (e.g., its nitrate content) that can be linked to ecological processes such as productivity (Jacox et al. 2018).

In the CCE, the timing of peak vertical flux of upwelled water (indicated by CUTI) varies by latitude, with northern latitudes having a later onset of maximum upwelling (Figure 13, left, shaded areas). The maximum climatological value of CUTI (Figure 13, left, dashed line) is at the end of April at lat 33°N (San Diego, California), the middle of June at lat 39°N (Point Arena, California), and the end of July at lat 45°N (Newport, Oregon). Values of CUTI at lat 39°N tend to be roughly a factor of two greater than at the other two latitudes. The magnitude of vertical nitrate flux (BEUTI) also varies greatly by latitude (Figure 13, right, shaded areas). At lat 39°N, BEUTI is about an order of magnitude larger at its peak than at the other latitudes, and this much larger amount of nutrient input in upwelled water likely contributes to the high productivity of lower trophic levels in this region of the coast. At lat 45°N, and to a lesser extent at lat 39°N, downwelling occurs in the winter due to poleward-blowing winds. (Note that a negative value of BEUTI accompanying downwelling suggests removal of nitrate, but a source is not identified).

During 2019, CUTI and BEUTI varied regionally in the CCE. At lat 45°N, both CUTI and BEUTI were highly variable, but were generally average to slightly above-average in the winter and spring (Figure 13, top, heavy solid lines). In summer and early fall, CUTI was average to below-average, while BEUTI was close to average; in late fall, CUTI and BEUTI were above-average for a period before declining below-average near the end of 2019, with negative values indicating at least one strong downwelling event (Figure 13, top, heavy solid lines). At lat 39°N, CUTI and BEUTI were also variable, but average to below-average in winter and spring, but average to above-average in summer and most of the fall (Figure 13, middle, heavy solid lines). In late fall, multiple strong downwelling events drove both CUTI and BEUTI below average (Figure 13, middle, heavy solid lines). At lat 33°N, CUTI and BEUTI values were variable, though far less so than the other two latitudes; as with lat 39°N, CUTI and BEUTI at lat 33°N were average to below-average in winter and spring, average to above-average in summer and fall, and average to below-average in late fall (Figure 10, bottom, heavy solid lines).

The high-frequency cycling between upwelling events and relaxation or downwelling periods pictured in Figure 13 appears critical for the uptake of nutrients by phytoplankton and the availability of phytoplankton for higher trophic levels. These cycles, or Lasker events (Lasker 1978), create a balance of the supply of nutrients in the upwelled water and the nutrient residence time to allow for phytoplankton growth. With insufficient upwelling, there are not enough nutrients for phytoplankton growth, while with extended upwelling, the nutrients are carried out to the open ocean. Jacox et al. (2016) described the optimal wind strength (moderate) and nutrient concentration (high) for promoting high phytoplankton biomass, while Wilkerson et al. (2006) concluded that an optimal window of 3–7 days of relaxation following an upwelling event was required for chlorophyll accumulation in the Central California region off Bodega. Lasker (1978) also found cycling shifts in the Southern California phytoplankton population between dinoflagellates and diatoms, with the larger dinoflagellates providing more caloric requirements of first feeding anchovy larvae.

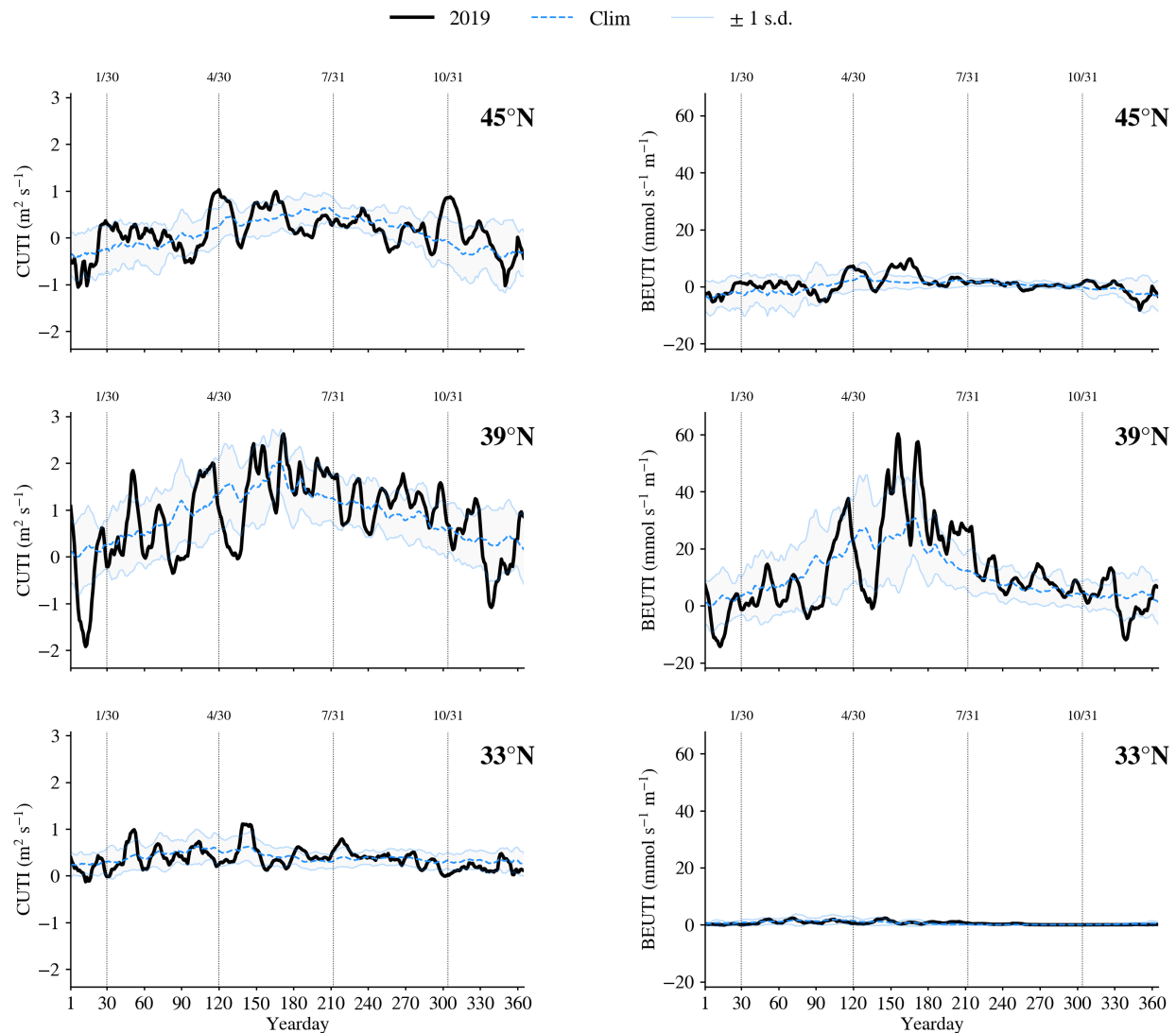


Figure 13. Daily 2019 values of Coastal Upwelling Transport Index (CUTI, left) and Biologically Effective Upwelling Transport Index (BEUTI, right) from 1 Jan–31 Dec, relative to the 1988–2019 climatology (blue dashed line) ± 1.0 SD (shaded area), at lats 33°, 39°, and 45°N. Daily data are smoothed with a 10-day running mean. Vertical lines mark the ends of Jan, Apr, Jul, and Oct. Daily 2019 BEUTI and CUTI values provided by M. Jacox, NMFS/SWFSC; detailed information about these indices can be found at <https://go.usa.gov/xG6Jp>.

Upwelling is an important feature along the U.S. West Coast, not just because it brings nutrients to surface waters where they can be taken up by phytoplankton to support primary production; upwelling also creates a band of relatively cool water along the coast during the spring and summer, which is suitable habitat for a diverse and productive portion of the CCE food web. A concern that has emerged in the CCE during the anomalously warm years that began with the 2013–16 marine heatwave is “habitat compression.” Santora et al. (2020) used this term to denote how offshore warming during the 2013–16 marine heatwave restricted the relatively cool upwelling habitat to a narrower-than-normal band along the coast. This compression of the upwelling habitat consequently altered pelagic species composition and distribution, from forage species to top predators, and

likely contributed to impacts such as increased rates of whale entanglements in fixed fishing gear. Santora et al. (2020) developed a Habitat Compression Index (HCI) to track latitudinal changes in the area of cool upwelled surface waters. The HCI is defined as the area of cool ($\leq 12^{\circ}\text{C}$) monthly averaged temperatures at a depth of 2 m, in a region extending from the coast to 150 km offshore between lats 35.5° and 40°N (roughly from Morro Bay to Cape Mendocino, California). These temperatures were extracted from the same ROMS model used to generate the CUTI and BEUTI indices. Figure 14 illustrates the strong HCI shift that occurred in 2014 and has continued since then, especially in winter. Similar levels of compression have been observed in previous years, such as in winter and spring in the years 1992–98; however, as Santora et al. (2020) showed, the temperature gradient between inshore and offshore water since 2014 has been steep, due to the large amount of anomalously warm water present in the northeastern Pacific Ocean in recent years (Figure 15); this strong inshore/offshore temperature gradient may be exacerbating the ecological impacts of the compressed area of the upwelling zone. We will continue to study this metric in relation to other indicators, in hopes of discerning its relative importance as an environmental driver at different scales and locations, given its degree of spatiotemporal variability (Figure 15). We plan to expand the HCI estimation efforts to examine other depth layers and other regions of the coast.

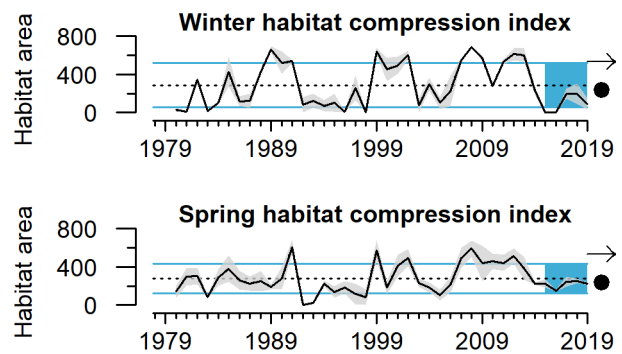


Figure 14. Mean winter (Jan–Mar) and spring (Apr–Jun) habitat compression index ($\text{SST} < 12^{\circ}\text{C} \times 100 \text{ km}^2$) for 1980–2019. Error envelope indicates ± 1.0 SE. Lines, colors, and symbols as in Fig 3a. Compression index estimates developed and provided by J. Santora, NMFS/SWFSC, and I. Schroeder, NMFS/SWFSC, UCSC.

2.3 Hypoxia and Ocean Acidification

Nearshore dissolved oxygen (DO) depends on many processes, including currents, upwelling, air–sea exchange, and community-level production and respiration in the water column and benthos. DO is required for organismal respiration; low DO can compress habitat and cause stress or die-offs for sensitive species. Waters with DO levels $< 1.4 \text{ mL/L}$ (2 mg/L) are considered to be hypoxic; such conditions may occur on the shelf following the onset of spring upwelling, and continue into the summer and early fall months until the fall transition mixes shelf waters. Upwelling-driven hypoxia occurs because upwelled water from deeper ocean sources tends to be low in DO, and microbial decomposition of organic matter in the summer and fall increases overall system respiration and oxygen consumption, particularly closer to the seafloor.

Low DO was a serious issue in the northern CCE in 2019, as it has been in other recent years. At station NH05 (5 nmi [nautical miles] off of Newport), water near bottom over the continental shelf fell below the hypoxia threshold in August; although the station was hypoxic for a shorter period of time than in 2018, the hypoxia was of similar intensity (Figure 16, top). Observed DO levels in the middle of the water column (depth = 150 m) at station NH25 (25 nmi offshore of Newport) were above the 1.4 mL/L threshold (Figure 16, bottom). Mild-to-severe

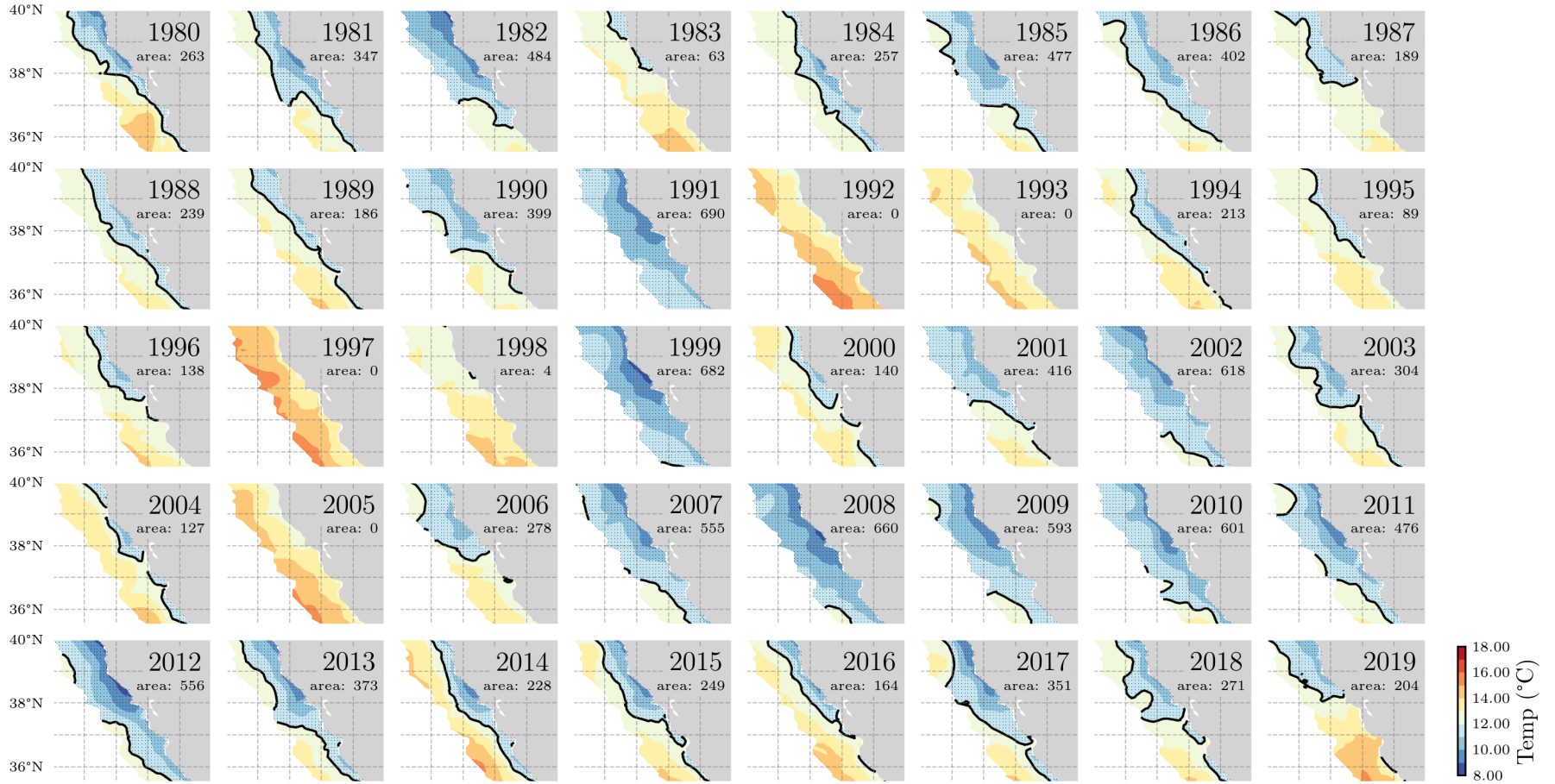


Figure 15. Areal extent of the HCI for the month of May for 1980–2019. Heavy contour is the offshore extent of the cool coastal habitat water. Compression index estimates developed and provided by J. Santora, NMFS/SWFSC, and I. Schroeder, NMFS/SWFSC, UCSC.

hypoxia was widespread in August and September 2019 in near-bottom waters over the continental shelf and slope off of Washington and Oregon, as indicated by DO readings taken from the NOAA Fisheries West Coast Groundfish Bottom Trawl Survey (Figure 17), though we note that fewer demersal DO readings were taken by this survey in 2019 than in prior years due to a reduction in survey effort. Demersal shelf waters off Washington were hypoxic in the late summer of 2019, although the hypoxia appeared to be less intense than in the same season in 2018 (Figure 17). Off Oregon, demersal shelf waters also experienced widespread hypoxia in late summer 2019, and the hypoxia spread further south along the Oregon coast than in the prior four years, extending just to the south of Cape Blanco (Figure 17).

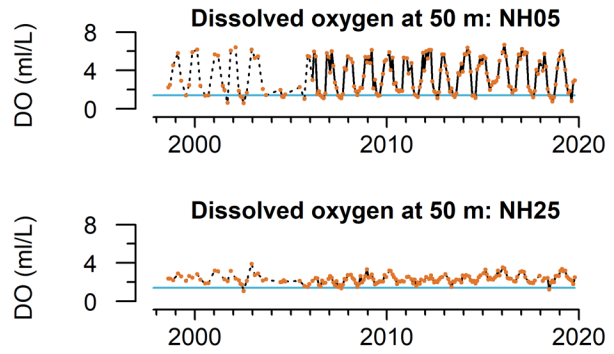


Figure 16. Dissolved oxygen at 50 m depth off Newport, OR, through 2019. Stations NH05 and NH25 are 5 and 25 nmi from shore, respectively. The blue line is the hypoxic threshold of 1.4 mL/L DO. The dotted black line indicates missing data. Lines, colors, and symbols as in Fig 3a. Newport Hydrographic (NH) line DO data are from J. Fisher, NMFS/NWFSC, OSU.

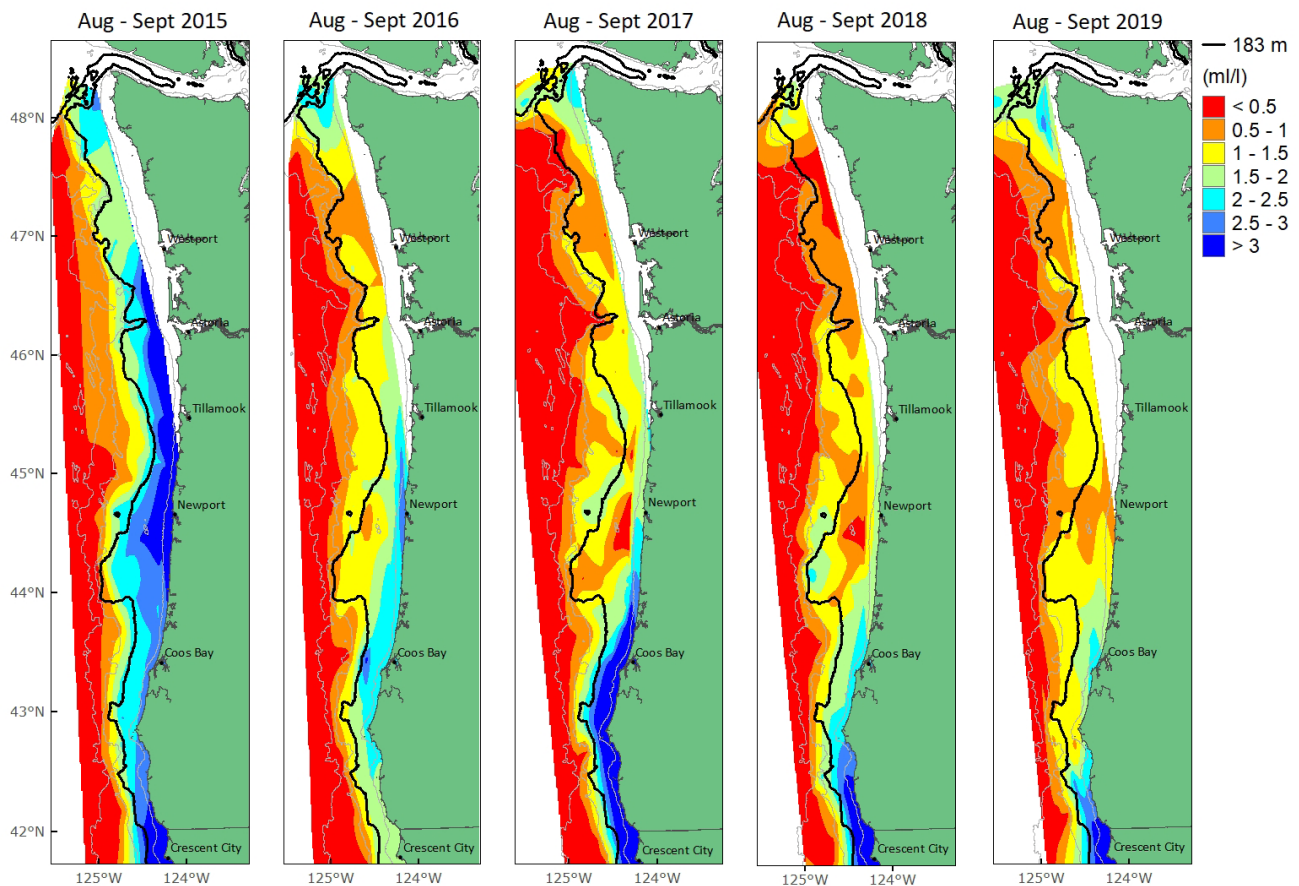


Figure 17. Annual maps of near-bottom DO levels (mL/L) during the months of Aug–Sep from 2015 (far left) through 2019 (far right). Source: NMFS/NWFSC West Coast Groundfish Bottom Trawl Survey.

In the CalCOFI region of the southern CCE (see Figure 4a), summer DO values displayed strong inshore-offshore and depth gradients, with higher values measured farther offshore and lower values measured at depth. At CalCOFI station 90.9 (461 km offshore), DO values at 150-m depths were well above the hypoxia threshold in the spring and summer 2019 (Figure 18, top). At station 93.3, located 27.4 km offshore, DO at 150 m was lower than at station 90.9 but still above the hypoxia threshold (Figure 18, bottom). Figure 19 provides additional DO information for this region, derived from the July 2019 CalCOFI survey; shown are maps of interpolated DO values derived from the sampling stations. DO estimates are shown for depths of 50 m, 150 m, and from the greatest depth sampled by the conductivity-temperature-depth (CTD) cast (near bottom at depths <500 m; at 500 m at all deeper stations). DO values were well above the hypoxia threshold at depths of 50 and 150 m (Figure 19, left and middle). At the greatest depths sampled, near-bottom DO was generally above the hypoxia threshold at coastal stations, except in some shallow portions of the Santa Barbara basin between the mainland and Santa Cruz and Santa Rosa islands (Figure 19, right). The deeper stations consistently had hypoxic water at 500-m depth, although that is typical of those sites, and most deep stations were close to or even above-average for DO at depth (Figure 19, right).

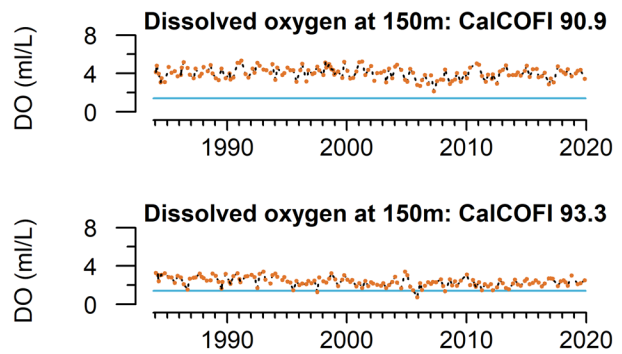


Figure 18. DO at 150 m off San Diego, CA (CalCOFI survey stations 90.9 and 93.3), through 2019. The blue line is the hypoxic threshold of 1.4 mL/L DO. Lines, colors, and symbols as in Fig 3b. DO data compiled by I. Schroeder, NMFS/SWFSC, UCSC, using CalCOFI data. CalCOFI data before April 2018 are from the bottle data database, while current data are from the final quality control CTD database.

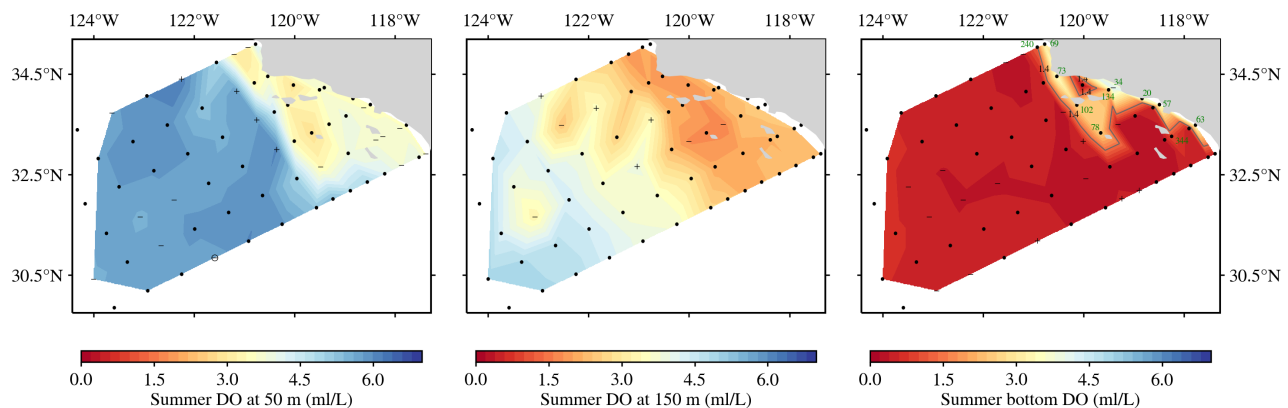


Figure 19. DO observations during the summer 2019 CalCOFI survey of the Southern CCE at 50 m (left), 150 m (middle), and on the bottom of the hydrographic cast (right). DO was sampled at hydrographic stations (marked with black dots). Hydrographic casts extended to the bottom or to a maximum depth of 500 m; only a small number of stations near shore or islands have bottom depths <500 m (labeled in green). The black dots are changed to either a minus (-) or plus (+) if the measured value was less or greater than 1 SD above the long-term mean, respectively. Also, if the measured value is the smallest or largest value ever sampled since 1984, the symbol is surrounded by a black circle. The 1.4 mL/L contour level is labeled if it exists. DO data compiled by I. Schroeder, NMFS/SWFSC, UCSC, using CalCOFI data.

Ocean acidification (OA), caused by anthropogenically increased levels of atmospheric CO₂, reduces pH and carbonate ion levels in seawater. A key indicator of OA is aragonite saturation state, a measure of the availability of aragonite (a form of calcium carbonate). Aragonite saturation <1.0 indicates corrosive conditions that have been shown to be stressful for many CCE species, including oysters, crabs, and pteropods (Barton et al. 2012, Bednarsek et al. 2014, Marshall et al. 2017, Hodgson et al. 2018). Upwelling, which drives primary production in the CCE, also transports hypoxic, acidified waters from offshore onto the continental shelf, where increased community-level metabolic activity can further exacerbate OA (Chan et al. 2008, Feely et al. 2008). As a result, aragonite saturation levels tend to be lowest during and following upwelling in the spring and summer, and highest during the winter. Rivers in the region tend to be undersaturated and may contribute further to corrosivity (Feely et al. 2018).

Off Newport, aragonite saturation state near the seafloor in 2019 was similar to 2018, and lower than in the anomalous years of 2014–15. Winter saturation state was consistently above the threshold of 1.0 at station NH05 (Figure 20, left, top), but indicated generally corrosive conditions at 150 m depth at station NH25 for most of the time series, including 2019 (Figure 20, left, bottom). Summer aragonite saturation states indicated corrosive waters at both stations for most of the time series, including 2019 (Figure 20, right). At these same stations, aragonite saturation horizon profiles show that more of the water column was above the saturation threshold (i.e., ≥1.0) in 2019 (Figure 21) than in 2018, but was within the range of previous observations.

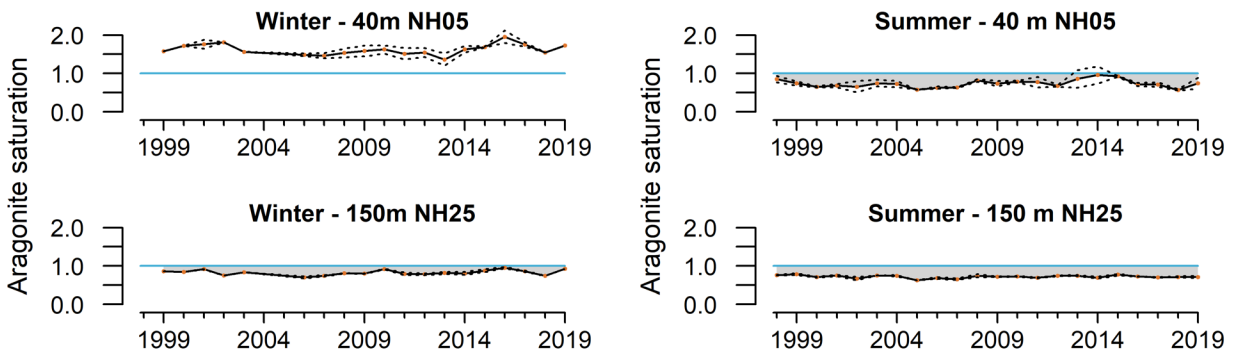


Figure 20. Winter (Jan–Mar, left, 1999–2019) and summer (Jul–Sep, right, 1998–2019) aragonite saturation values at two stations off Newport, OR. Stations NH05 and NH25 are 5 and 25 nmi from shore, respectively. The blue line is the threshold value of 1.0 for aragonite saturation state. Lines, colors, and symbols as in Fig 3a. Data provided by J. Fisher, NMFS/NWFSC, OSU.

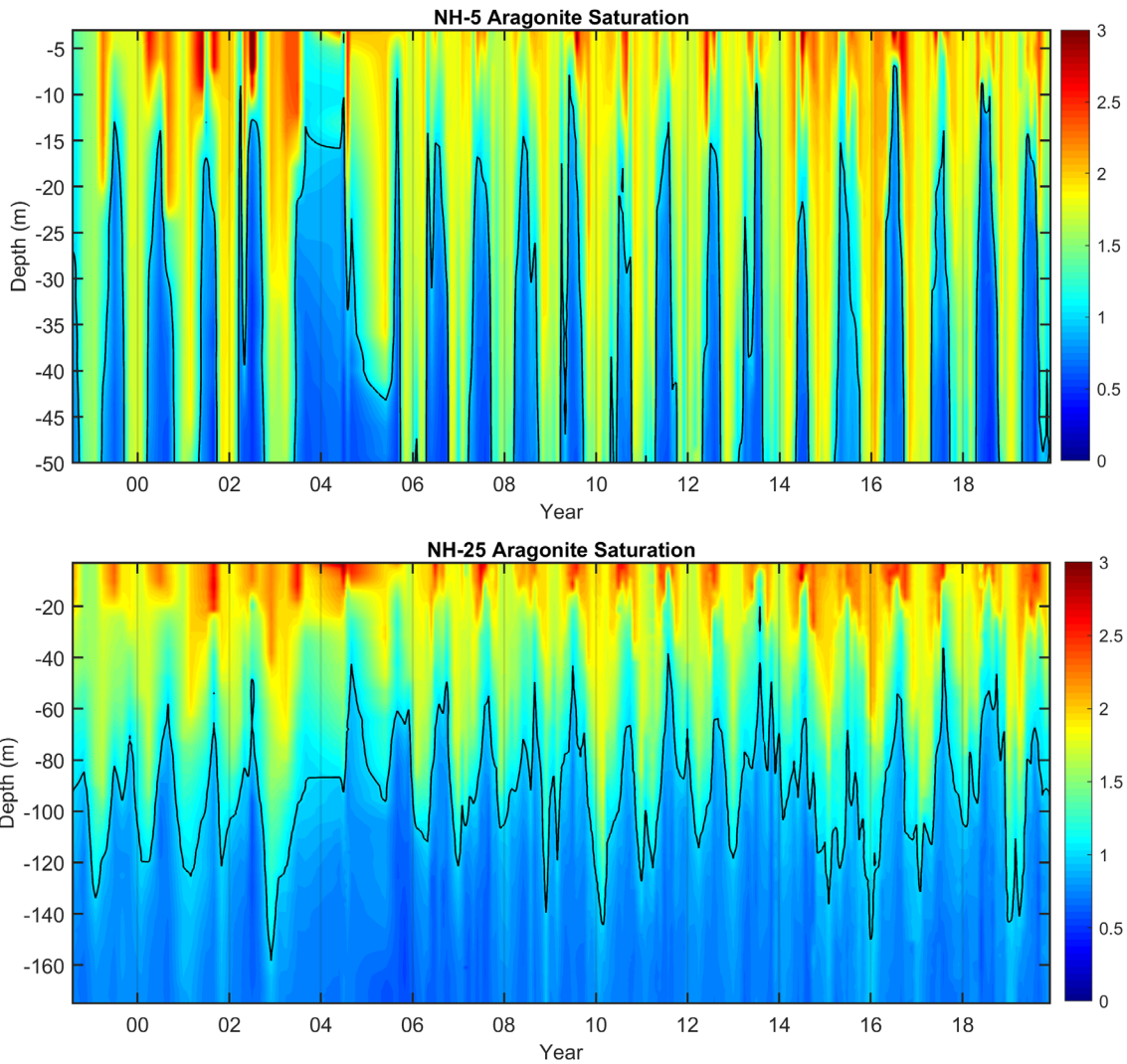


Figure 21. Aragonite saturation vertical profiles for stations NH05 and NH25 off of Newport, OR. Black line indicates the depth at which aragonite saturation state = 1.0, a biological threshold below which seawater can be especially corrosive to shell-forming organisms. Stations NH05 and NH25 are 5 and 25 nmi offshore, respectively. Data provided by J. Fisher, NMFS/NWFSC, OSU.

Forecasts of dissolved oxygen and aragonite saturation in spring and summer of 2020 are available for the northern portion of the CCE, using a forecasting system originally developed at the University of Washington Joint Institute for the Study of the Atmosphere and Ocean (JISAO). The model system is called J-SCOPE (JISAO's Seasonal Coastal Ocean Prediction of the Ecosystem). The J-SCOPE forecast system provides short-term skilled forecasts of ocean conditions off of Washington and Oregon based on dynamically downscaled 6- to 9-month forecasts from the global-scale NOAA Climate Forecasting System model. J-SCOPE forecasts have been extended to include seasonal predictions of habitat quality for sardines (*Sardinops sagax*; Kaplan et al. 2016, Siedlecki et al. 2016). Each January and April, the J-SCOPE modelers produce an ensemble of three forecasts that project ocean conditions through September and include variables like temperature, dissolved oxygen, chlorophyll, aragonite saturation state (ocean acidification), and sardine habitat, in addition to other dynamics such as the timing and intensity of upwelling.

According to the J-SCOPE ensemble forecast of the 2020 summer upwelling season (May–August), sea surface temperatures of coastal waters in the northern CCE are expected to be near the average of recent years until late summer (July–August), when they will become warmer, but these warm anomalies do not extend to subsurface habitats (consistent with the forecast of ENSO neutral conditions; data not shown here). DO on the bottom is forecast to be below-average over the continental shelf, with hypoxia on the shelf off Oregon and Washington developing in June (earlier than average for recent years) and remaining for the rest of the upwelling season (Figure 22). However, the three model ensemble members had high disagreement for the DO projection, resulting in high uncertainty surrounding this forecast. Aragonite on the bottom is expected to be undersaturated (i.e., more corrosive) throughout the upwelling season for most of the bottom waters in the region, except for shallow nearshore waters on the Washington shelf through spring (Figure 23). Surface waters are expected to be supersaturated in aragonite throughout the season (not shown). Other J-SCOPE forecasts for 2020 project that chlorophyll-*a* concentrations will be near average values for recent years early in the upwelling season but lower over the Washington and Oregon shelves later in the upwelling season; and that waters throughout the region will have suitable temperature and salinity conditions for sardines, though in recent years sardine population size has been low and much of this habitat has not been occupied.

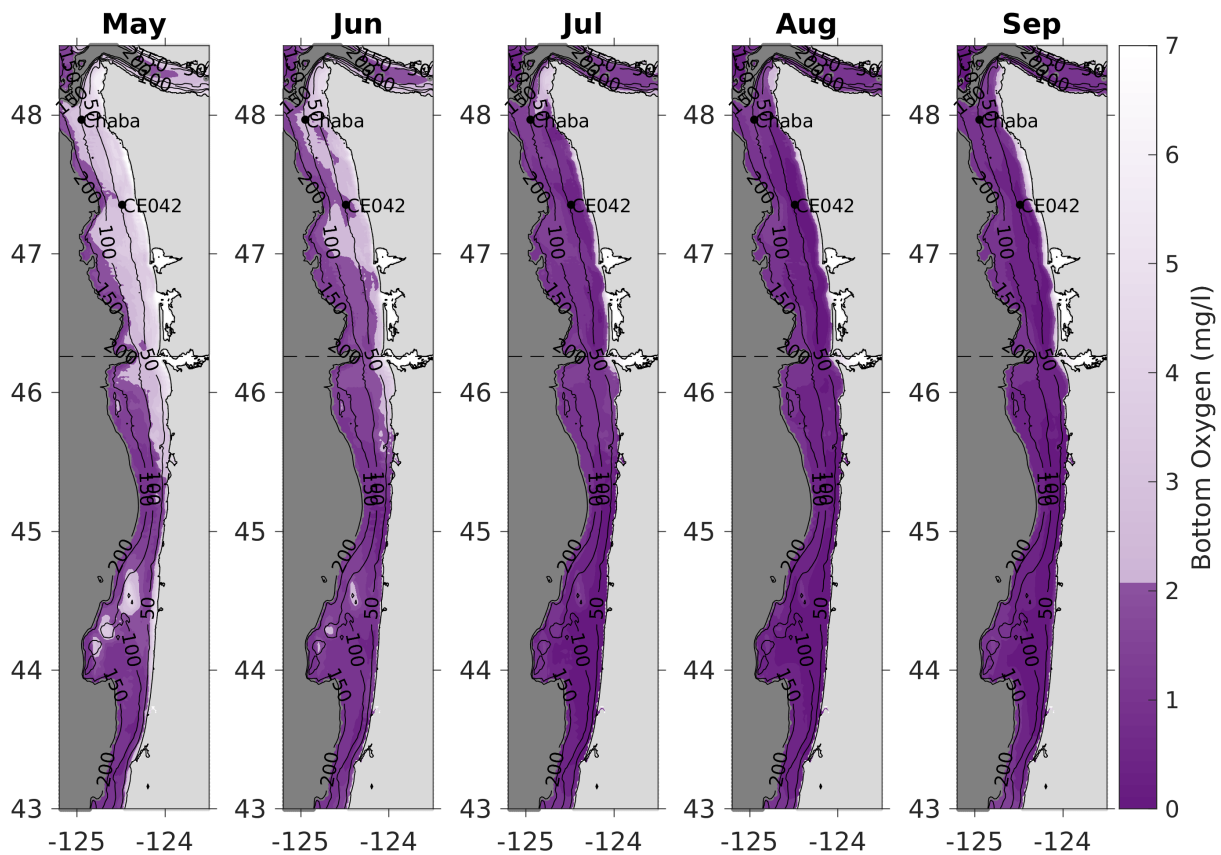


Figure 22. J-SCOPE forecasts of bottom DO (mg/L) for May–Sep 2020, averaged over all 3 ensemble members. Hypoxia ($O_2 < 2$ mg/L) is shown in dark purple, and offshore areas are shaded dark gray. The black horizontal dashed line indicates the boundary between Washington and Oregon waters. Black contours indicate bathymetry on the shelf. J-SCOPE ensemble forecast maps provided by the J-SCOPE team, <http://www.nanoos.org/products/j-scope/forecasts.php>.

The detailed forecasts for temperatures, chlorophyll and sardines can be viewed at the [J-SCOPE website](#).⁸ Additional forecasts for Pacific hake and Dungeness crab will be available in future years, and similar types of seasonal forecasts at the spatial scale of the full California Current are expected in the future as well. By making these forecasts available to PFMC and other partners, we hope to provide useful, skilled forecast information that assists with decision-making prior to the periods at which most productivity and harvest occurs in key fishery sectors.

2.4 Hydrologic Indicators

Freshwater habitat conditions are critical for salmon and other anadromous species, and for estuaries that support many marine species. Indicators are reported based on a hierarchical spatial framework and are summarized by freshwater ecoregion (Figure 4b, as derived from Abell et al. [2008] and [Freshwater Ecoregions of the World](#)⁹) or, where possible, by salmon evolutionarily significant units (ESUs, sensu Waples 1995). Within ecoregions, we summarized data by Chinook salmon ESUs. Status and trends for all freshwater indicators are estimated using space–time models (Lindgren and Rue 2015), which account for temporal and spatial autocorrelation.

The freshwater indicators presented here focus on salmon habitat conditions as related to snowpack, streamflow, and temperature. Snow-water equivalent (SWE) is the total water content in snowpack, which provides a steady source of cool, fresh water that is vital for salmon in the warm summer months (Munsch et al. 2019). Maximum streamflows in winter and spring are important for habitat formation, and in California can be important for removing a polychaete worm that is the obligate host of the salmon parasites *Ceratonova shasta* and *Parvicapsula minibicornis* (Alexander et al. 2014, True et al. 2017); however, extreme discharge relative to historic averages can potentially cause scouring of eggs from salmon redds (DeVries 1997), thereby reducing abundance and productivity (Greene et

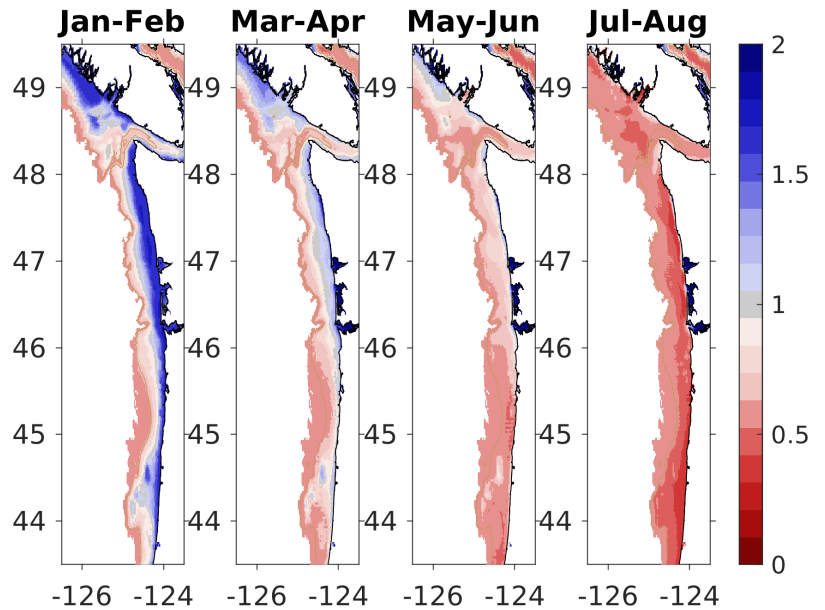


Figure 23. J-SCOPE forecasts of bottom aragonite saturation state (Ω) for Jan–Aug 2020, averaged over all 3 ensemble members. For reference, $\Omega = 1$ is broadly considered the boundary between undersaturated and saturated conditions, but stressful conditions for juvenile oysters begin to occur before the waters become undersaturated ($\Omega \leq 1.3$). The 200-m isobath is outlined by the beige contour line. J-SCOPE ensemble forecast maps provided by the J-SCOPE team.

⁸ <http://www.nanoos.org/products/j-scope/forecasts.php>

⁹ <http://www.feow.org>

al. 2005, Zimmerman et al. 2015). Below-average minimum streamflows in summer and fall can restrict habitat for in-stream juveniles and migrating adults (Bradford and Heinonen 2008), and high summer water temperatures can cause impaired physiology and increased mortality for both juveniles (Marine and Cech 2004, Richter and Kolmes 2005) and returning adults (Jeffries et al. 2012). All freshwater indicators are influenced by climate and weather patterns, and intensifying climate change is expected to exacerbate high temperatures, low SWEs, and extreme flow events.

In 2019, SWE in the two northern ecoregions (Salish Sea/WA Coast and Columbia River Glaciated) declined relative to 2018 (Figure 24), and drought conditions were declared in parts of Washington. In contrast, SWE was average in the Columbia Unglaciaded ecoregion in 2019, and above average for Sacramento/San Joaquin and coastal California and Oregon. All regions have increasing trends over the most recent five years, due to rebounds since the extreme lows of 2015 (Figure 24). Because the official SWE estimate is made on 1 April for each calendar year, SWE for the 2019–20 winter is not represented in Figure 24, which was presented to PFMC in March 2020. However, the updated map in Figure 25 shows that SWE measured on 1 April 2020 varied considerably by ecoregion; stations in much of Washington, northern Idaho, and northern Oregon exceeded the long-term median, whereas stations in California, central and southern Oregon, and much of southern Idaho were at or below the long-term median (Figure 25).

Mean maximum stream temperatures in August were determined from 446 U.S. Geological Survey (USGS) gages with temperature-monitoring capability. While these gages did not necessarily operate simultaneously throughout the period of record, at least two gages provided data each year in all ecoregions. Stream temperature records are limited in

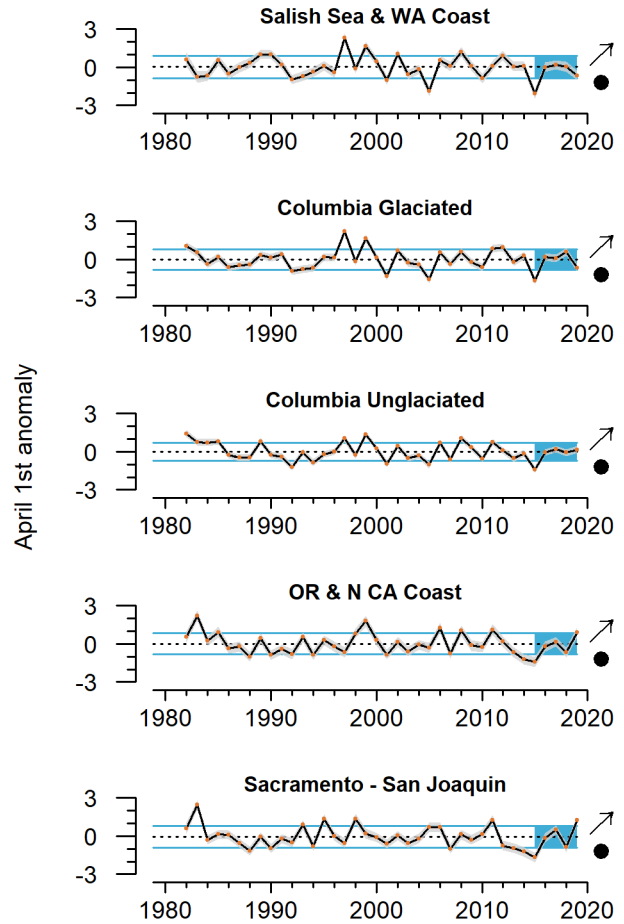


Figure 24. Anomalies of 1 April SWE in 5 CCE freshwater ecoregions through 2019. Ecoregions are mapped in Fig 4b. Error envelopes represent the 2.5% and 97.5% upper and lower credible intervals. Symbols to the right follow those in Fig 3a, but were evaluated based on whether the credible interval overlapped zero (slope of the 5-year trend) or the long-term (5-yr) mean. SWE data derived from the California Department of Water Resources snow survey (<http://cdec.water.ca.gov/>) and the Natural Resources Conservation Service’s SNOTEL sites in WA, OR, CA, and ID (<http://www.wcc.nrcs.usda.gov/snow/>).

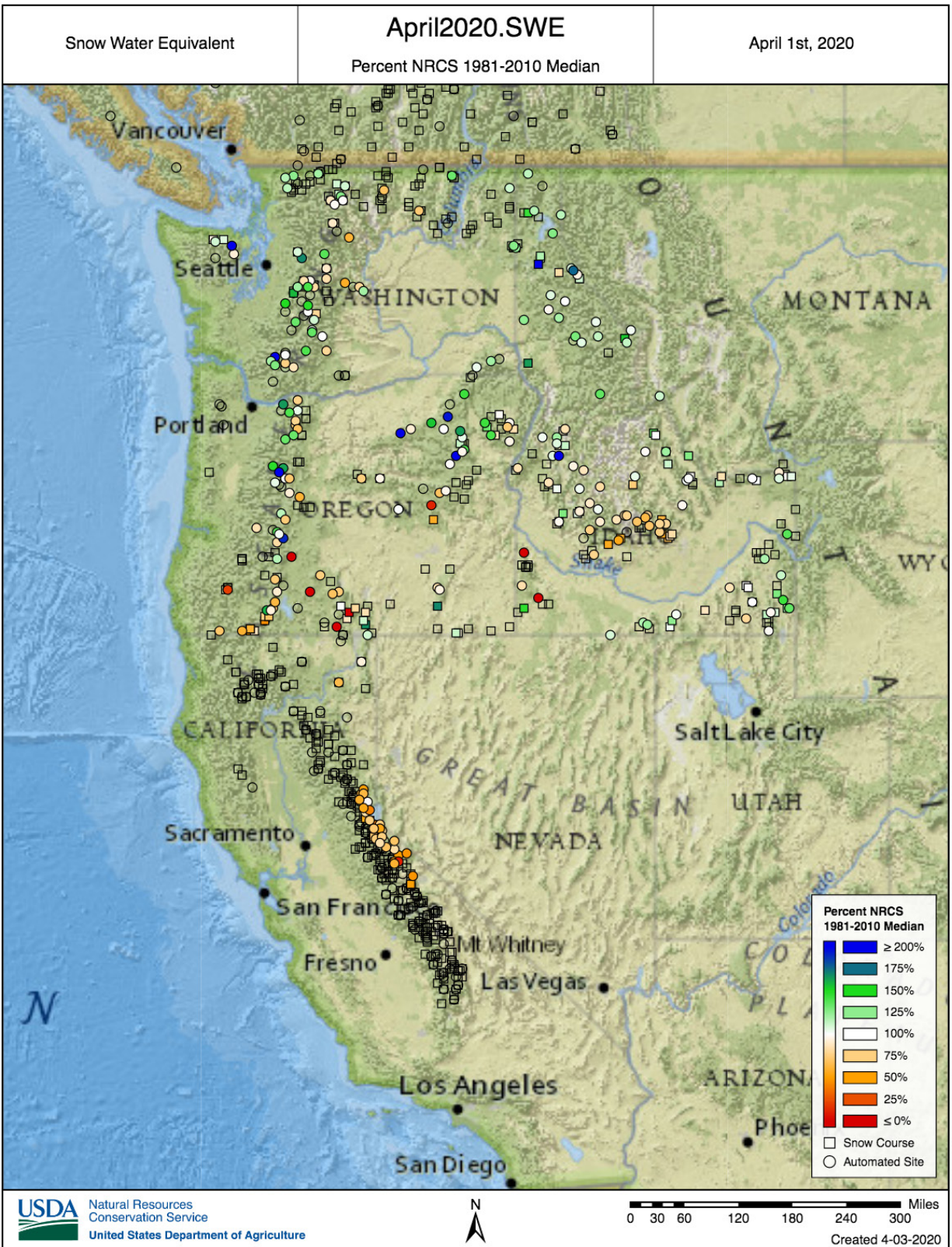


Figure 25. Mountain snowpack on 1 April 2020, at select monitoring sites relative to 1981–2010 median values. Open circles are stations that lack either current data or long-term median data. Snowpack data obtained from interactive map products produced by the Natural Resources Conservation Service (NRCS), presented as SWE percentile compared to period of record (https://www.wcc.nrcs.usda.gov/snow/snow_map.html).

California, so the Sacramento/San Joaquin and Southern California Bight ecoregions were combined. Maximum August stream temperatures continued to exhibit strong ecoregional differences; for example, the Salish Sea/Washington Coast streams were much cooler on average than California streams. The most recent five years have been marked by largely average values in all ecoregions, with the exception of the Salish Sea and Washington Coast, which had much higher temperatures in the last five years compared to the period of record (Figure 26). Recent trends in maximum August stream temperatures have been relatively stable; the recent decline in Sacramento/San Joaquin and Southern California streams is not statistically significant.

Streamflow indicators are derived from active USGS stream gages with records of at least 30 years' duration. We use standardized anomalies of streamflow time series from 213 individual gages. Daily means were used to calculate annual one-day maximum and seven-day minimum flows, corresponding to flow parameters to which salmon populations are most sensitive. Throughout the California Current, both minimum and maximum streamflow anomalies have exhibited variability in the most recent five years. At the ecoregion scale, minimum streamflows were consistent with SWE, exhibiting generally increasing trends since lows in 2015. In particular, minimum flow increased over the past five years for the Columbia Unglaciaded, Oregon/California Coast, and Sacramento/San Joaquin ecoregions (Figure 27). Minimum flow over the past five years in the Southern California Bight has been relatively stable, but was among the lowest on record for the ecoregion over the past several decades.

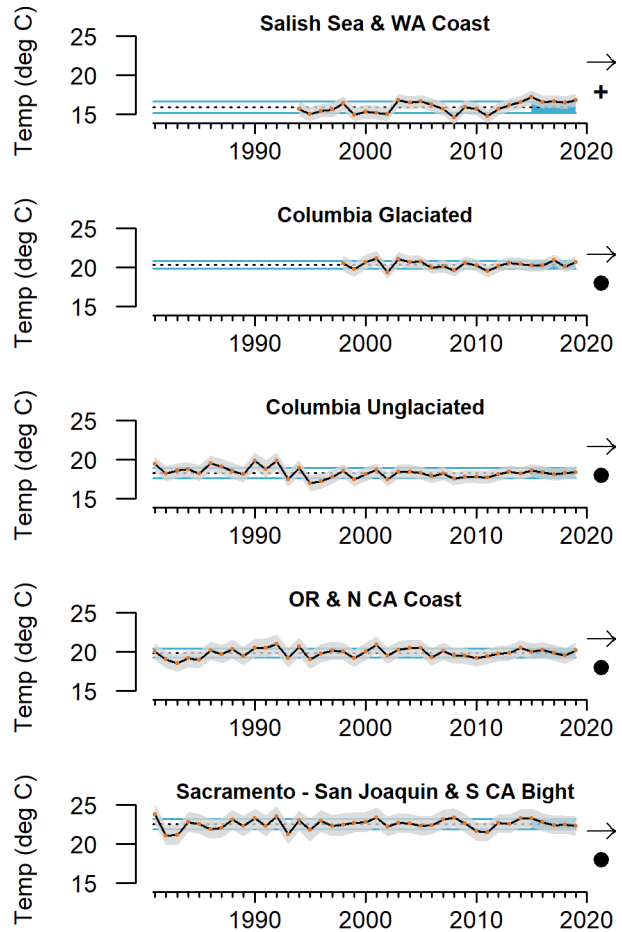


Figure 26. Mean maximum stream temperature in August measured at 466 USGS gages in 6 ecoregions (Sacramento/San Joaquin and Southern California Bight ecoregions combined), 1981–2019. Gages include both regulated (subject to hydropower operations) and unregulated systems, although trends were similar when these systems were examined separately. Error envelopes represent the 2.5% and 97.5% upper and lower credible intervals. Symbols follow those in Fig 3a, but were evaluated based on whether the credible interval overlapped zero (slope of the 5-yr trend) or the long-term (5-year) mean. Stream temperature data provided by the U.S. Geological Survey (<http://waterdata.usgs.gov/nwis/sw>).

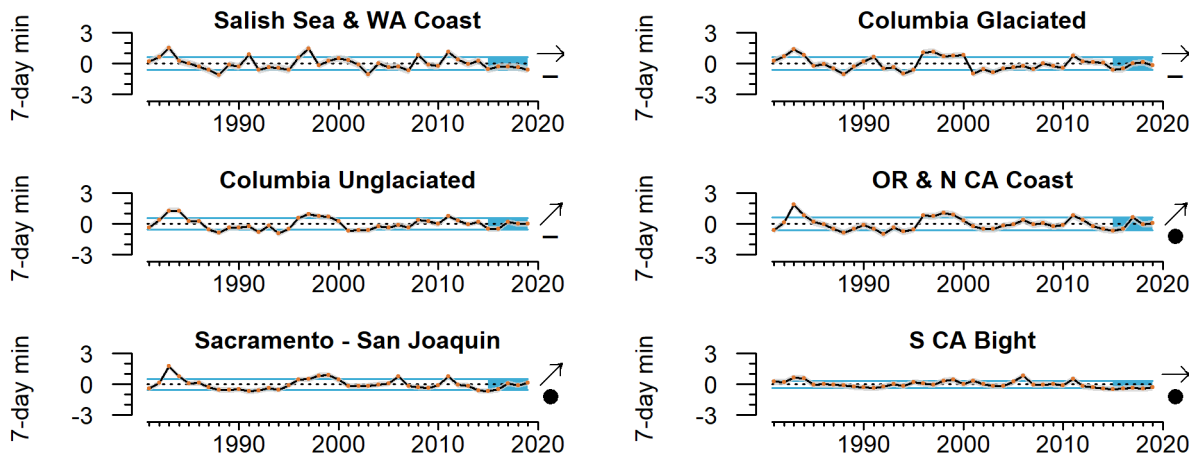


Figure 27. Anomalies of the 7-day minimum streamflow measured at 213 gages in 6 ecoregions, 1981–2019. Gages include both regulated (subject to hydropower operations) and unregulated systems, although trends were similar when these systems were examined separately. Error envelopes represent the 2.5% and 97.5% upper and lower credible intervals. Symbols follow those in Fig 3a, but were evaluated based on whether the credible interval overlapped zero (slope of the 5-yr trend) or the long-term (5-year) mean. Minimum streamflow data provided by USGS.

Because high rates of maximum late-winter flow are generally beneficial for juvenile salmon in inland regions but detrimental to northern coastal populations, flow conditions during egg incubation (after spawning) may have been favorable in recent years across a wide range of the Pacific Coast. The Salish Sea/Washington Coast and Columbia Glaciated ecoregions experienced downturns in maximum flow in 2019, and the Salish Sea/Washington Coast experienced a negative short-term trend (Figure 28). Maximum flow has been trending higher since 2015 in the Southern California Bight, Sacramento/San Joaquin, and Unglaciaded Columbia Basin. The Columbia Glaciated and Oregon/California Coast ecoregions had highly variable 1-day maximum flows from 2015–19, resulting in no clear short-term trend for either ecoregion.

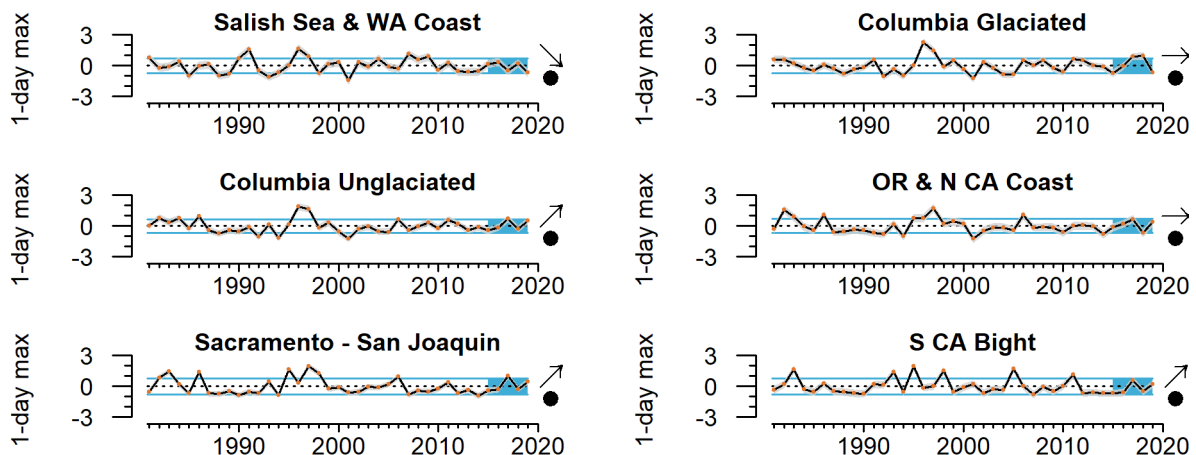


Figure 28. Anomalies of the 1-day maximum streamflow measured at 213 gages in 6 ecoregions, 1981–2019. Gages include both regulated (subject to hydropower operations) and unregulated systems, although trends were similar when these systems were examined separately. Error envelopes represent the 2.5% and 97.5% upper and lower credible intervals. Symbols follow those in Fig 3a, but were evaluated based on whether the credible interval overlapped zero (slope of the 5-yr trend) or the long-term (5-year) mean. Minimum streamflow data provided by USGS.

We also summarized streamflows at the finer scale of individual Chinook salmon ESUs. These results are presented in quad plots, showing flow anomalies and 95% credible intervals to indicate which ESUs had significant trends from 2015–19, or short-term averages that differed from the long-term means. Significance is associated with credible intervals that do not overlap with zero on a given axis; these credible intervals take into account spatial correlations between different gages within a given ESU (S. Munsch, unpublished data). ESUs in Puget Sound, Washington, and Oregon coastal sites and the Lower Columbia experienced decreasing trends in maximum flows since 2015, while other ESUs experienced stable or increasing maximum flows, particularly the Middle Columbia, Snake River, and California Coast ESUs (Figure 29, left). Several ESUs—Klamath/Trinity, Sacramento winter, Central Valley spring, and Upper Columbia spring—had five-year average maximum flows that were greater than long-term averages (Figure 29, left). Because high rates of winter flow are generally beneficial for juvenile salmon in inland regions but detrimental to northern coastal populations, these trends suggest improving flow conditions during egg incubation across much of the CCE. Minimum flows have generally been below-average but increasing since the very low flows of 2015, with the strongest short-term increases in southern and inland ESUs (Figure 29, right). ESUs in the northwest tended to be the furthest below average, including three Columbia Basin ESUs, Puget Sound, and the Washington Coast. Time series summarized in these quad plots can be found in Appendix F of Harvey et al. (2020).

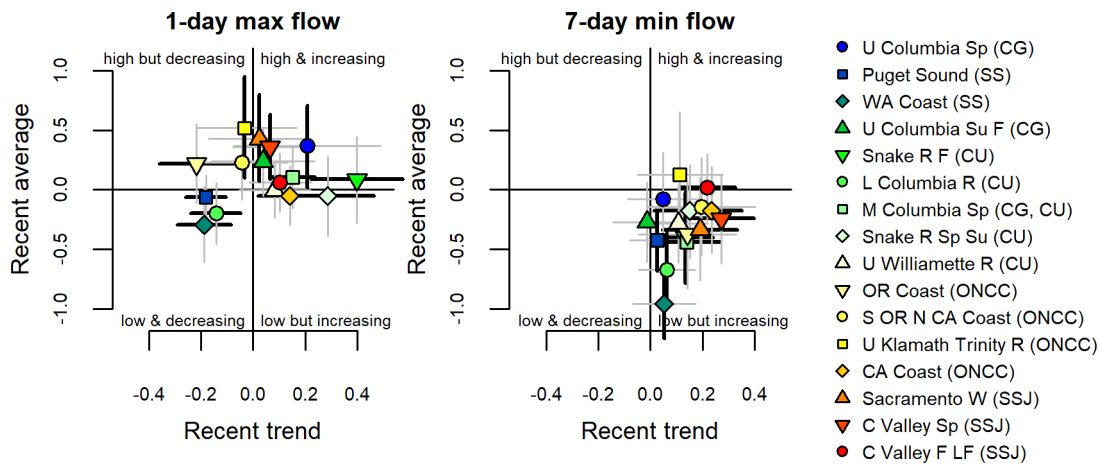


Figure 29. Recent (5-year) trend and average of maximum and minimum streamflow anomalies in 16 freshwater Chinook salmon ESUs in the CCE through 2019. Symbols of ESUs are color-coded from north (blue) to south (red). Error bars represent the 2.5% and 97.5% upper and lower credible intervals. Grey error bars overlap zero, while heavy black error bars differ from zero. Abbreviations in the legend refer to the ESU’s freshwater ecoregion, shown in Fig 4b (CG = Columbia Glaciated; SS = Salish Sea; CU = Columbia Unglaciated; ONCC = OR/NorCal Coastal; SSJ = Sacramento/San Joaquin). Lines and symbols as in Fig 3c. Min and max streamflow data provided by USGS.

3 Focal Components of Ecological Integrity

The CCIEA Team examines many indicators related to the abundance and condition of key species, the dynamics of community structure, and ecological interactions. Many CCE species and processes respond very quickly to changes in ocean and climate drivers, while other responses may lag by many years. These dynamics are challenging to predict. Between 2014 and 2016, many ecological metrics indicated conditions of poor productivity at lower trophic levels and poor foraging conditions for many predators. In 2017–18, there were some signs that indicator species abundance, condition, and composition were returning to more average conditions, although there were many exceptions that implied residual effects of the anomalous warming events. In 2019, ecological indicators implied average to above-average productivity in the Northern and Southern portions of the CCE, but average to below-average conditions in the Central CCE. The marine heatwave that developed in mid-2019 may have affected portions of the system later in the year, but we have relatively little ecological data to demonstrate impacts at this time.

3.1 Northern Copepod Biomass Anomaly

Copepod biomass anomalies represent interannual variation for two groups of copepod taxa: “northern copepods,” which are cold-water species rich in wax esters and fatty acids that appear to be essential for pelagic fishes, and “southern copepods,” which are warm-water species that are smaller and have lower fat content and nutritional quality. In summer, northern copepods usually dominate the coastal zooplankton community observed along the Newport Hydrographic Line (Figures 4a and 4c), while southern copepods dominate during winter. Positive values of northern copepods correlate with stronger returns of Chinook salmon to Bonneville Dam and coho salmon to coastal Oregon (Peterson et al. 2014). El Niño events and positive PDO regimes can promote higher southern copepod biomass (Keister et al. 2011, Fisher et al. 2015).

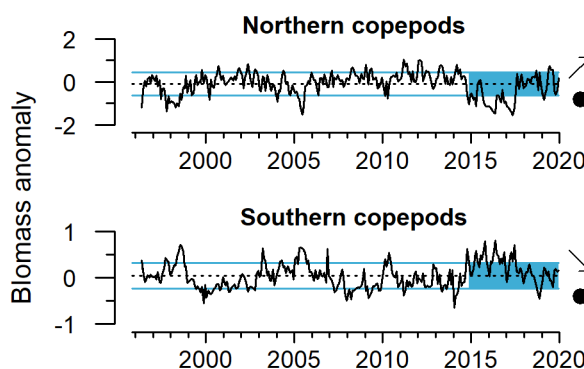


Figure 30. Monthly northern (top) and southern (bottom) copepod biomass anomalies from Newport Hydrographic Line station NH05, 1996–2019. Lines, colors, and symbols as in Fig 3a. Copepod biomass anomaly data provided by J. Fisher, NMFS/NWFSC, OSU.

In 2019, northern copepods continued an overall increasing trend since the extreme lows during the 2014–16 marine heatwave. They were ~1 SD above the mean in spring–summer 2019, but declined by September (Figure 30, top). The spring–summer anomaly was among the highest of the time series, despite weak equatorial El Niño conditions. However, the northern copepods appeared relatively late and declined relatively early, resulting in a short duration of the northern copepod community. Southern copepods were near average for most of 2019, continuing a decline since the heatwave (Figure 30, bottom). The values of these two indicators suggest average to above-average feeding conditions for pelagic fishes off central Oregon in 2019, with the best copepod ratios in the summer.

3.2 Euphausiid Size off of Trinidad Head

Krill are among the most important prey for fishes, mammals, and seabirds in the CCE. Two species of particular importance are *Thysanoessa spinifera* and *Euphausia pacifica*. *E. pacifica* has been sampled multiple times per season off of Trinidad Head (Figures 4a and 4c) since late 2007. Mean length of adult *E. pacifica* is one indicator of krill as a resource for predators. *E. pacifica* length cycles from short individuals in winter that grow into longer individuals by summer. *E. pacifica* lengths were very low during the first half of 2019 (Figure 31), coincident with El Niño conditions during the 2018–19 winter. This marked a decrease relative to 2018, when lengths were generally above-average and consistent with conditions associated with typical seasonal upwelling. Krill lengths had been gradually increasing after poor growth in 2014 at the onset of marine heatwave conditions in the CCE. The 2019 results suggest that krill production in the northern CCE continues to be impacted by ocean forcing, such as recent warming and the weak NPGO.

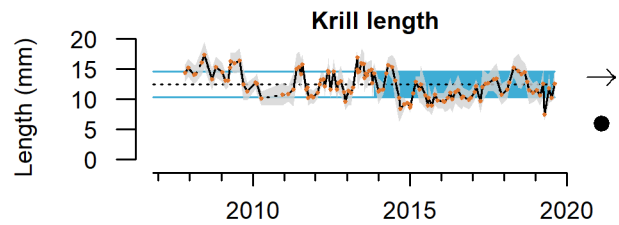


Figure 31. Mean krill carapace length (mm) off of Trinidad Head, CA, 2007–19. Grey shaded envelope indicates ± 1.0 SD. Lines, colors, and symbols as in Fig 3a. Krill data provided by E. Bjorkstedt, NMFS/SWFSC, Humboldt State University (HSU), and R. Robertson, Cooperative Institute for Marine Ecosystems and Climate (CIMEC) at HSU.

3.3 Harmful Algal Blooms

Harmful algal blooms (HABs) of diatoms in the genus *Pseudo-nitzschia* have been of recurring concern along the U.S. West Coast in recent years. Certain species of *Pseudo-nitzschia* produce the toxin domoic acid, which can accumulate in filter feeders and extend through food webs to cause harmful or lethal effects on people, marine mammals, and seabirds (Lefebvre et al. 2002, McCabe et al. 2016). Because domoic acid can cause amnesic shellfish poisoning in humans, fisheries that target shellfish (including razor clam *Siliqua patula*, Dungeness crab *Metacarcinus magister*, rock crab *Cancer* spp., and spiny lobster *Panulirus interruptus*) are closed, or operate under a health advisory in the recreational sector, when concentrations exceed regulatory thresholds for human consumption. Domoic acid regulatory thresholds are currently set by the U.S. Food and Drug Administration (FDA); domoic acid levels ≥ 20 parts per million (ppm) trigger actions for all seafood and tissues except Dungeness crab viscera, for which the level is >30 ppm (California applies this to rock crab viscera as well). We present monthly maximum domoic acid concentrations in razor clams and Dungeness crabs for Washington, Oregon, and California in Figure 32; results are summarized at the individual coastal county level in Appendix E of Harvey et al. (2020).

Extremely toxic HABs of *Pseudo-nitzschia* are influenced by ocean conditions and have been documented in 1991, 1998–99, 2002–03, 2005–06, and 2015–19. In the northern CCE, they have been found to coincide with or closely follow El Niño events or positive PDO regimes

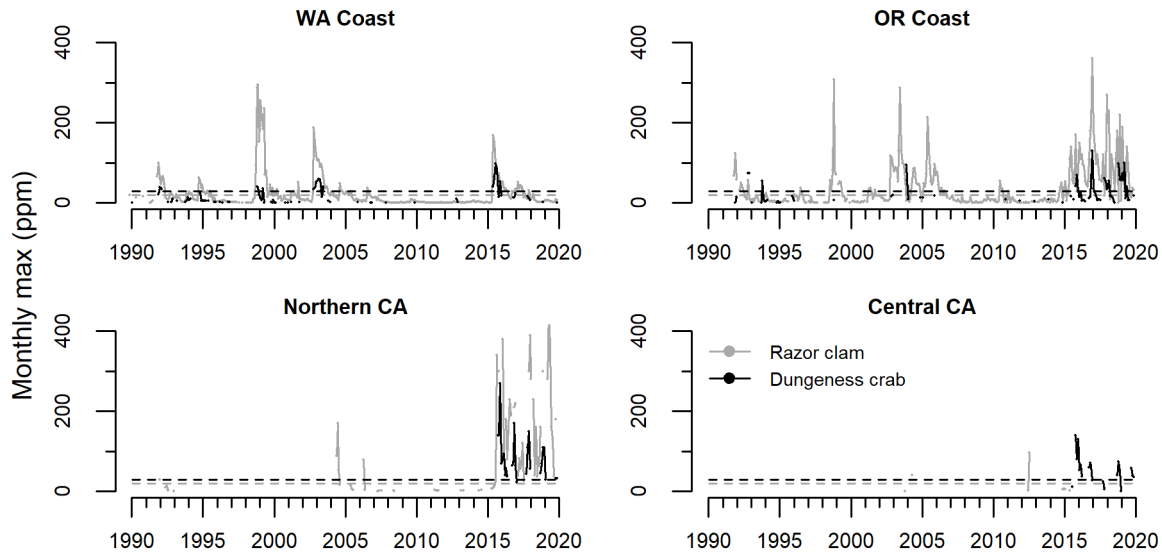


Figure 32. Monthly maximum domoic acid concentration (ppm) in razor clams (gray) and Dungeness crab viscera (black) through 2019 for WA, OR, NorCal (Del Norte to Humboldt counties), and Central CA (Sonoma to San Luis Obispo counties). Horizontal dashed lines are the management thresholds of 20 ppm (clams) and 30 ppm (crab viscera). WA data are provided by the Washington State Department of Health, OR data from the Oregon Department of Agriculture, and CA data from the California Department of Public Health.

and track regional anomalies in southern copepod species (McCabe et al. 2016, McKibben et al. 2017). Fishery closures may result in tens of millions of dollars in lost revenue and a range of sociocultural impacts in coastal economies (Dyson and Huppert 2010, NMFS 2016, Ritzman et al. 2018), and can also cause “spillover” of fishing effort into other fisheries. The largest and most toxic HAB of *Pseudo-nitzschia* ever recorded on the U.S. West Coast occurred in 2015, coincident with the 2013–16 marine heatwave, and caused the longest-lasting and most geographically widespread HAB-related fisheries closures on record (McCabe et al. 2016, Moore et al. 2019).

In 2019, domoic acid concentrations in shellfish varied regionally. There were no domoic acid-related razor clam or Dungeness crab harvest closures in Washington state (Figure 32, top left), where harvest conditions have remained safe since 2018; previous closures occurred most recently in 2015, 2016, and 2017, coincident with the anomalous warming events in the CCE.

In contrast to Washington, domoic acid affected both the timing and spatial extent of Oregon razor clam and Dungeness crab fisheries during 2019. Domoic acid levels in razor clams have consistently exceeded safe levels since 2014 along much of the Southern Oregon coast, especially from Heceta Head south to the California border (Douglas, Coos, and Curry counties; Harvey et al. 2020, Appendix E). As a result, razor clam harvesting in southern Oregon was closed for much of 2019, although this restriction was temporarily lifted during September–October 2019. Elevated domoic acid levels later closed all Oregon razor clam fisheries in December 2019 (Figure 32, upper right). Domoic acid levels in crab tissues also contributed to extended delays in opening the 2018–19 Oregon commercial Dungeness crab fishery in southern Oregon, from Cape Arago to the California border (Figure 32, upper right).

California experienced a similar mosaic of shellfish harvest closures, some of which were driven by HAB dynamics. In northern California, the razor clam fishery remained closed throughout 2019 due to elevated domoic acid levels, extending a closure that began in 2016 (Figure 32, lower left). While domoic acid levels in Dungeness crab from some regions exceeded regulatory thresholds in late 2019 (Figure 32, lower panels), these cleared prior to the opening of the 2019–20 commercial fishery. There were no domoic acid-related closures of spiny lobster or rock crab fisheries in southern California during 2019 (Harvey et al. 2020, Appendix E); however, the northern rock crab fishery is still closed in two areas due to domoic acid concerns (data not shown; see [the CDFW website](#)¹⁰), and these areas have not been open since November 2015.

3.4 Regional Forage Availability

This section describes trends in forage availability, based on spring/summer research cruises that have been conducted independently in three different regions (see Figure 4c) for decades. The species shown below represent a substantial portion of the available forage in the regions sampled by the cruises. *We consider these regional indices of relative forage community composition, availability, and variability, not indices of absolute abundance of coastal pelagic species (CPS).* Absolute abundance estimates should come from PMFC adopted stock assessments (e.g., PFMC 2019) and comprehensive monitoring programs; coastwide scientific monitoring of several federally managed CPS stocks is outlined in [Section 3.5](#).

The three regional surveys that produce forage community indicator data use different methods (e.g., gear selectivity, timing, frequency, and survey objectives); thus, the amplitudes of a given species' time series from a particular region are not necessarily comparable to that species' time series from the other regions. This problem has confounded the CCIEA Team in past reporting because effectively analyzing and communicating the composition and status of a diverse forage assemblage spread across three regions with different sampling methods is difficult. Past approaches have included presenting stacks of standard time series plots grouped by region, or the use of quad plots; however, we have long felt that these placed an undue interpretive burden on readers, and also failed to address the challenge of making informed cross-regional comparisons.

For the last two years we have used an approach that employs two forms of cluster analysis: one part of the analysis groups species that tend to co-occur in each region, and the other part of the analysis groups consecutive years of statistically similar species compositions (see Thompson et al. 2019a). This allows us to identify years in which a region's forage community made a significant transition from one set of species to another. It also allows us to compare regions to see if significant transitions occurred at the same time, which may help us identify if concurrent changes in the rest of the system (climate, oceanography, fisheries, predators, etc.) are related to the forage community. The analysis also includes nonmetric multidimensional scaling (NMDS) to look across all years and identify the key forage species and assemblages in each year for each surveyed region. Analytical methods for this approach are described in Thompson et al. (2019a). Related time series for all three regions can be found in Appendix G of Harvey et al. (2020).

¹⁰ <https://wildlife.ca.gov/Fishing/Ocean/Health-Advisories>

3.4.1 Northern CCE

Forage community data from the Northern CCE come from a NOAA survey off Washington and Oregon in late June (see Figure 4c) called the Juvenile Salmon and Ocean Ecosystem Survey (JSOES). JSOES uses a surface trawl to target juvenile salmon (*Oncorhynchus* spp.); the trawl also catches pelagic fishes, squid, and gelatinous zooplankton (Brodeur et al. 2005, Morgan et al. 2019). Because JSOES is a daytime survey that employs a surface trawl, it is not suitable for effective quantitative monitoring of pelagic species that undergo diel vertical migration (DVM) or that tend to be deeper in the water column. Thus, to avoid sampling bias, we focused on surface-oriented or non-DVM species like salmon, market squid, and gelatinous zooplankton. We excluded data from midwater and DVM species such as sardine, anchovy, whitebait smelt (*Allosmerus elongatus*), jack mackerel (*Trachurus symmetricus*), and Pacific herring (*Clupea pallasii*).

Overall, the cluster analysis (Figure 33, right) shows that the Northern CCE forage assemblage sampled by JSOES has displayed several recent shifts since the onset of the 2013–16 marine heatwave, most recently an increase in juvenile salmon, market squid, and several gelatinous zooplankton in 2018 and continuing into 2019. These trends are depicted by the colors and lines within the grid. The relative abundance of a group over the course of the time series is indicated by color, from very rare (dark blue) to very abundant (dark red) relative to the group's time series mean (white). Horizontal lines separate the community into subgroups that tend to co-occur (e.g., market squid, pompano [*Peprilus simillimus*], water jelly [*Aequorea victoria*], and egg yolk jelly [*Phacellophora camtschatica*] tend to co-occur). Vertical lines indicate years in which a statistically significant shift in forage composition occurred (e.g., from 2017 to 2018; prior shifts occurred following the onset of the marine heatwave, from 2014 to 2015, and in 2017, a year marked by very poor juvenile salmon catches). The dendrograms indicate the hierarchical clustering of co-occurring species groups (dendrogram to left of grid) and of years with statistically similar forage community compositions (dendrogram above the grid), following the methods of Thompson et al. (2019a). Some species (e.g., pompano, water jelly, egg yolk jelly) that were abundant during the previous marine heatwave were less abundant in 2018–19. Catches of market squid have shown an increasing trend in the last five years through 2019, the highest year on record (Appendix G, Harvey et al. 2020). Juvenile salmon catches in the same period have been variable, with 2017 catches declining to among the lowest observed since the late 1990s. Most recently in 2019, catches of juvenile Chinook, coho, and sockeye salmon (*Oncorhynchus nerka*) were close to average, whereas chum salmon (*O. keta*) catches were above average and contributed to a positive five-year trend. Catches of *Chrysaora fuscescens* jellyfish (sea nettles) have increased since 2015 following the onset of the marine heatwave, and are near average values. In contrast, catches of pompano, egg yolk jelly, and water jelly, all of which peaked in 2015 and 2016, have declined.

On the left of Figure 33, an NMDS plot arranges individual years along two standardized multivariate axes that represent significant tendencies in community composition (as described in Thompson et al. 2019a). Years with similar community compositions tend to occur close to one another on the plot. The names of species appear on the plot as well, with their positions indicating their loadings on the two NMDS axes. The forage community sampled by the JSOES cruise in 2019 appears in the upper left quadrant in roughly the same area as the community

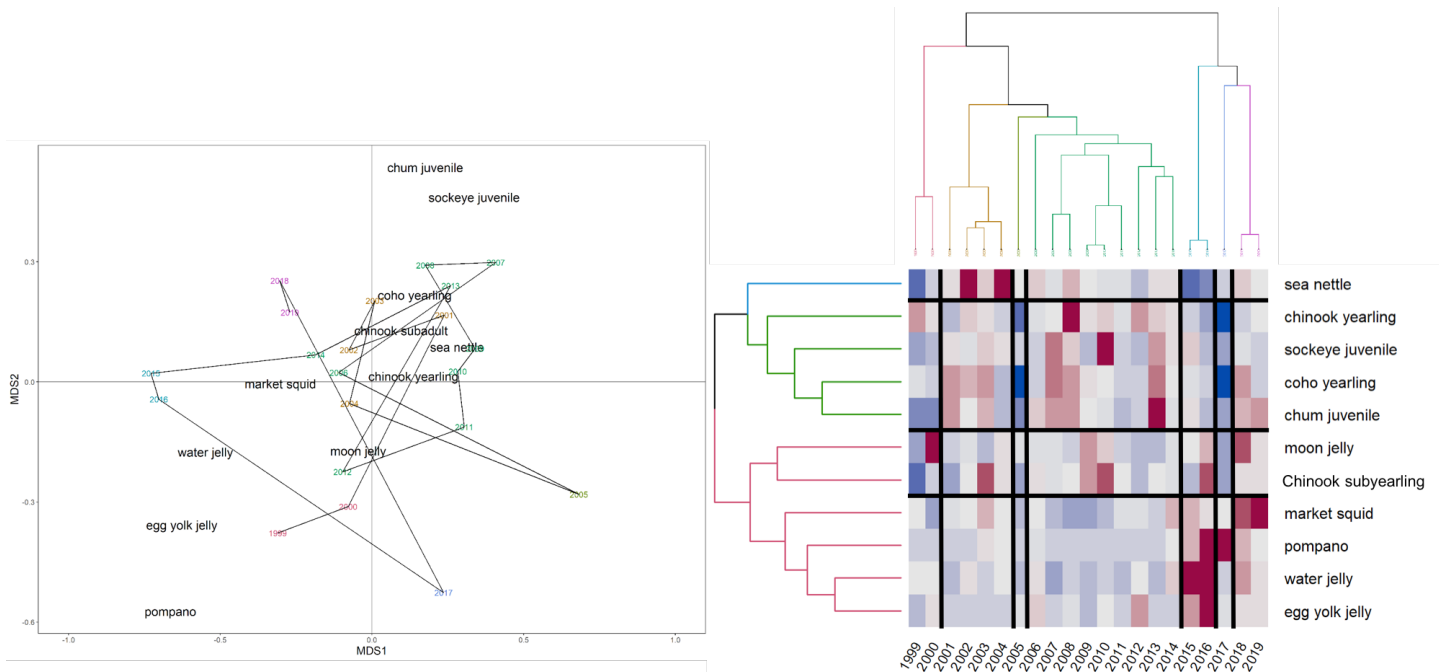


Figure 33. Multivariate analyses of forage dynamics in the Northern CCE through 2019. The plot on the left depicts NMDS results, with years color-coded to correspond with the horizontal chronological clustering branches on the top right. In the center, the dendrogram with horizontal lines indicates clusters of typically co-occurring species; vertical lines indicate temporal shifts in community structure. The heat map on the right is colored based on the Z-score for each taxon, with colors indicating relative abundance (red = abundant, blue = rare). Horizontal bars indicate clusters of typically co-occurring species, dark vertical bars demarcate deep breaks in assemblage structure between years. Pelagic forage data from the Northern CCE provided by B. Burke, NMFS/NWFSC, and C. Morgan, NMFS/NWFSC, OSU. Data derived from surface trawls taken in June during the NWFSC Juvenile Salmon and Ocean Ecosystem Survey (JSOES; <https://www.nwfsc.noaa.gov/research/divisions/fe/estuarine/oeip/kb-juvenile-salmon-sampling.cfm>).

from 2018 (both of which had high catches of market squid and moderate-to-high catches of at least one type of yearling salmon). The location of the 2018 and 2019 data differed dramatically from the 2017 point, which was influenced primarily by very low catches of salmon.

Some prominent forage species like anchovy, sardine, herring, and mackerel are caught by this survey, but not very efficiently, because they tend to be deeper in the water column during daylight hours, and thus are not reported as catch-per-unit-effort (CPUE). However, researchers have tracked the proportion of hauls in which at least one individual of a given species is captured in order to get a general sense of their prevalence. In 2018–19, the prevalence data reflect a community composed of juvenile salmon and market squid, and relatively frequent occurrence of herring, while warmer-water species like mackerel and water jellies declined relative to 2015–17 (see Thompson et al. 2019b, their Figure 29).

Finally, limited krill data are available for the Northern CCE from a related survey (Brodeur et al. 2019), which has been operating since 2011 as a northern extension of the forage sampling in the Central CCE, described in the next section. This survey covers offshore waters from approximately Willapa Bay, Washington to the Oregon/California border, and

krill are sampled at night in the upper ~40 m of the water column. In 2019, estimated krill densities within the survey area were ~400 individuals per tow (Figure 34). Adult krill catches within the survey areas have been low since 2015, following the onset of coastal impacts of the 2013–16 marine heatwave. Densities prior to that were several orders of magnitude higher than at present. It is possible that krill were present in this area but perhaps at different depths or locations than those sampled by this survey. For example, the JSOES survey did observe krill in daytime surface trawls in June 2019, and large numbers of krill eggs and various larval stages were captured during the marine heatwave years (data not shown). Thus, krill may have been present in the Northern CCE over the past several years, but distributed in a manner that made them less accessible to many consumers.

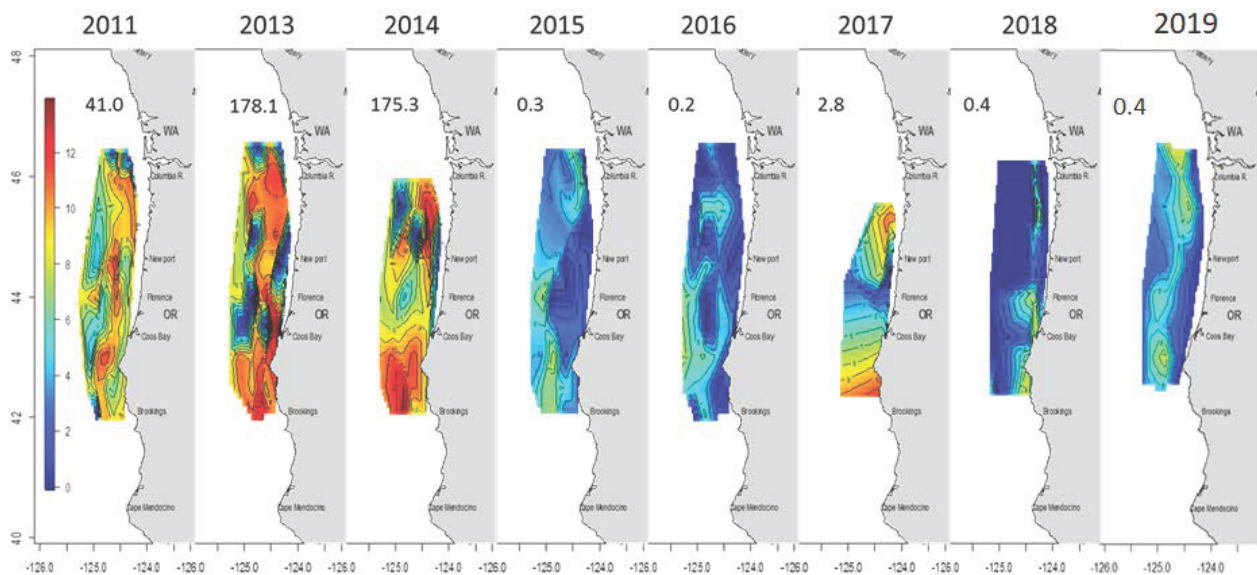


Figure 34. Spatiotemporal distributions of krill off of OR and WA, May–Jun 2011–19 (no data from 2012). Colors represent CPUE ($\times 10^3$) of krill per standardized tow. Data provided by R. Brodeur, NMFS/NWFSC.

3.4.2 Central CCE

Forage data for the Central CCE are from the “core area” of the NOAA Juvenile Rockfish Recruitment and Ecosystem Assessment Survey (JRREAS; see Figure 4c), a springtime midwater trawl survey that targets pelagic young-of-the-year (YOY) rockfishes (*Sebastes* spp.), but also samples other YOY and adult forage species, market squid, adult krill, and gelatinous zooplankton (Sakuma et al. 2016).

The composition of the 2019 Central CCE forage assemblage was similar to that of 2018, driven primarily by large catches of adult anchovy. In 2019, adult anchovy catches strongly increased for a second straight year and were higher than in any previous year on record (Figure 35, right; Harvey et al. 2020, Appendix G). Adult sardine catches in 2019 were higher than they had been in a decade. Market squid remained abundant, as did several types of myctophids, notably blue lanternfish (*Tarletonbeania crenularis*). The Central CCE assemblage in 2018–19 represented a significant temporal shift from the assemblage in 2013–17, when juvenile rockfish, hake, and flatfish were abundant (Figure 35, right). Catches of these taxa declined to low abundances in the past two years.

In the NMDS plot for the Central CCE forage community, the 2019 data grouped in the lower left quadrant, previously most closely associated with 1998 and 1999 (Figure 35, left). The two groups with the strongest loadings in this quadrant were adult anchovy and adult sardine, both of which were abundant in 2019 catches relative to the long-term averages of their respective time series (Harvey et al. 2020, Appendix G).

There were other noteworthy findings from JRREAS (data not shown). Krill catches were among the lowest of the time series (Harvey et al. 2020, Appendix G). These catches, coupled with the relatively small size of krill observed off of Trinidad Head in 2019 (Figure 31) and the poor catches observed off of Oregon (Figure 34), represent potential constraints for the pelagic food web in 2019. Catches of *Aurelia* and *Chrysaora fuscescens* jellyfish were near time series averages, and were lower than the dramatic catches in 2018 (Harvey et al. 2020, Appendix G).

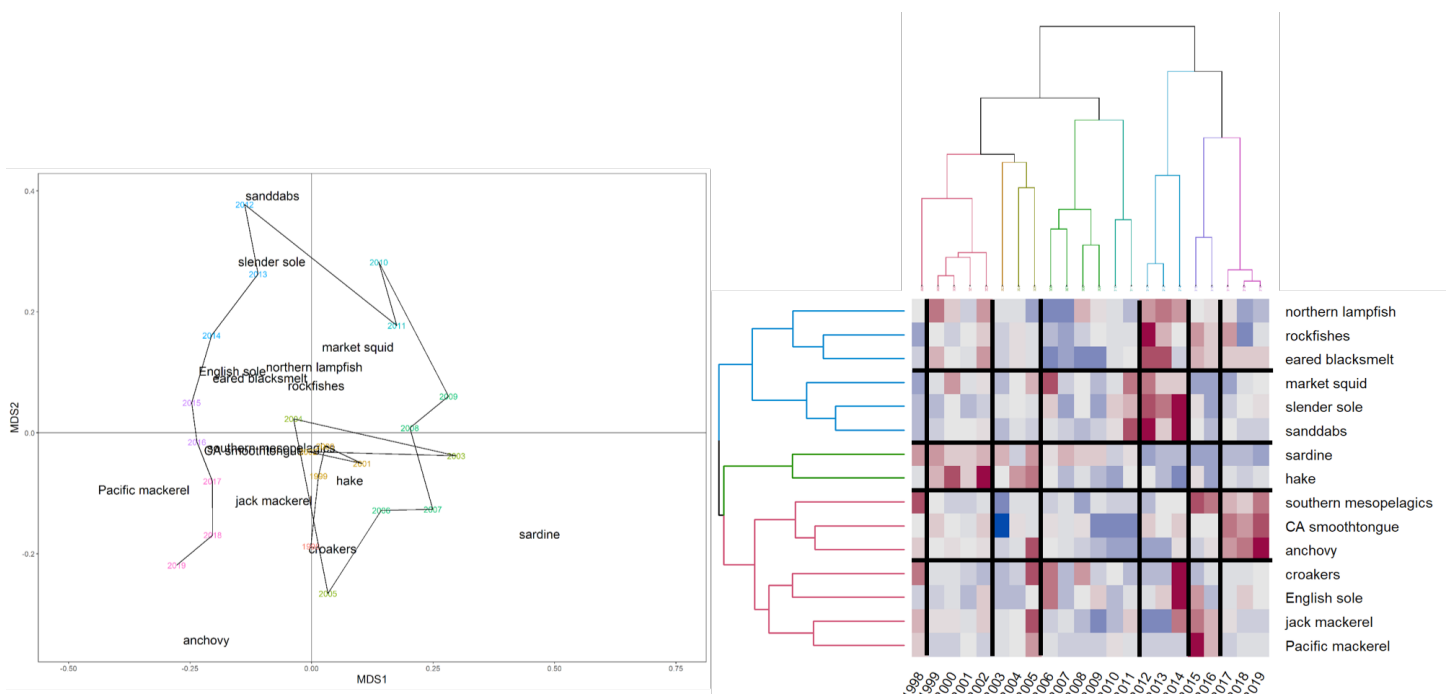


Figure 35. Multivariate analyses of forage dynamics in the Central CCE through 2019. The plot on the left depicts NMDS results, with years color-coded to correspond with the horizontal chronological clustering branches on the top right. In the center, the dendrogram with horizontal lines indicates clusters of typically co-occurring species; vertical lines indicate temporal shifts in community structure. The heatmap on the right is colored based on the Z-score for each taxon, with colors indicating relative abundance (red = abundant, blue = rare). Horizontal bars indicate clusters of typically co-occurring species, dark vertical bars demarcate deep breaks in assemblage structure between years. Pelagic forage data from the Central CCE provided by J. Field and K. Sakuma, NMFS/SWFSC, from the SWFSC Juvenile Rockfish Recruitment and Ecosystem Assessment Survey (<https://go.usa.gov/xGMfR>).

3.4.3 Southern CCE

Forage indicators for the Southern CCE come from CalCOFI larval fish surveys conducted in the spring across all core stations of the CalCOFI survey (see Figure 4c), using oblique vertical tows of fine mesh Bongo nets to 212-m depth (McClatchie 2014). The survey collects a variety of fish larvae and invertebrate paralarvae (<5 days old) from several taxonomic and functional groups. Larval biomass is assumed to correlate with regional abundance of parent stocks.

The southern forage assemblage has experienced six substantial shifts from 1998–2019, including shifts coinciding with the onset of the warm anomalies (post-2014) and the relaxation of the warm anomalies (post-2016; Figure 36, right). Since 2017, the community has been characterized by abundant larval anchovy, California smoothtongue (*Leuroglossus stilbius*), and warm-water mesopelagic fishes. Larval anchovy abundance was the greatest in the history of the CalCOFI time series (Harvey et al. 2020, Appendix G). Larvae of species such as rockfish and mackerel, abundant prior to 2017, were less common and showed low or declining catches over the past five years; other commercially important species (e.g., market squid) show increasing catches since 2014, while larval sardine have been relatively rare since 2010.

The Southern CCE larval forage community in 2019 grouped in the lower left quadrant of the NMDS plot along with data from 2017 and 2018, continuing a progressive shift in composition with a trajectory toward larval anchovy (Figure 36, left).

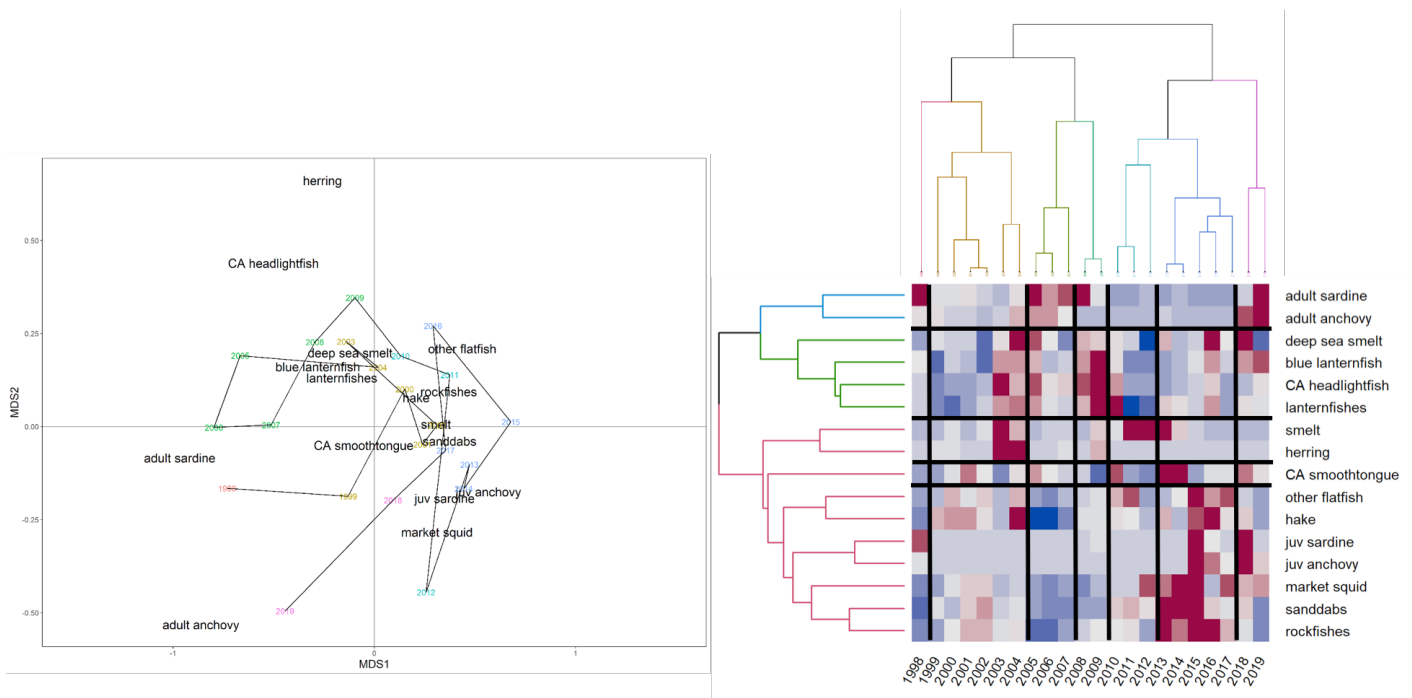


Figure 36. Cluster analysis of key forage species in the Southern CCE through 2019. The plot on the left depicts NMDS results, with years color-coded to correspond with the horizontal chronological clustering branches on the top right. In the center, the dendrogram with horizontal lines indicates clusters of typically co-occurring species; vertical lines indicate temporal shifts in community structure. The heat map on the right is colored based on the Z-score for each taxon, with colors indicating relative abundance (red = abundant, blue = rare). Horizontal bars indicate clusters of typically co-occurring species, dark vertical bars demarcate deep breaks in assemblage structure between years. Pelagic forage data from the Southern CCE provided by A. Thompson, NMFS/SWFSC, derived from spring CalCOFI surveys.

3.4.4 Pyrosomes

Pyrosomes (*Pyrosoma atlanticum*) are pelagic tunicates known to have a subtropical distribution, and historically have been occasionally observed in Southern and Central California waters of the CCE; over the past several years they have been far more abundant, and the increase has been attributed to the 2014–16 marine heatwave, when anomalously warm ocean conditions may have favored pyrosome feeding and reproduction. Pyrosomes are aggregate filter feeders that consume pico- and microplankton, and in some areas have been shown to cause the depletion of chlorophyll-*a* standing stocks. Mass occurrences of pelagic tunicates have impacts on human activities, damaging fishing nets and clogging cooling-water intakes of coastal hydropower facilities.

Recent work by Miller et al. (2019) examined the spatial distribution, abundance, and size variability of pyrosomes in the CCE. Pyrosome abundance was significantly greater in 2012–19 than in 1983–2001, and the recent persistent abundance peaks were unprecedented. Relative biomass trends showed abundance in the CCE shifting from south to north from 2013 to 2018, while in 2019 abundance was vastly reduced north of Cape Mendocino and predominantly located in the Central CCE (Figure 37). In 2014–15, pyrosome biomass was concentrated mostly off of California, but spread north in 2016. In 2017 and 2018, pyrosome biomass was greatest off of Washington and Oregon, and the mean latitude of coastwide

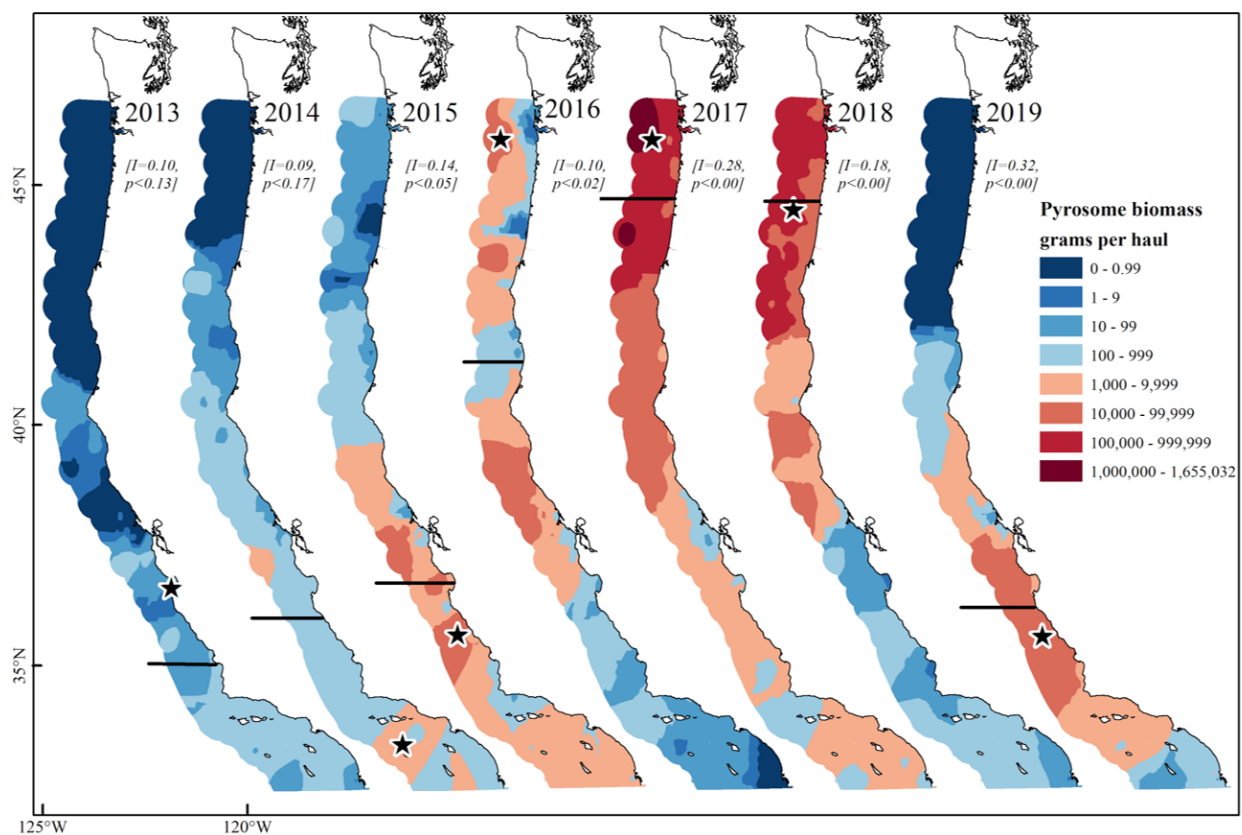


Figure 37. *Pyrosoma atlanticum* biomass (grams of wet weight per haul) during May–Jun in the CCE, 2013–19. Solid lines represent the latitudes at which the coastwide biomass means occurred for each year. The star represents the station with that year's maximum catch. The Moran's I and p-values are presented for each year. Moran's I suggests spatial clustering (0 to 1), spatial randomness (0), or spatial dispersion (–1 to 0). Sampling methods in all regions were consistent with the JRREAS survey described in Section 3.4.2; map reproduced from Miller et al. (2019), Fig 8.

pyrosome biomass was off of Central Oregon. In contrast, pyrosome biomass south of San Francisco Bay in 2018 was orders of magnitude lower than in 2017. However, in 2019 the pyrosome distribution shifted dramatically to the south: a single pyrosome was caught in NOAA surveys off of Oregon and Washington, while pyrosome biomass was again high in the Central California region, reaching levels similar to or greater than in 2015.

3.5 Coastal Pelagic Species

Acoustic surveys have been used in most years since 2006 to map the distribution and estimate the abundances of coastal pelagic fish species (CPS) in the coastal region from Vancouver Island, Canada, to San Diego, California (e.g., Demer et al. 2012, Zwolinski et al. 2012, Stierhoff et al. 2020). Surveys cover waters out to at least the 1,000-fathom isobath, or 65 km from shore. The five most abundant CPS comprising the forage fish assemblage in this domain include northern anchovy, Pacific herring, Pacific sardine, jack mackerel, and Pacific mackerel (*Scomber japonicus*). The acoustic–trawl method combines data from echosounders, which record CPS echoes, and trawls, which produce information about these fish species and size compositions contributing to the CPS echoes.

Results from the summer 2019 CPS survey documented a continued increase in total forage fish biomass in the CCE since 2016. Northern anchovy made up the largest relative proportion of the 2018 and 2019 biomass (Figure 38) and dominated the acoustic proportion of CPS samples from the U.S.–Mexico Border to Bodega Bay in both years (Figure 39). Jack mackerel represented the second-largest biomass proportion, dominating samples from Bodega Bay to the Washington–Oregon border. Pacific herring were the third-largest biomass proportion, dominating from the Washington–Oregon border northward to Vancouver Island.

During summer 2019, Pacific sardines and Pacific mackerel, the two species whose population sizes and demographics are estimated via stock assessments, represented a relatively small proportion of CPS in trawl clusters (Figure 39) and made up a small proportion of the cumulative CPS biomass (Figure 38, bottom). The northern stock of Pacific sardine had an estimated biomass of approximately 33,000 mt, approximately the same as it has been since 2014 (Figure 38, top). Prior to 2014, Pacific sardine had dominated the CPS fish assemblage (Figure 38). During the transition period from sardine dominance in 2013 to anchovy dominance in 2018, while the U.S. Pacific sardine fishery was closed, NOAA recognized an unusual mortality event for California sea lions, and multiple species of seabirds experienced reproductive failures (e.g., McClatchie et al. 2016, Thompson et al. 2019b).

These acoustic–trawl survey results are generally consistent with the results of the regional forage surveys in [Section 3.4](#). The acoustic–trawl survey and the forage surveys demonstrate very high abundance of anchovy in the Central and Southern CCE (Figures 35, 36, 38, and 39). Also, the acoustic–trawl survey found that sardine declined from 2006 to 2013, and then, despite the marine heatwave of 2013–16, sardine recruitment remained low even though sardine productivity is often associated with warmer conditions in the CCE. Consistently, sardine larval CPUE from the Southern CCE has been low since 2010 (Figure 36), with similar values to those observed during the low sardine abundance of the late 1980s. In contrast, the JRREAS cruise results for spring 2019 indicated an increase in adult sardine catches (Figure 35), while the acoustic–trawl survey from summer 2019 did

not indicate an increase in abundance for the northern stock of Pacific sardine (Figure 38). One possible explanation for this difference is that the northern stock of sardines was more evenly distributed in 2019 (Stierhoff et al. 2020), which may mean more were present in the JRREAS sampling domain in 2019 than in other recent years, giving the impression of a local increase in abundance despite overall low and stable abundance of the stock.

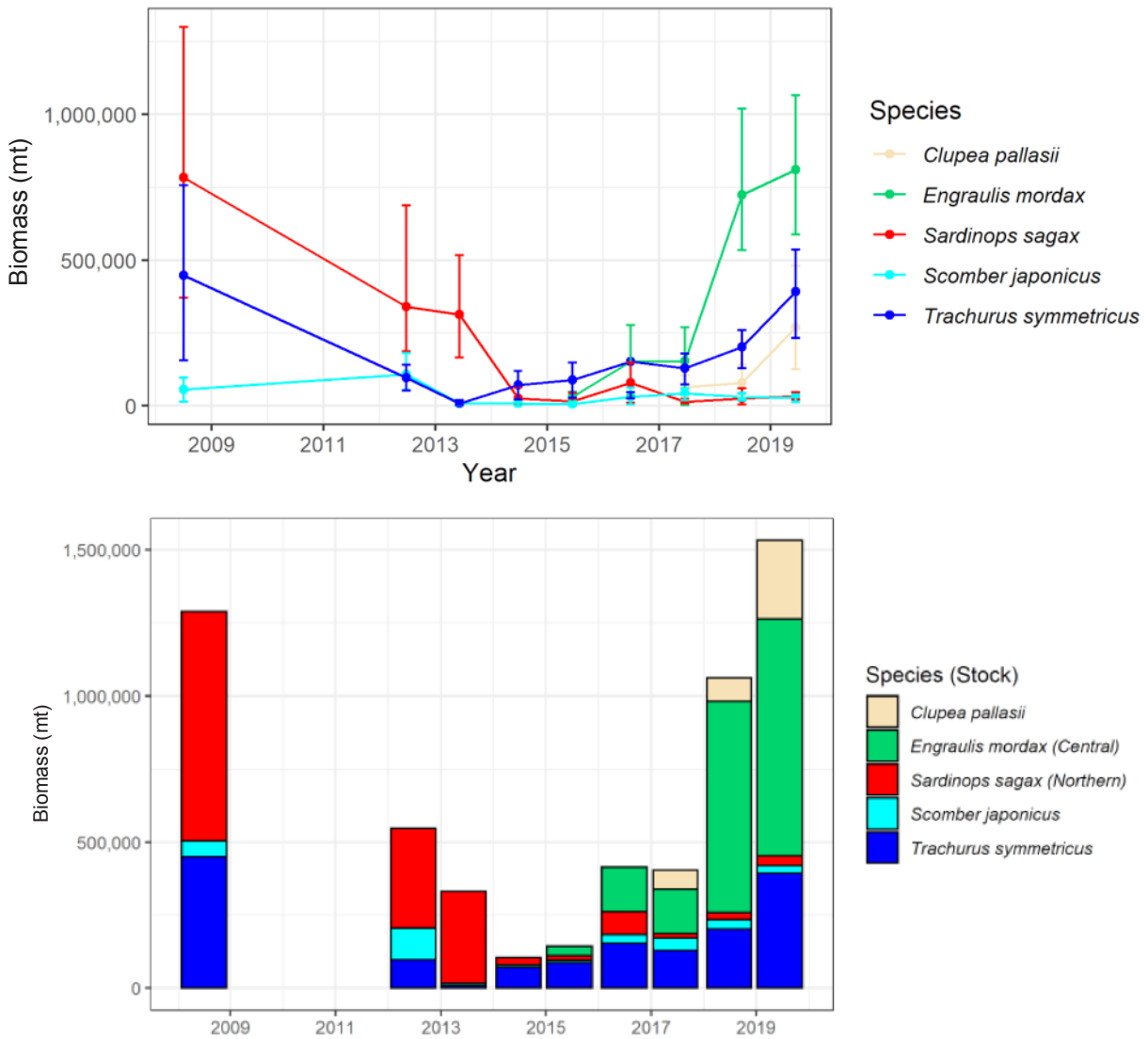


Figure 38. Estimated (top) and cumulative (bottom) biomasses (mt) of the 5 most abundant coastal pelagic fish species (CPS) in the CCE, 2008 and 2012–19, based on coastwide summer acoustic-trawl surveys; summer surveys were not conducted in 2009–11 (cf. Stierhoff et al. 2020, Figs 28 and 29). Error bars are 95% confidence intervals. Biomasses of northern anchovy prior to 2015 and of Pacific herring prior to 2017 are not reported. CPS data and plots provided by K. Stierhoff and D. Demer, NMFS/SWFSC, and J. Zwolinski, NMFS/SWFSC, UCSC.

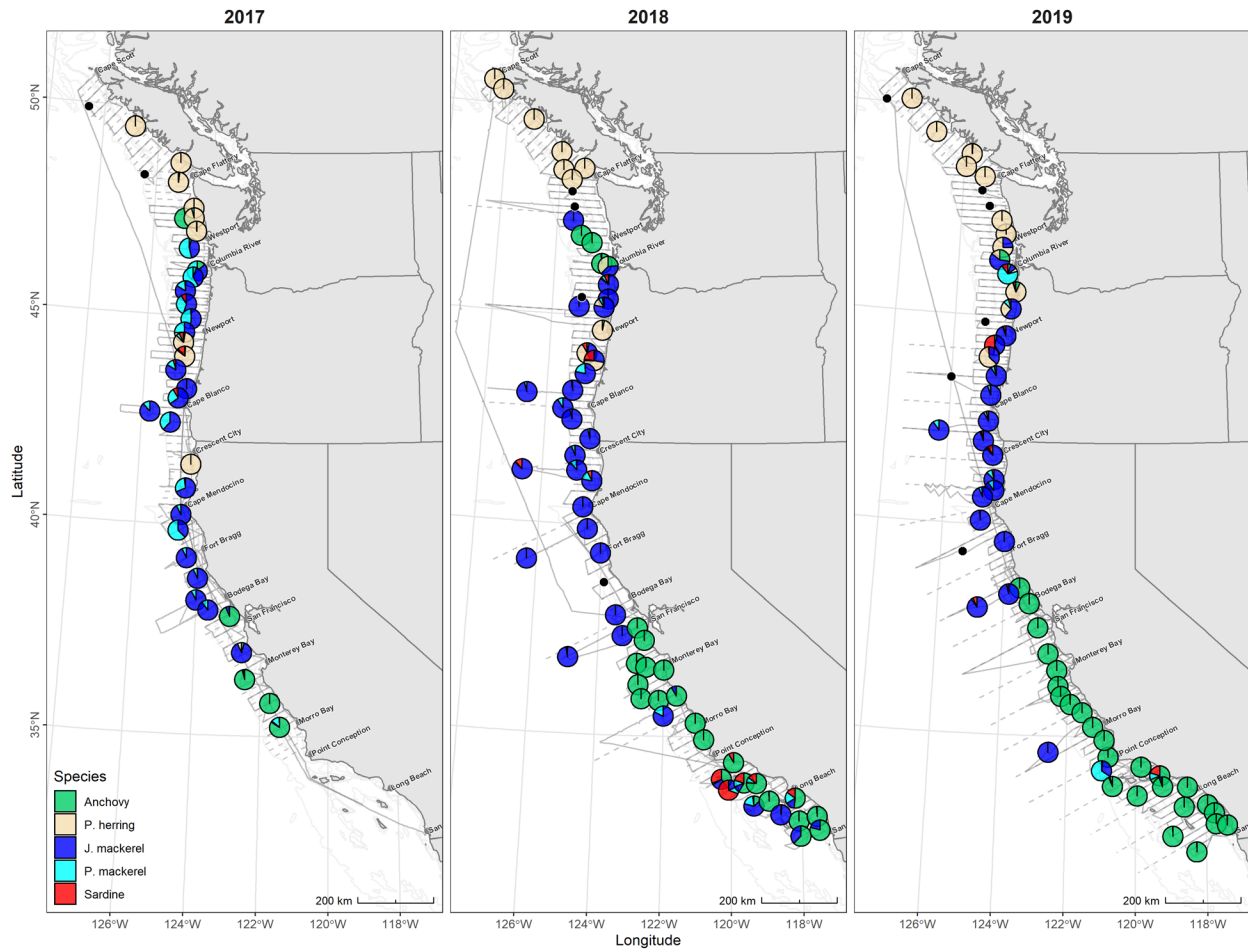


Figure 39. Acoustic proportions of coastal pelagic fish species (CPS) in trawl clusters during 2017 (adapted from Zwolinski et al. 2019, Fig 13b), 2018 (from Stierhoff et al. 2019, Fig 11b), and 2019 (from Stierhoff et al. 2020, Fig 9b). Black points indicate trawl clusters with no CPS. Dashed lines were planned acoustic transects, solid lines are the vessel track. CPS data and plots provided by K. Stierhoff and D. Demer, NMFS/SWFSC, and J. Zwolinski, NMFS/SWFSC, UCSC.

3.6 Salmon

For indicators of the abundance and reproductive potential of naturally spawning Chinook salmon populations, we compare the trends in spawning escapement throughout the CCE to evaluate the coherence in production dynamics, and also to get a more complete perspective of their status across the greater portion of their range. When available, we use escapement time series back to the 1970s; however, some populations have shorter time series (for example, Central Valley spring starts in 1995 and Central Valley winter starts in 2001; Coastal California data began in 1991 but have not been updated since 2015 and thus will no longer be included in our analyses). We summarize escapement trends in quad plots (see Figure 3); time series are available in Harvey et al. (2020), Appendix H. Trends are evaluated for the most recent ten-year period in order to capture population dynamics across multiple generations, given the spatial segregation of successive year classes of salmon.

Most Chinook salmon escapement data are updated through 2018. Across the CCE, average escapements over the last decade were mostly within 1 SD of long-term averages (Figure 40, y-axis), while trends over the last decade were more variable by region (Figure 40, x-axis). In California, average escapements of Chinook salmon ESUs over the last decade were within 1 SD of long-term means, though 2018 escapements were among the lowest on record in several ESUs, particularly in the Central Valley (see Harvey et al. 2020, Appendix H). California ESUs had neutral trends over the last decade, though some sharp declines occurred ~5 years ago (Harvey et al. 2020, Appendix H). In the Northwest, most mean escapements in the past decade were within 1 SD of average; the exception was above-average Snake River fall Chinook salmon escapements, due to relatively large escapements in 2009–16 relative to the time series that began in the mid-1970s (Harvey et al. 2020, Appendix H). Escapement trends for Northwest stocks over the past decade were mostly neutral, but Willamette spring Chinook salmon had a positive trend while Snake River spring–summer Chinook salmon had a negative trend.

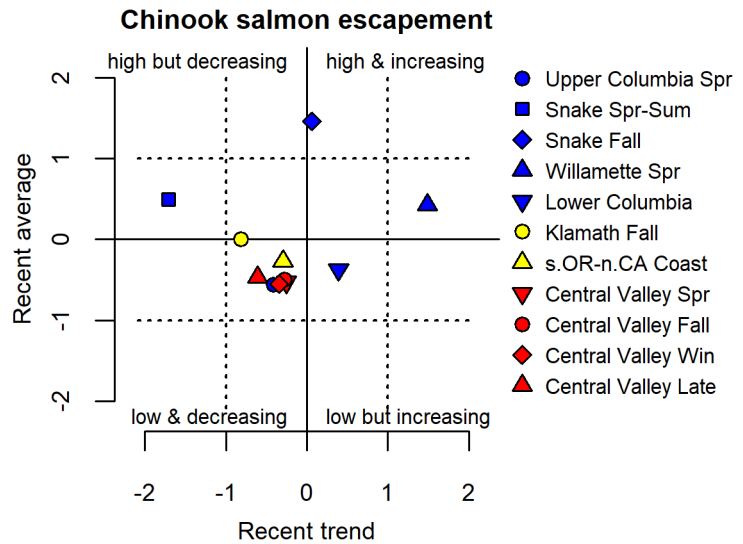


Figure 40. Recent (10-yr) trend and average of Chinook salmon escapement, with most systems updated through 2018. *Recent trend* indicates the escapement trend from 2008–18. *Recent average* is mean natural escapement (includes hatchery strays) from 2008–18. Lines and symbols as in Fig 3c. Chinook salmon escapement data derived from the [California Department of Fish and Wildlife](#),* [PFMC preseason reports](#),[†] and [NWFSC's Salmon Population Summary database](#),[‡] with data provided directly from the Nez Perce Tribe, the Yakama Nation Tribe, and from Streamnet's Coordinated Assessments database (cax.streamnet.org; see website for a list of all participating data-compiling agencies).

* <https://www.dfg.ca.gov/fish/Resources/Chinook/CValleyAssessment.asp>

† <https://www.pcouncil.org/safe-documents-3/>

‡ <https://www.webapps.nwfsc.noaa.gov/sps>

We also evaluate time series of juvenile salmon catches from a NOAA survey conducted in the Northern CCE in ocean waters off Oregon and Washington (see Figure 4c). This is also the survey that generated the forage assembly data for the Northern CCE shown in Figure 33. Annual catches of juvenile coho and Chinook salmon from surveys during June in this region can serve as indicators of salmon survival during their first few weeks at sea, which is a critical window for the productivity of salmon populations (e.g., Miller et al. 2013). In 2019, catches of subyearling and yearling Chinook salmon and yearling coho salmon were all very close to long-term averages (Figure 41). The five-year catch trends were neutral but variable for all groups. Juvenile salmon captured off Oregon and Washington in 2019 generally appeared to be in good condition.

Long-term associations between oceanographic conditions, food web structure, and salmon productivity (Burke et al. 2013, Peterson et al. 2014) support projections of returns of Chinook salmon to Bonneville Dam and smolt-to-adult survival of Oregon Coast coho salmon. The suite of indicators is depicted in the “stoplight chart” in Table 1, and includes many indicators (including PDO, ONI, SSTa, deep-water temperature, copepod biomass anomalies, and juvenile salmon catch) shown elsewhere in this report. Indicators for 2020 Chinook salmon returns to the Columbia River reflect a range of conditions, from poor in smolt years 2016 and 2017, to more mixed conditions in smolt year 2018. Taken as a whole, these indicators are consistent with average returns of Chinook salmon to the Columbia River in 2020 relative to the past two decades; this derives from the fact that a large portion of Chinook salmon returning in 2020 went to sea in 2018. Conditions in smolt year 2019 were a mix of good, intermediate, and poor conditions, consistent with average to below-average returns of coho salmon to the Oregon coast in 2020.

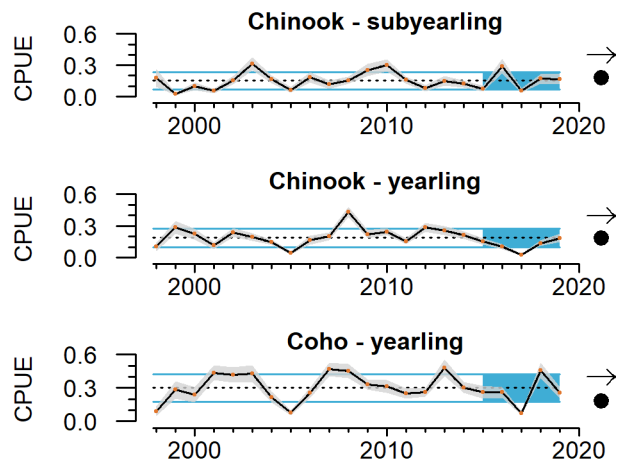


Figure 41. At-sea juvenile Chinook and coho salmon catch ($\text{Log}_{10}(\text{no}/(\text{km} + 1))$) in Jun, 1998–2019, off WA and OR. Lines, colors, and symbols as in Fig 3a. Data for at-sea juvenile salmon provided by B. Burke, NMFS/NWFSC, with additional calculations by C. Morgan, OSU/CIMRS. Data are derived from surface trawls taken during NWFSC Juvenile Salmon and Ocean Ecosystem Survey (JSOES) cruises.

Table 1. “Stoplight” table of basin-scale and local/regional conditions for smolt years 2016–19 and 2019 projected adult returns for coho and Chinook salmon that inhabit coastal OR and WA waters in their marine phase. Green/circle = favorable conditions (the top third of all years examined). Yellow/square = intermediate conditions (the middle third of all years examined). Red/diamond = poor conditions (the bottom third of all years examined). Courtesy of B. Burke and K. Jacobson, NMFS/NWFSC, and J. Fisher, C. Morgan, and S. Zeman, OSU/CIMRS.

Scale of indicators	Smolt year				Adult return outlook, 2020	
	2016	2017	2018	2019	Coho	Chinook
Basin-scale						
PDO (May–Sep)	Red diamond	Yellow square	Yellow square	Red diamond	Red diamond	Yellow square
ONI (Jan–Jun)	Red diamond	Yellow square	Green circle	Red diamond	Red diamond	Green circle
Local and regional						
SST anomalies	Red diamond	Yellow square	Yellow square	Red diamond	Red diamond	Yellow square
Deep-water temperature	Yellow square	Red diamond	Red diamond	Red diamond	Red diamond	Red diamond
Deep-water salinity	Yellow square	Yellow square	Green circle	Red diamond	Red diamond	Green circle
Copepod biodiversity	Red diamond	Red diamond	Yellow square	Yellow square	Yellow square	Yellow square
Northern copepod anomaly	Red diamond	Red diamond	Yellow square	Green circle	Green circle	Yellow square
Biological spring transition	Red diamond	Red diamond	Yellow square	Yellow square	Yellow square	Yellow square
Winter ichthyoplankton biomass	Yellow square	Yellow square	Yellow square	Red diamond	Red diamond	Yellow square
Winter ichthyoplankton community	Red diamond	Red diamond				
Juvenile Chinook salmon catch (Jun)	Red diamond	Red diamond	Yellow square	Yellow square	Yellow square	Yellow square
Juvenile coho salmon catch (Jun)	Yellow square	Red diamond	Green circle	Yellow square	Yellow square	Yellow square

A somewhat more quantitative analysis based on Table 1 estimates a reasonable probability of modest increases in returns of fall Chinook and coho salmon in 2020 relative to 2019, but comparable returns of spring Chinook salmon. In this analysis, annual Chinook salmon counts at Bonneville Dam (Figure 42, top and middle) and Oregon Coast coho smolt-to-adult survival (Figure 42, bottom) over the last two decades are regressed against the aggregate mean ranking of indicators in Table 1, with a 1-yr lag for coho and a 2-yr lag for Chinook salmon. The highest-ranking years at the left of the panels in Figure 42 tend to produce the highest returns and survival. The 2018 stoplight indicators had a relatively low mean rank of 11.8, for which the model equation projects returns of 131,000 spring and 379,000 fall Chinook salmon at Bonneville Dam in 2020 (Figure 42, top and middle, solid arrows). The 2019 stoplight indicators had an even lower mean rank of 15.1, for which the model projects smolt-to-adult survival of 1.9% for Oregon Production Index Hatchery (OPIH) coho in 2019 (Figure 42, bottom, solid arrow). The stoplight indicator ranking of 15.1 in 2019 also corresponds to 2021 Bonneville counts of 104,000 spring Chinook and 294,000 fall Chinook (Figure 42, top and middle, dashed arrows). The relationships of past salmon returns to stoplight means explain between 25% (coho) and 58% (fall Chinook) of variance. This is a fairly simple analysis, however, given that each indicator in Table 1 is given equal weight, a tenuous assumption due to differences in functional importance among different indicators and the high degree of correlation between some indicators.

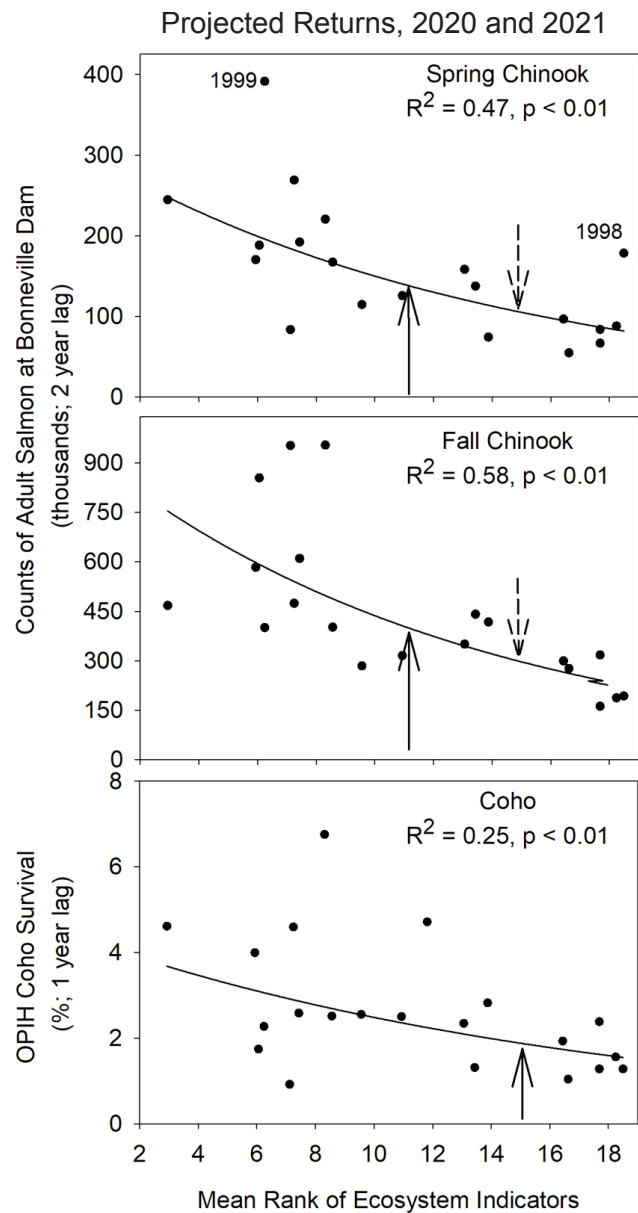


Figure 42. Salmon returns versus the mean rank of ecosystem “stoplight” indicators from Table 1. Arrows show the forecasted returns of Chinook salmon to Bonneville Dam in 2020 (solid) and 2021 (dashed), and of OPIH coho salmon to Oregon Coast streams in 2020 (solid). Data courtesy of B. Burke, NMFS/NWFSC.

To address these caveats, we include a more robust quantitative analysis for Chinook salmon returns to the Columbia River. The analysis uses an expanded set of ocean indicators plus principal components analysis and dynamic linear modeling to produce salmon forecasts for the same systems (see Burke et al. 2013). The principal components analysis essentially is used for weighted averaging of the ocean indicators, reducing the

total number of indicators while retaining the bulk of the information from them. The dynamic linear modeling technique relates salmon returns to the principal components of the indicator data, and the approach used here also incorporates dynamic information from sibling regression modeling. The model fits very well to data for spring and fall Chinook salmon at the broad Columbia River scale (Figure 43). Model outputs with 95% confidence intervals estimate 2020 Bonneville Dam counts of spring Chinook salmon that are similar to returns from 2017–19 (Figure 43, top), and potential increases of fall Chinook salmon at Bonneville Dam in 2020 relative to 2019, but still well below the returns of 2013–15 (Figure 43, bottom). (In past years, a similar model was run for coho salmon returns to the OPIH region, but that model was not updated this year.) Although these analyses represent a general description of ocean conditions, we must acknowledge that the importance of any particular indicator will vary among salmon species and populations in these basins. NOAA scientists and partners are working toward stock-specific salmon forecasts by using methods that can optimally weight the indicators for each response variable in which we are interested (Burke et al. 2013).

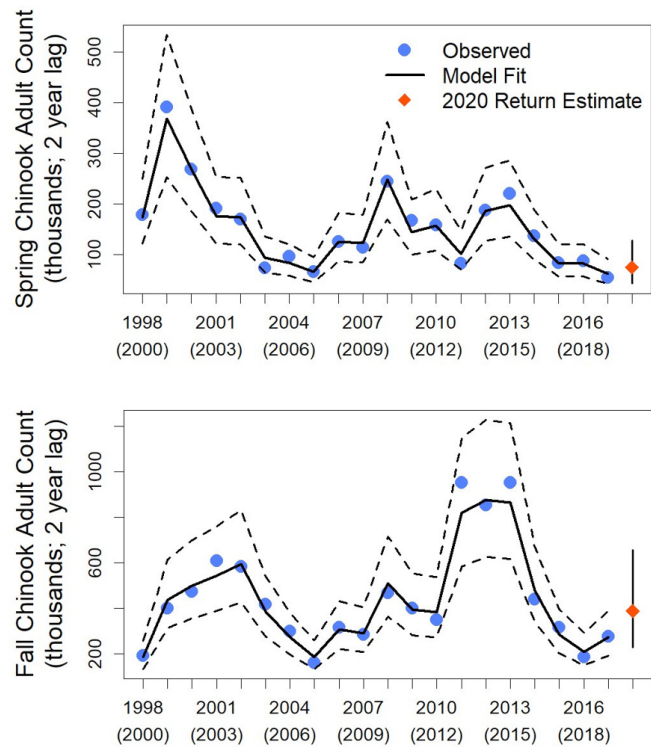


Figure 43. Time series of observed and projected spring Chinook salmon adult counts (top) and fall Chinook salmon adult counts (bottom), by out-migration year. In each plot, the dark line represents the model fit and lighter lines represent 95% confidence intervals. Projections (for return year 2020) were created from a DLM (Dynamic Linear Model) with log of sibling counts and first principal component of ocean indicators as predictor variables. Courtesy of B. Burke, NMFS/NWFSC.

We are working to develop similar indicator-based outlooks for returns of Chinook salmon in California. As a first iteration, a recent study by Friedman et al. (2019) found that returns of naturally produced Central Valley fall Chinook salmon correlated with spawning escapement of parent generations, egg incubation temperature between October and December at Red Bluff Diversion Dam (Sacramento River), median flow in the Sacramento River in February following fry emergence, and a marine predation index based on the abundance of common murre (*Uria aalge*) at Southeast Farallon Island. For fall Chinook salmon cohorts returning to the Central Valley in 2020, these four indicators imply relatively low returns for naturally produced age-3 Chinook salmon, the dominant age group for this system (Table 2). Age-3 fish returning in 2020 were the progeny of a parent generation with very low escapement in 2017, then experienced poor

Table 2. Table of conditions for naturally produced Central Valley fall Chinook salmon returning in 2020, from spawning years 2016–18. Indicators reflect each cohort’s parent generation escapement, egg incubation temperature, flow during juvenile stream residence, and seabird predation in the early marine phase. Shading indicates age-3 Chinook salmon, the dominant age class returning to the Central Valley. Courtesy of N. Mantua, NMFS/SWFSC.

Spawning escapement (t = 0)	Incubation temp. Oct-Dec (t = 0)	February median flow (t + 1)	Seabird Marine Predation Index (t + 1)	Chinook age in fall 2020
2016: 56,000 (low)	11.8°C (poor)	48,200 cfs (very high)	near average	4
2017: 18,000 (very low)	11.8°C (poor)	5,525 cfs (very low)	near average	3
2018: 72,000 (low)	11.7°C (poor)	21,700 cfs (high)	near average	2

incubation temperature in the 2017–18 winter and very low streamflow in early 2018, likely coupled with typical avian predation pressure as they went to sea later in 2018. Age-4 fish (produced in 2016) and age-2 jacks (2018) have mixed signals thanks to better juvenile flow regimes. Importantly, this summary of indicators is only relevant to naturally produced fall Chinook salmon in this river system; hatchery-reared fall Chinook salmon, which make up the majority of fall Chinook salmon from the Central Valley, are buffered from much of the variability (e.g., in temperature and flow) that affects naturally produced fish.

3.7 Groundfish Stock Abundance and Community Structure

The CCIEA Team regularly presents the status of groundfish biomass and fishing pressure based on the most recent stock assessments. This year’s report includes updated information for ten stocks (big skate [*Beringraja binoculata*], longnose skate [*B. rhina*], three substocks of cabezon [*Scorpaenichthys marmoratus*], Pacific hake, sablefish [*Anoplopoma fimbria*], cowcod [*Sebastes levis*], and combined gopher/black-and-yellow rockfish [*Sebastes carnatus/S. chrysomelas*]), plus many catch-only projections. This leaves splitnose rockfish (*S. diploproa*) as the only full assessment done prior to 2010.

All assessed groundfish stock biomasses are above biomass limit reference points (LRPs); thus, no assessed stocks were considered to be in an overfished status (Figure 44, x-axis). Yelloweye rockfish (*S. ruberrimus*) is still rebuilding toward its target reference point (TRP; dashed vertical line in Figure 44), but is above the overfished level (i.e., its biomass is greater than the LRP), meaning that it remains under a protective rebuilding plan from PFMC. However, cowcod is now above its TRP, indicating that it is rebuilt after the stock was declared overfished in 2000 and was placed under a rebuilding plan. Regarding fishing intensity, nearly all groundfish stocks were being sustainably harvested below the overfishing proxy as of their most recent assessments (Figure 44, y-axis). “Overfishing” occurs when catches exceed overfishing limits (OFLs), but not all stocks are managed by OFLs. For summary purposes, our best alternative is to compare fishing rates to proxy rates that are based on a stock’s spawner potential ratio (SPR). Three rockfish stocks—rougheye rockfish (*S. aleutianus*), splitnose rockfish (*S. diploproa*), and the southern stock of China rockfish (*S. nebulosus*)—were near the proxy for overfishing (dashed horizontal line in Figure 44) in their most recent assessments. The rougheye rockfish assessment was most recently updated in 2013, while China rockfish were last updated in 2015 and splitnose rockfish in 2009. The current fishing mortality rates of these species are likely different from those in Figure 44.

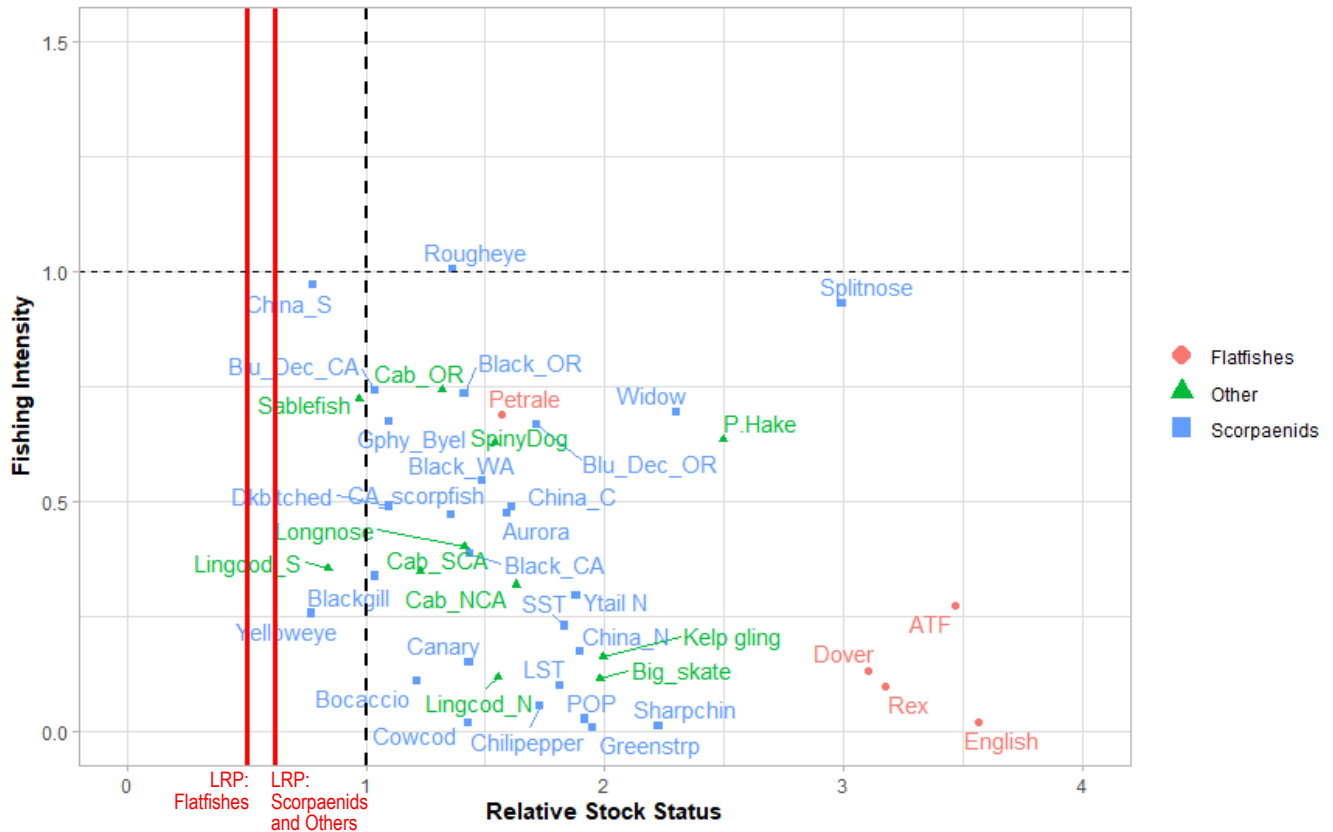


Figure 44. Stock status of CCE groundfish. *Relative Stock Status* is the ratio of the current year to the unfished spawning output (in millions of eggs). *Fishing Intensity* uses the fishing rate to achieve a specific spawner potential ratio (SPR), defined as $F \div F_{SPR}$, where SPR is the maximum sustainable yield (MSY) proxy. The horizontal line is the fishing intensity rate reference; above the line is above the reference level and indicates overfishing. Vertical lines are the biomass target reference points (TRP; dashed line) and limit reference points (LRPs; red lines); left of the TRP indicates an overfished status. Symbols indicate taxonomic groups. All points represent values from the most recent PFMC-adopted stock assessments. Groundfish stock status data provided by J. Cope, NMFS/NWFSC, derived from NOAA Fisheries stock assessments.

3.8 Highly Migratory Species

Biomass and recruitment patterns for highly migratory species (HMS), including several stocks managed by PFMC, are derived from the most recent assessments of key HMS target stocks. These assessments (which range from 2015–18) have not been updated since last year’s technical memorandum (Harvey et al. 2019), and thus we have no new information on HMS indicators for this report.

3.9 Marine Mammals

3.9.1 Sea lion production

California sea lions are permanent residents of the CCE, breeding in the California Channel Islands and feeding throughout the CCE in coastal and offshore habitats. They are also indicators of prey availability in the Central and Southern CCE (Melin et al. 2012). Two indices are particularly sensitive measures of prey availability to California sea lions: pup production and pup growth during the period of maternal nutritional dependence. Sea lion pup count at San Miguel Island is a result of successful pregnancies, and relates to prey availability and nutritional status for adult females from October to June. Pup growth from birth to age seven months is related to prey availability to adult females during lactation from June to February.

In 2019, California sea lion pup births at San Miguel Island were about 1 SD above the long-term mean for the third consecutive year, representing a sharp increase from pup counts in 2015–16 and leading to an overall increasing short-term trend (Figure 45, top). Furthermore, pup growth rates for each of the four cohorts from 2016–19 were at or above the long-term average (Figure 45, bottom). These indicators represent a substantial improvement in feeding conditions for the San Miguel colony relative to cohorts in 2012–15, which experienced unusually high stranding rates and reduced pup growth rates associated with poor foraging conditions for nursing females in the Central and Southern CCE during the period of pup nutritional dependence (Wells et al. 2013, Leising et al. 2014, Leising et al. 2015, McClatchie et al. 2016).

The improved growth of pups in the recent cohorts indicates that nursing females experienced better foraging conditions during 2016–19. Favorable ocean conditions for anchovy and sardine have resulted in the return of anchovy as the most frequently occurring California sea lion prey near the colony (present in >85% of adult female sea lion diets) in the past four years and the resurgence of sardine in the diet in 2018 (48%). Hake, market squid, and Pacific and jack mackerel also had high occurrences in 2018, resulting in a diverse diet of high-quality prey for nursing females that likely contributed to the positive trends in the pup indices. Preliminary data from the 2019–20 fall–winter field seasons indicate that nursing females at the San Miguel Island colony fed heavily on anchovy during that period.

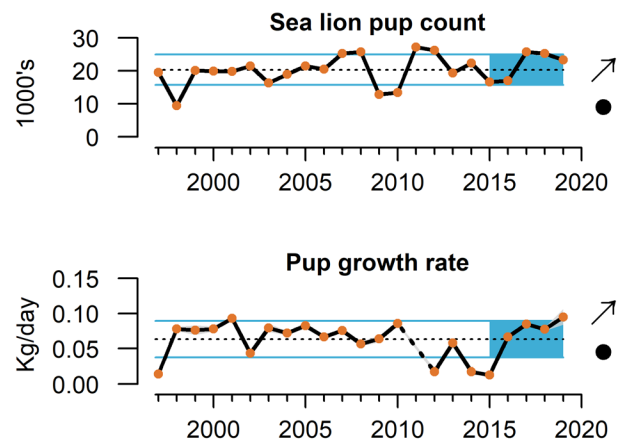


Figure 45. California sea lion pup counts, and estimated mean daily growth rate of female pups between 4–7 months of age, on San Miguel Island for the 1997–2019 cohorts. Lines, colors, and symbols as in Fig 3a. California sea lion data provided by S. Melin, NMFS/AFSC.

3.9.2 Whale entanglement

The number of whale entanglements reported along the U.S. West Coast has increased considerably since 2014, particularly for humpback whales (*Megaptera novaeangliae*). While ~50% of entanglement reports cannot be attributed to a specific gear type, Dungeness crab fishing gear is the most common source that has been identified during this period. The dynamics of entanglement risk and reporting are complex, and they are affected by shifts in oceanographic conditions and prey fields, changes in whale populations, changes in distribution and timing of fishing effort, and increased public awareness leading to improved reporting (Santora et al. 2020). Pelagic habitat compression as shown in Figure 12 may further exacerbate interactions between whales and other ecosystem components (Santora et al. 2020).

There were 26 confirmed entanglement reports on the U.S. West Coast in 2019, higher than any year prior to 2014, although fewer confirmed reports were made than in 2015–18 (Figure 46; see also NOAA 2020). As in previous years, the majority of confirmed reports (17) were of entangled humpback whales, followed by gray whales (*Eschrichtius robustus*; eight confirmed reports) and one confirmed report of an entangled minke whale (*Balaenoptera acutorostrata*). There were no confirmed reports of entangled blue whales (*B. musculus*). Also as in previous years, the majority of reports in 2019 were observations of entangled whales in California, though entanglements were known to include gear from all three coastal states (NOAA 2020). Gear involved in confirmed entanglements in 2019 included commercial and recreational Dungeness crab gear, commercial rock crab gear, gillnets, and unknown gear (NOAA 2020). Significant actions were taken in 2019 to address the increased entanglement reports, including closures and delays of Dungeness crab seasons in California and late-season reductions of allowable Dungeness crab gear in Washington in response

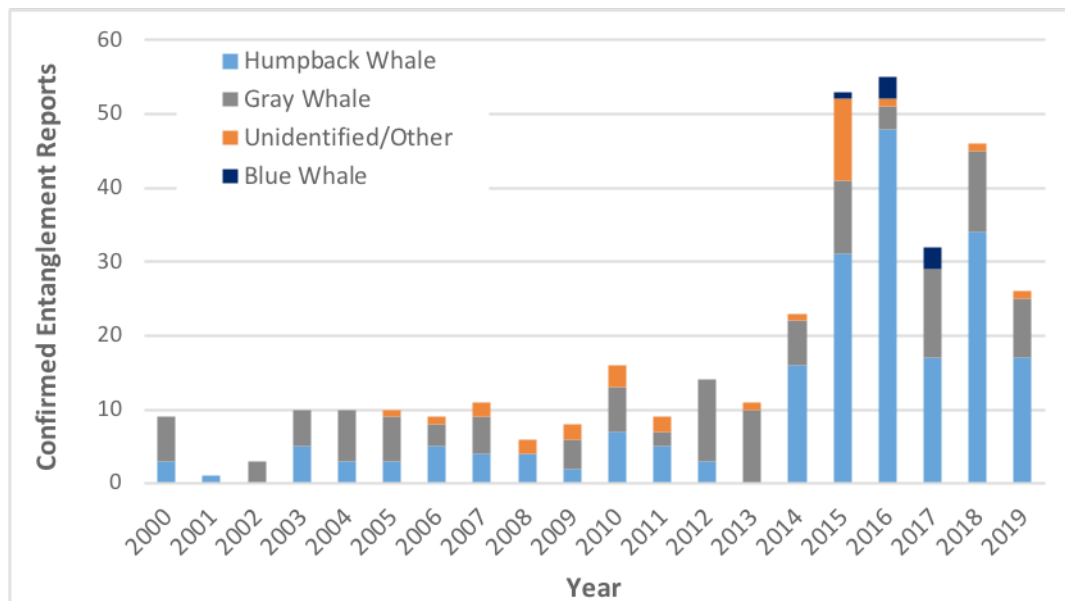


Figure 46. Confirmed numbers of whales (by species) reported as entangled in fishing gear or other anthropogenic materials along the U.S. West Coast, 2000–19. Whale entanglement data provided by D. Lawson, NMFS/WCR.

to entanglement risk, and commitments by all three states to develop conservation plans to reduce entanglements in Dungeness crab fisheries (NOAA 2020). While these actions likely contributed to reducing entanglement risks in 2019, other factors—such as continued exposure of whales to gear that was lost during the season, or foraging in nearshore waters on abundant anchovy—likely contributed to entanglement risks in 2019.

3.10 Seabirds

Seabird indicators (at-sea densities, diet, productivity, and mortality) constitute a portfolio of metrics that reflect population health and condition of seabirds as well as links to lower trophic levels and other conditions in the CCE. To highlight the status of different seabird guilds and relationships to their marine environment, multiple focal species are monitored throughout the CCE. The species we report on in the sections below represent a breadth of foraging strategies, life histories, and spatial ranges.

3.10.1 Seabird population productivity

Seabird population productivity, as measured through variables related to reproductive success, tracks marine environmental conditions and often reflects forage production near breeding colonies. Here we present standardized anomalies of fledgling production per pair of breeding adults for five focal species on Southeast Farallon Island (SEFI) in the Central CCE. The five species represent a range of feeding habits while on their colonies.

1. Rhinoceros auklets (*Cerorhinca monocerata*) forage primarily on pelagic fishes in shallow waters over the continental shelf, generally within 50 km of colonies, returning to the colony after dusk to deliver multiple whole fish to their chicks.
2. Common murre forage primarily on pelagic fishes in deeper waters over the shelf and near the shelf break, generally within 80 km of colonies, returning to the colony during daylight hours to deliver single whole fish to their chicks.
3. Cassin's auklets (*Ptychoramphus aleuticus*) forage primarily on zooplankton in shallow water over the shelf break, generally within 30 km of colonies; they forage by day and night and return to the colony at night to feed chicks.
4. Brandt's cormorants (*Phalacrocorax penicillatus*) forage primarily on pelagic and benthic fishes in waters over the shelf, generally within 20 km of breeding colonies, returning to the colony during the day to deliver regurgitated fish to their chicks.
5. Pigeon guillemots (*Cephus columba*) forage primarily on small benthic and pelagic fish over the shelf, generally within 10 km of colonies, returning to the colony during the day to deliver a single fish to their chicks.

Fledgling production of most of these five species at SEFI was very poor in 2019. While Brandt's cormorant experienced relatively high fledgling production consistent with other observations over the past five years, the other four species had fledgling production anomalies that were ≥ 1 SD below the long-term average in 2019 (Figure 47). Cassin's auklets, common murre, and rhinoceros auklets in particular experienced pronounced declines in 2019 relative to 2018. Poor fledgling production may be related to the forage patterns in the central CCE (Figure 35). For example, low availability of krill likely contributed to

poor production of Cassin’s auklets, which mainly prey on krill. For piscivorous birds, anchovy prey were highly abundant in this area (e.g., Figures 35 and 39), but in many cases the anchovy were too large for seabird chicks to ingest, and other prey types such as juvenile rockfish were not as available in 2019 (see Section 3.10.2). This may illustrate the importance of having not only a productive forage base, but also a diverse forage base that can support a range of feeding guilds and provide opportunities for prey-switching if readily available prey are not suitable for chick provisioning.

Some seabird colonies elsewhere in the CCE had average or above-average fledgling production in 2019, indicating spatial variation in seabird feeding conditions. For example, fledgling production for common murre and Brandt’s cormorants was relatively high at Yaquina Head, Oregon, in 2019 (Thompson et al. 2019b), and rhinoceros auklet production at Destruction Island, Washington, was average in 2019 (S. Pearson, WDFW, personal communication). Birds at these colonies had access to several available forage species. Fledgling production at these colonies was probably also improved owing to relatively low disturbance and predation pressure from bald eagles (*Haliaeetus leucocephalus*) and gulls (family Laridae) on these colonies in 2019 compared to other years over the past decade (Porquez et al. 2019).

3.10.2 Seabird diets

Seabird diet composition during the breeding season tracks marine environmental conditions and often reflects production, diversity, and availability of forage in areas near seabird colonies in different regions of the CCE.

The first key finding from seabird diet studies pertains to the relatively good production of fledglings at seabird colonies in the Northern CCE, such as at Destruction Island and Yaquina Head. Birds at these colonies tend to feed in relatively nearshore waters, where forage species such as smelts (family Osmeridae) are abundant and may supplement forage from open waters;

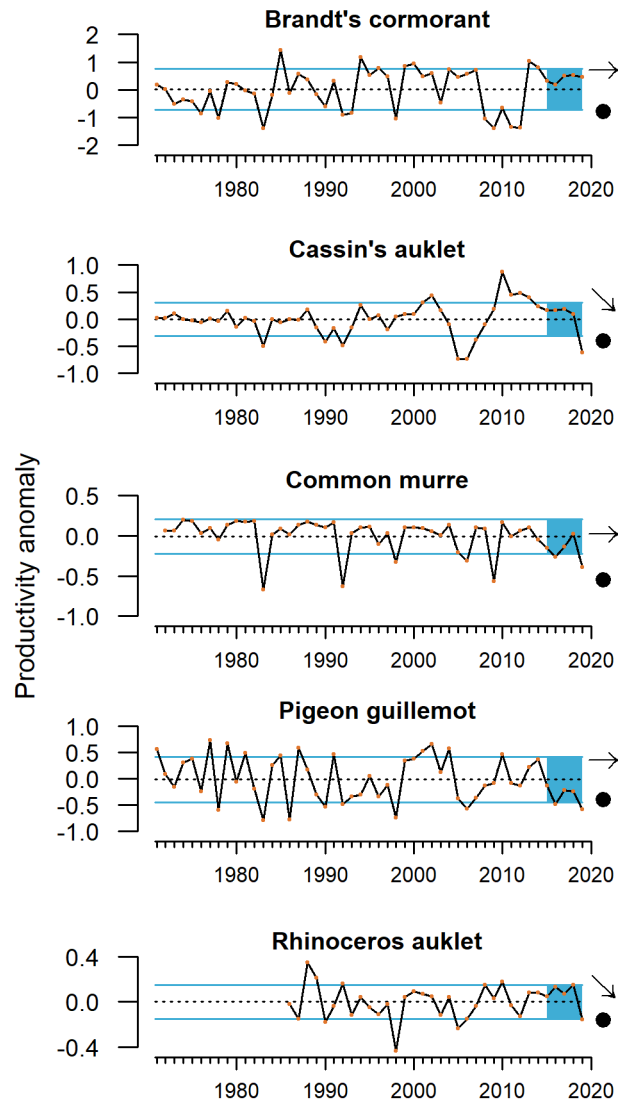


Figure 47. Standardized productivity anomalies (annual productivity, defined as annual number of chicks fledged/pair of breeding adults, minus long-term mean) for 5 seabird species breeding on Southeast Farallon Island (SEFI) through 2019. Lines and symbols as in Fig 3a. Seabird fledgling production data at nesting colonies on SEFI provided by J. Jahncke, Point Blue Conservation Science.

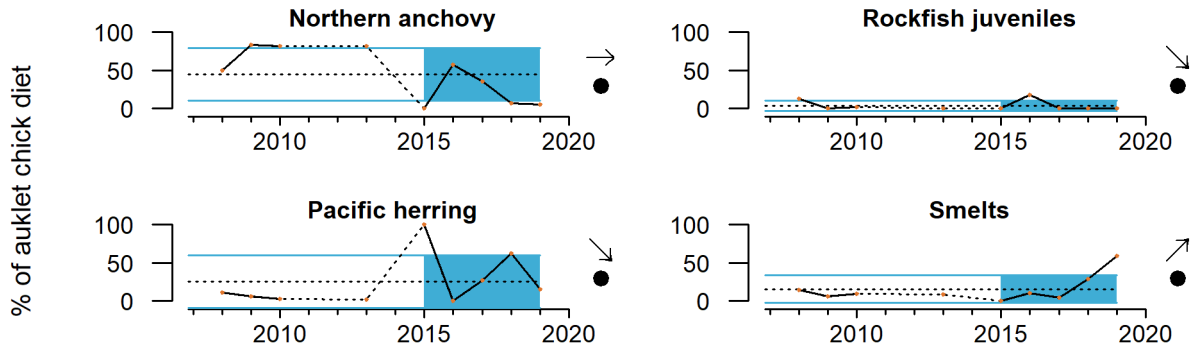


Figure 48. Rhinoceros auklet chick diets at Destruction Island, WA, through 2019. Lines, colors, and symbols as in Fig 3a. Data courtesy of S. Pearson, Washington Rhinoceros Auklet Ecology Project (scott.pearson@dfw.wa.gov).

smelts are not sampled effectively by the forage surveys described elsewhere (e.g., Figure 33), but seabird diets from these colonies suggest that smelt were abundant in 2019. At Destruction Island, the percentage of smelts in the diets of rhinoceros auklets provisioning chicks was the highest ever recorded and showed a significant positive short-term trend (Figure 48). Proportions of anchovies and herring in rhinoceros auklet diets were below average in 2019, and the proportion of juvenile rockfish continued to be low since a peak in 2016.

Similarly, at Yaquina Head, the proportion of smelts in the diet of common murre provisioning chicks was above average in 2019, after a below-average value in 2018 (Figure 49). The combined proportions of herring and sardine in the murre diet were below average in 2019 and showed a significant short-term decline. The proportion of Pacific sand lance (*Ammodytes hexapterus*) in the common murre diet was below average in 2019. The proportion of flatfishes in the murre diet was above average for the second straight year and showed a significant positive short-term trend. The proportion of juvenile rockfish in the murre diet was well below average for the fifth straight year, and considerably lower than peaks in 2008 and 2010.

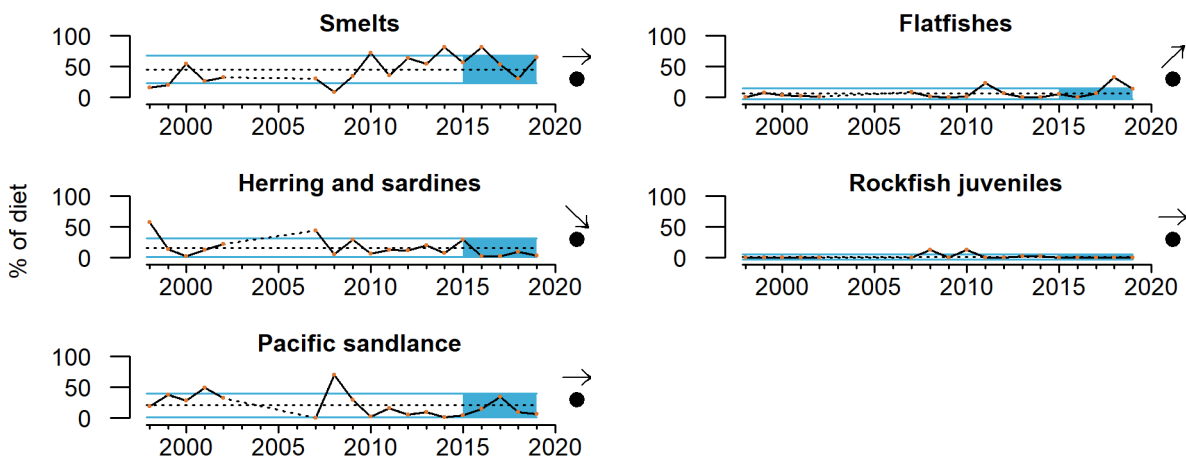


Figure 49. Common murre chick diets at Yaquina Head, OR, through 2019. Lines, colors, and symbols as in Fig 3a. Data provided by R. Suryan, Yaquina Head Seabird Colony Monitoring Project (rob.suryan@noaa.gov).

At SEFI in Central California, piscivorous seabirds have shown increasing reliance on anchovy and decreasing reliance on juvenile rockfish over the past five years. The proportions of anchovy in the diets of Brandt’s cormorants, rhinoceros auklets, and common murres provisioning chicks on SEFI were well above average in 2019 and showed significant positive short-term trends, while the proportions of rockfish in these species’ diets were well below average in 2019 and showed significant negative short-term trends (Figure 50). Pigeon guillemots showed a similar decline in juvenile rockfish. In addition, the proportion of salmonids in common murre diets at SEFI was well below average in 2019. Finally, diet data for Cassin’s auklets, which feed heavily on krill, were only current through 2018 at the time this report was completed. This is prior to the 2019 decline in krill seen off Central California (see Section 3.4). The proportion of *Euphausia pacifica* in the diet of SEFI Cassin’s auklets was above average in 2018 and showed a significant positive short-term trend, while the proportion of *Thysanoessa spinifera* in the Cassin’s auklet diet was near average, but the recent mean was significantly greater than the long-term mean.

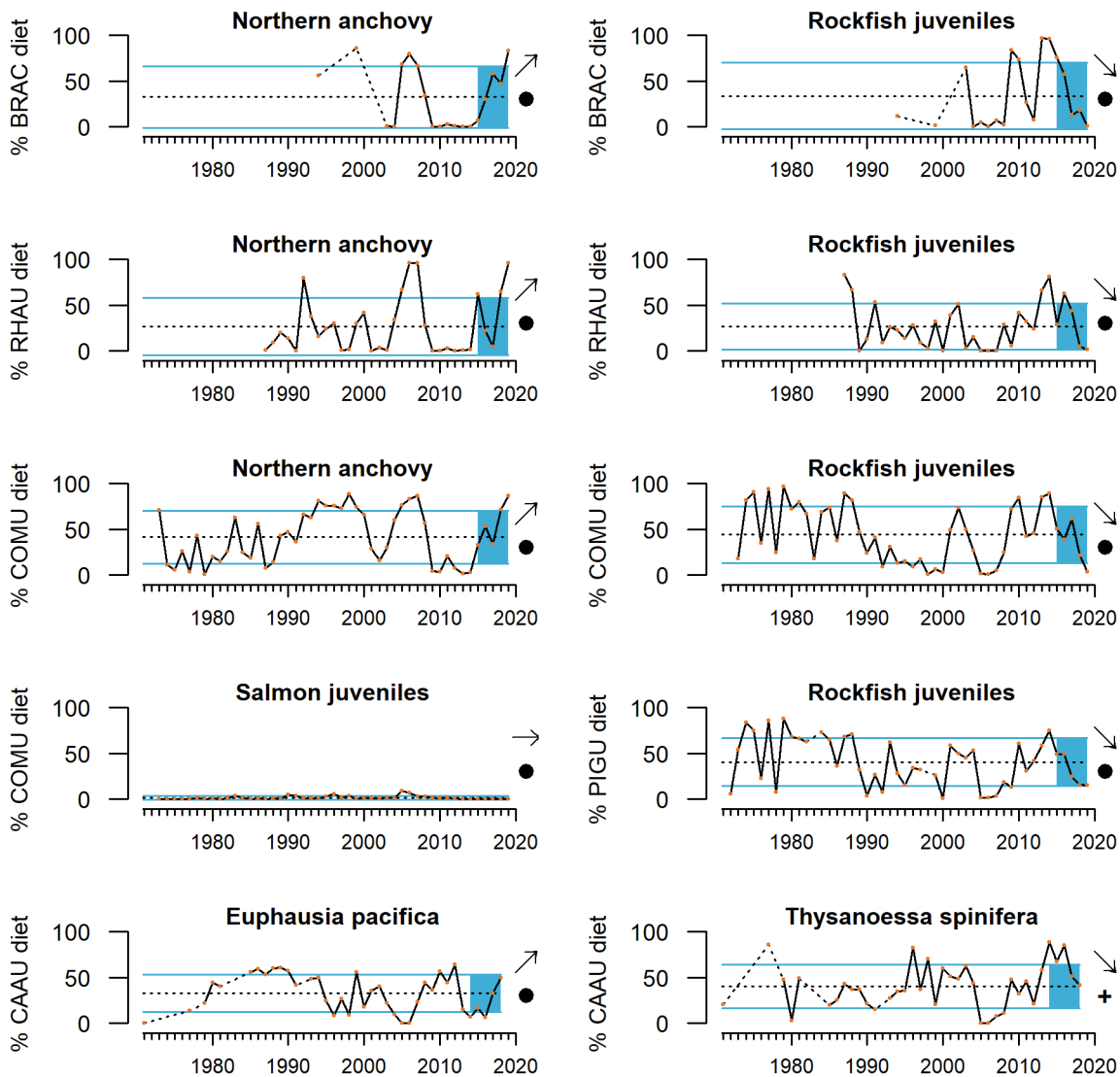


Figure 50. SEFI seabird diets through 2019. BRAC = Brandt’s cormorant; RHAU = rhinoceros auklet; COMU = common murre; PIGU = pigeon guillemot; CAAU = Cassin’s auklet. Lines, colors, and symbols as in Fig 3a. Data provided by J. Jahncke, Point Blue Conservation Science (jjahncke@pointblue.org).

At another central California site, Año Nuevo Island, researchers noted that anchovy accounted for nearly 100% of the diets of rhinoceros auklets provisioning chicks in both 2018 and 2019; other prey resources like rockfish juveniles, market squid, and Pacific saury (*Cololabis saira*), were very rarely delivered to chicks (data not shown). The size of anchovies returned to chicks on Año Nuevo Island in 2019 was close to the time series average and has increased since 2014–16 (Figure 51). Researchers expressed concern that individual anchovy were too large to be ingested by rhinoceros auklet chicks, which may have contributed to the below-average fledgling production observed at Año Nuevo Island (Bathwick et al. 2019) as well as elsewhere in Central California (e.g., Figure 47), despite the abundance of anchovy in this region.

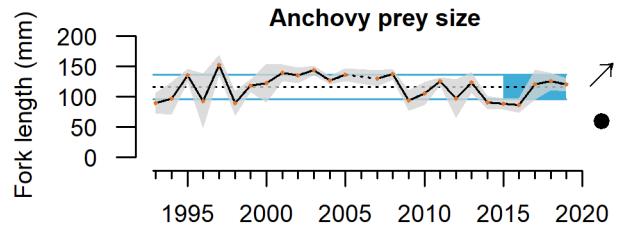


Figure 51. Fork length of northern anchovy brought to rhinoceros auklet chicks at Año Nuevo Island, 1993–2019. Error envelope shows ± 1.0 SD. Lines, colors, and symbols as in Fig 3a. Data provided by R. Carle, Oikonos/Point Blue Conservation Science (ryan@oikonos.org).

Collectively, these seabird diet indicators likely reflect both the variability of forage community composition and the plasticity or opportunistic nature of predator foraging and diet. While there have been shifts in dominant prey species over time, northern anchovy featured prominently in diets of multiple seabird predators in 2019, particularly in the Central CCE, likely tracking availability as indexed by forage indicators (high anchovy, low rockfish; see Figure 35).

3.10.3 Seabird mortality

Seabird mortality can track seabird populations as well as environmental conditions at regional and larger spatial scales. Monitoring of beached birds (often by citizen scientists) provides information on the health of seabird populations, ecosystem health, and unusual mortality events. CCIEA ESRs from the anomalously warm and unproductive years of 2014–16 noted major seabird mortality events in each year. These “wrecks”—exceptional numbers of dead birds washing up on widespread beaches—impacted Cassin’s auklets in 2014, common murrens in 2015, and rhinoceros auklets in 2016.

In the Northern CCE and the northernmost Central CCE (Washington to Northern California), the University of Washington-led Coastal Observation and Seabird Survey Team (COASST) documented beached birds at average to below-average levels for four focal species in the winter of 2018–19 (Figure 52). The Cassin’s auklet encounter rate was at baseline levels in 2018 (the latest year of data available at the time this report was completed), as it has been since its unusual mortality event in 2014. The common murre encounter rate was average in 2019 and showed a significant negative short-term trend since its unusual mortality event in 2015. The northern fulmar (*Fulmarus glacialis*) encounter rate was just below average in 2018 (the latest year of data) and showed a significant negative short-term trend, although preliminary data from late 2019 and early 2020 suggests a recent increase in beached northern fulmars. The sooty shearwater (*Ardenna grisea*) encounter rate in 2019 was below average, as it has been since a peak

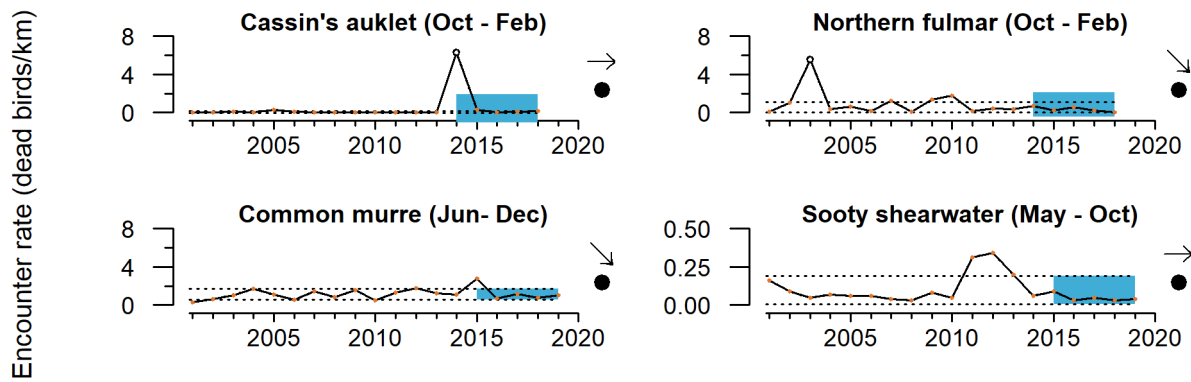


Figure 52. Encounter rate of bird carcasses on WA, OR, and NorCal beaches through 2019. The mean and trend of the last 5 years is evaluated versus the mean and SD of the full time series without outliers (open circles). Dashed lines indicate upper and lower SD of the full time series with outliers removed. Blue shaded box indicates the evaluation period and the upper and lower SD of the full time series with the outliers included. Data provided by the Coastal Observation and Seabird Survey Team (<https://depts.washington.edu/coasst/>).

from 2011–13. Although encounter rates of indicator species in the COASST survey were near their long-term means in 2019, there was a significant common murre mortality event in northern California that is not evident in the spatially aggregated data shown in Figure 52. Elevated numbers of dead adult common murres on beaches were documented during the breeding season in Humboldt and Mendocino Counties in Northern California. In Mendocino County, spring encounter rates were roughly an order of magnitude above normal (data not shown), and birds appeared emaciated. These areas are north of the northern extent of the abundant anchovy biomass shown in Figure 39.

Preliminary information also suggests that unusually high post-breeding mortality of rhinoceros auklets occurred in Washington and Oregon in the fall of 2019, possibly indicating declining foraging conditions for these primarily piscivorous birds in the latter half of 2019 in the Northern CCE. Data from this rhinoceros auklet mortality event were not available at the time this report was completed.

Further south within the Central CCE (Bodega Bay, California, to Point Año Nuevo, California), the BeachWatch program observed no major wrecks among focal species in 2019 (Figure 53). The Brandt's cormorant encounter rate was just below average in spring–fall 2019 and showed a significant negative short-term trend following a peak in 2015. The Cassin's auklet encounter rate continued at low baseline levels in 2017–18 (the most recent year of data). The common murre encounter rate was >1 SD above average in 2019, which continues an increasing recent trend; however, common murre encounter rates remain well below the peak from the wreck in 2014–15. The sooty shearwater encounter rate was close to average in spring–fall 2019; the peak it experienced in 2015 was not sharp enough to result in a short-term negative trend. The northern fulmar encounter rate was just below average in 2017–18.

The BeachCOMBERS program conducts another survey of beached seabirds on California beaches from Point Año Nuevo to Malibu. We have previously reported on two survey regions: north (Point Año Nuevo to Lopez Point, California) and central (Lopez Point to Rocky Point, California). These data have not been updated since last year's report (Harvey et al. 2019); they were current through 2018, generally finding encounter rates at average to below-average levels.

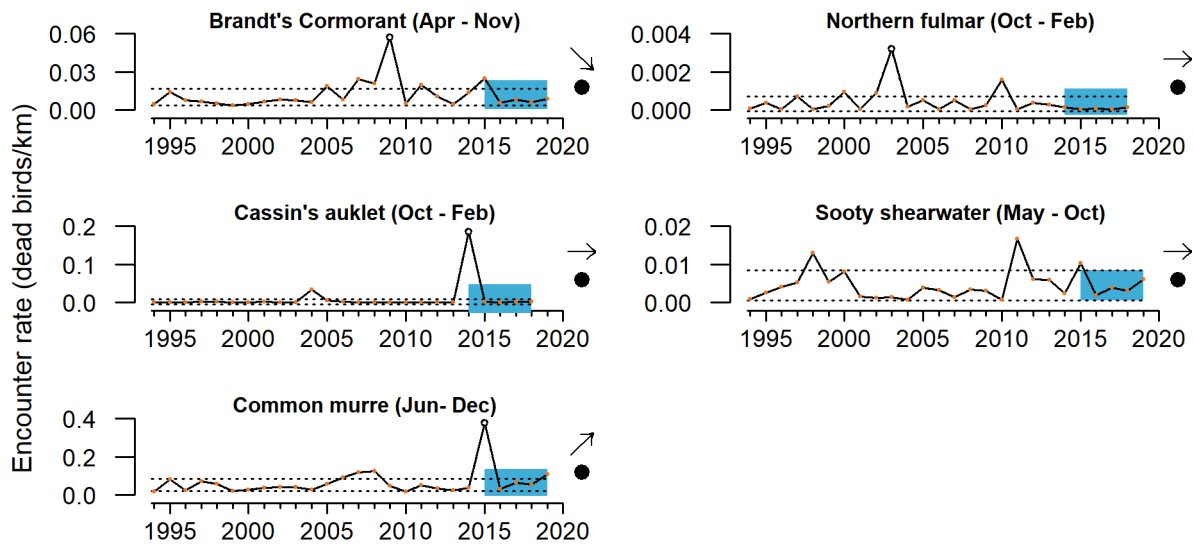


Figure 53. Encounter rate of bird carcasses on beaches in north-central California through 2018 and 2019. The mean and trend of the last five years is evaluated versus the mean and SD of the full time series but with the outliers removed. Open circles indicate outliers. Dotted lines indicate the upper and lower SD of the full time series with outliers removed. The blue box indicates the evaluation period and the upper and lower SD of the full time series with the outliers included. Data provided by BeachWatch (<https://farallones.noaa.gov/science/beachwatch.html>).

3.10.4 Seabird at-sea densities

Seabird densities on the water during the breeding season can track marine environmental conditions and may reflect regional production and availability of forage. Data from this indicator type can establish habitat use and may be used to detect and track seabird population movements or increases/declines as they relate to ecosystem change. We monitor and report at-sea densities of three focal species in the Northern, Central, and Southern CCE. These data are collected on the same springtime research cruises that sample forage assemblages (see [Section 3.4](#)). Sooty shearwaters migrate to the CCE from the Southern Hemisphere in spring and summer to forage near the shelf break on a variety of small fish, squid and zooplankton. Common murres and Cassin's auklets are resident species that feed primarily over the shelf; Cassin's auklets prey mainly on zooplankton and small fish, while common murres target a variety of pelagic fish.

At-sea density patterns varied within and across seabird species among the three regions of the CCE. Sooty shearwater at-sea density anomalies underwent significant short-term declines in both the Northern (NCC) and Southern (SCC) regions from 2015–19, and saw a significant short-term increase in the Central (CCC) region (Figure 54). The negative trends in the NCC and SCC were driven by steep declines after a peak in 2015, while the 2019 positive anomaly for sooty shearwaters in the CCC was the highest in the time series. Sooty shearwater distributions in the CCE are thought to be strongly linked to prey availability, given that they do not breed in the Northern Hemisphere. Given previous observations of high frequencies of anchovy in sooty shearwater diets (Wiens and Scott 1975, J. Zamon, unpublished data) and the ability of sooty shearwaters to track ocean features associated with high anchovy abundance (Phillips et al. 2018), the high density of sooty shearwaters in the Central CCE in

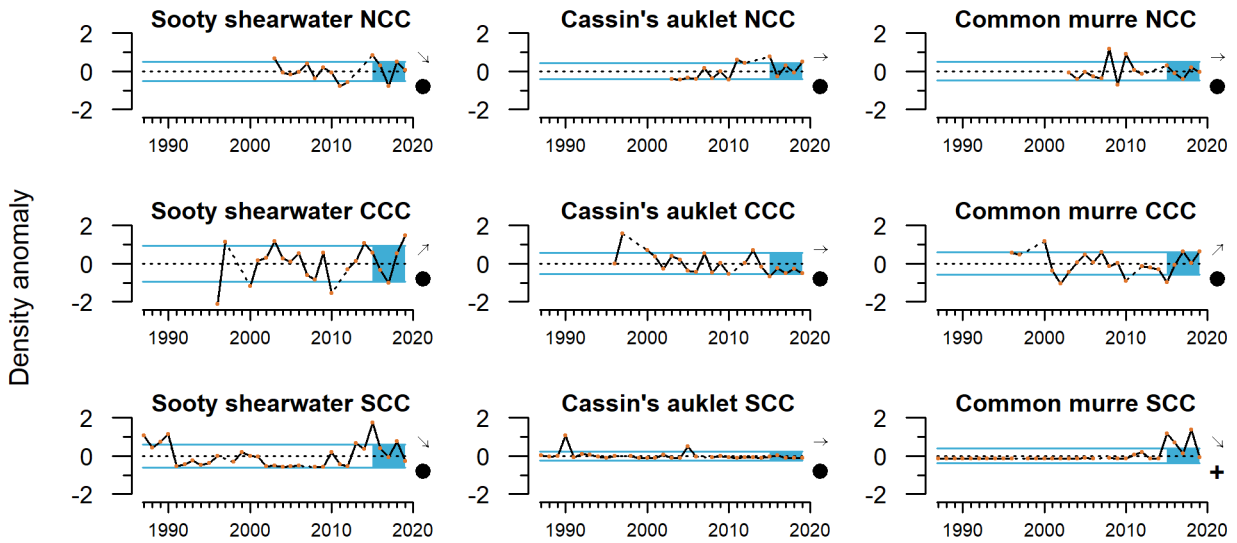


Figure 54. At-sea density anomalies of 3 seabird species in spring–summer in 3 CCE regions (NCC, CCC, SCC) through 2019. NCC = Northern CCE, data from 2003–19; CCC = Central CCE, data from 1996–2019; SCC = Southern CCE, data from 1987–2019. Geographic regions correspond to Fig 4c. Lines, colors, and symbols as in Fig 3a. Seabird abundance data from NCC collected and provided by J. Zamon, NMFS/NWFSC. Seabird abundance data from CCC (collected on the SWFSC Juvenile Rockfish Recruitment and Ecosystem Assessment Survey) and SCC (collected on the CalCOFI surveys) courtesy of B. Sydeman, Farallon Institute.

2019 may have been related to anchovy distributions. Cassin’s auklet at-sea density anomalies were high in the NCC in 2019 but showed no recent trends in any of the regions, and recent average densities have been within ± 1 SD of the long-term regional means. Common murre at-sea density anomaly trends were neutral over the last five years in the NCC, but showed a significant short-term increase in the CCC and short-term decrease in the SCC; despite near-average densities in 2019, recent common murre density anomalies in the SCC continued to be high relative to the long-term mean. In the NCC, sooty shearwaters and common murres were again aggregated near the Columbia River plume, likely attracted to concentrations of forage fishes, squid, or krill. In the SCC, it appears that recent sooty shearwater and common murre upticks relative to the 1990s and much of the 2000s have subsided.

4 Human Activities

4.1 Coastwide Landings by Major Fisheries

Fishery landings data are current through the end of 2019 (data accessed April 2020). Overall, total commercial landings across the U.S. West Coast have been highly variable in recent years, driven by large changes in landings of shrimp, market squid, and Pacific hake from 2015–19 (Figure 55). Total landings decreased 10% from 2018 to 2019, and total landings in 2019 were very close to the time series mean. Pacific hake made up 70% of all 2019 landings. Commercial landings of salmon and CPS finfish over the last five years were >1 SD below the average of the time series. Groundfish (excluding hake) have increased modestly after being at lows since the mid-2000s, but remain low relative to the rest of the time series. Pacific hake landings increased to the highest levels of the time series during 2015–19, while shrimp landings decreased from 2015–19, but remain within ± 1 SD of time series averages. Market squid landings have been highly variable throughout the time series; in 2019, market squid landings were among the lowest of the time series and were roughly 1 SD below average. Landings of crab were close to average in 2019. HMS and other species landings have been consistently within ± 1 SD of time series averages over the last 20+ years, though both are approaching lows for their respective time series.

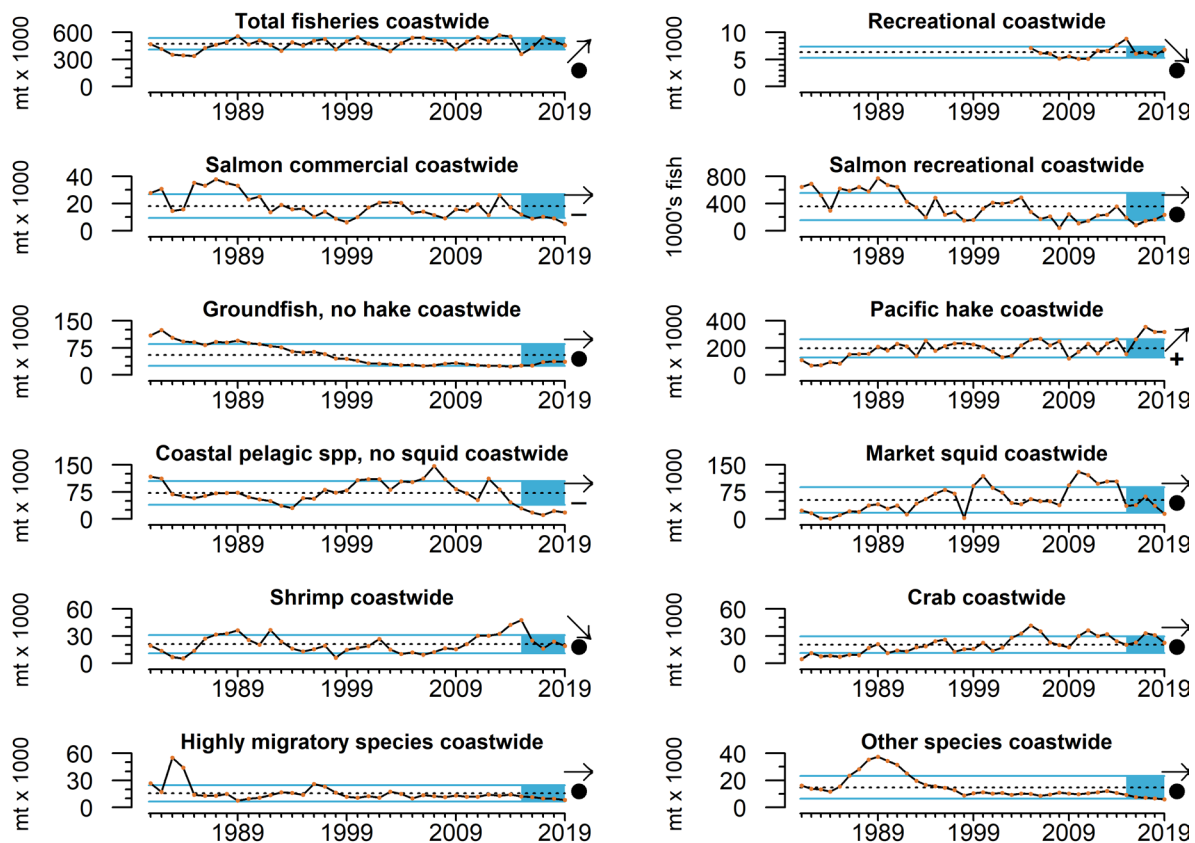


Figure 55. Annual landings of U.S. West Coast commercial (data from [PacFIN](http://pacfin.psmfc.org)^{*} and NORPAC [North Pacific Groundfish Observer Program]) and recreational (data from [RecFIN](http://www.recfin.org/)[†] and the CDFW Pelagic Fisheries and Ecosystem Data Sharing Index) fisheries, including total landings across all fisheries, 1981–2019. Lines, colors, and symbols as in Fig 3a.

^{*} <http://pacfin.psmfc.org>

[†] <http://www.recfin.org/>

Methods for calculating total landings in recreational fisheries have changed recently, leading to shorter comparable time series and different estimates from previous reports. Recreational landings (excluding Pacific salmon and Pacific halibut [*Hippoglossus stenolepis*]) were close to the time series average in 2019, but have had a declining trend from 2015–19 (Figure 55). The decline in recreational landings has been driven primarily by decreases in yellowfin tuna (*Thunnus albacares*), yellowtail (*Seriola lalandi dorsalis*), and lingcod (*Ophiodon elongatus*) landings in California, and decreases in albacore tuna (*Thunnus alalunga*) and black rockfish (*Sebastes melanops*) landings in Oregon and Washington. Landings for recreationally caught salmon (Chinook and coho) showed no trends and were within 1 SD of the time series mean, but landings were in the lower range of time series observations (Figure 55). Additional information on state-by-state landings are available in Harvey et al. (2020), Appendix K.

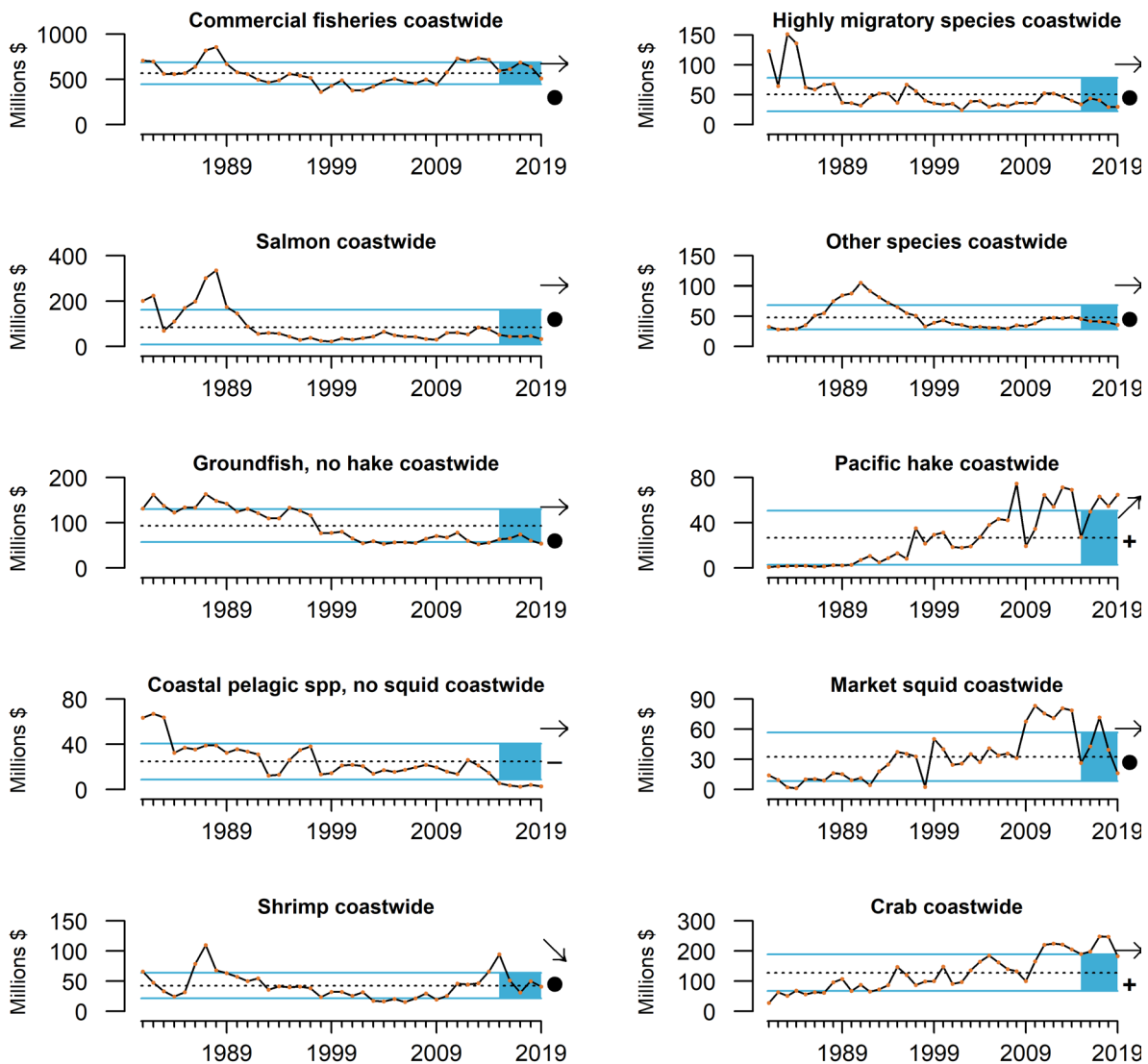


Figure 56. Annual revenue (ex-vessel value in 2019 dollars) of U.S. West Coast commercial fisheries (data from PacFIN), 1981–2019. Pacific hake revenue includes shoreside and at-sea hake revenue values from PacFIN, NORPAC, and NMFS Office of Science and Technology. Lines, colors, and symbols as in Fig 3a.

Total revenue across all U.S. West Coast commercial fisheries in 2019 was \$510M, a decrease of 20% from 2018 revenue (\$640M; Figure 56). Over the last five years, total landings revenue showed no clear trend and was within 1 SD of the time series average; however, revenue declines have been steep over the last two years (particularly in 2019), driven primarily by decreases in crab and market squid fisheries and a high proportion of hake, which have a relatively low price per pound compared to other species in the landings. Over the last five years (2015–19), revenues from Pacific hake and crab fisheries were >1 SD above their respective time series averages, while CPS finfish revenue was >1 SD below the time series average. Revenues from commercial fisheries targeting other species groups remained fairly stable from 2015–19, with the exception of shrimp, which had a steep decrease in revenue from 2015 to 2017, but remained within 1 SD of the long-term average. State-by-state revenues are available in Harvey et al. (2020), Appendix K.

4.2 Bottom Trawl Contact with Seafloor

Benthic marine species, communities, and habitats can be impacted by geological events (e.g., earthquakes, fractures, and slumping), oceanographic processes (internal waves, sedimentation, and currents), and human activities (bottom contact fishing, mining, and dredging). Such disturbances can lead to mortality of vulnerable benthic species and disruption of food web processes. These effects may differ among types of seafloor habitat (hard, mixed, or soft sediments) and may be particularly dramatic in sensitive environments (e.g., seagrass, algal beds, coral and sponge reefs, or rocky substrates) relative to soft sediments. The exploration of resources (e.g., oil, gas, and minerals) and marine fisheries often tend to operate within certain habitat types more than others, and long-term impacts of these activities may cause negative changes in biomass and the production of benthic communities. Thus, spatially explicit indicators are necessary to provide information for spatial management of specific human activities in relation to these resources.

We developed estimates of distances trawled by federally managed groundfish bottom trawl fisheries from 1999 to 2018, the most recent year for which data were available. We calculated trawling distances based on set and haul-back locations. Data come from state logbooks as reported to PacFIN and processed by NWFSC's West Coast Groundfish Observer Program. Processing includes removing tows that appear to have errors in the logbook entries (e.g., set or haul-back location is on land; vessel speed necessary to make the tow was >5 knots; etc.). These data are presented here in two ways. The first is at a coastwide scale and broken out by ecoregion (Northern, Central, and Southern CCE), substrate type (hard, mixed, and soft), and depth zone (shelf, upper slope, and lower slope). The second approach presents much finer spatial resolution of bottom trawl contact (2 × 2-km grid cells across the shelf and slope).

At the scale of the entire coast, federal groundfish bottom trawl gear contact with seafloor habitat remained consistently at low levels from 2014–18 relative to the available time series (Figure 57, top). During this period, the vast majority of bottom trawl gear contact occurred in soft shelf and upper slope habitat (Figure 57, bottom). The Northern CCE has seen the most bottom trawl fishing gear contact with seafloor habitat, with nearly four times more distance trawled than in the Central and >40 times more than in the Southern CCE, where very little bottom trawling has occurred during the available time series. A shift in trawling effort from shelf to upper slope habitats was observed during the mid-2000s, which in part corresponded to depth-related spatial closures implemented by PFMC.

To examine finer-scale bottom contact by bottom trawl gear in federally managed fisheries, we used the same logbook data to estimate distances trawled on a 2×2 -km grid from 2002 to 2018. For each grid cell, we mapped: a) the total distance trawled in the most recent year of available data (2018); b) the 2018 departure (anomaly) from the long-term mean for the cell; and c) the most recent five-year trend in the cell (Figure 58). Note that the number of cells included in the five-year trend analysis is greater than in the 2018 anomaly analysis because there must be data from at least three vessels in a given cell for the period of analysis in order to conform to data confidentiality requirements.

Cumulative trawl distances within a given 2×2 -km cell in 2018 were generally less than 50 km, though some cells (e.g., off of Central Washington and just north of Cape Mendocino) had as much as 200 km of total trawling (Figure 58a). Distance trawled in 2018 was >1 SD above average (anomalously high relative to the available 2002–18 time series) in the red cells in Figure 58b, with notable concentrations off of Central Washington, multiple bands off of Northern and Central Oregon, and just north of Cape Mendocino. Distance trawled was >1 SD below average (anomalously low) in the dark blue cells in Figure 58b, with notable areas off of Northern Washington, a stretch of trawlable bottom south of Cape Blanco into northern California, and south of Cape Mendocino. Increasing trends from 2014–18 are shown in red in Figure 58c and indicate a short-term increase in trawl distance greater than 1 SD of the time series average for a cell. Areas with increasing five-year trends are concentrated off of Central Washington, Central and Northern Oregon, and north of Cape Mendocino. Decreasing trends from 2014–18 (in dark blue, five-year trends that declined by at least 1 SD of the time series average for a cell) occurred in many areas, with concentrations off of much of Washington, south of Cape Blanco, and south of Cape Mendocino (Figure 58c).

Because it highlights the variation of status and trends of trawling activity in specific areas across the CCE, the fine-scale spatial indicator of trawl distance provides more information than the time series of the total coastwide distance trawled, which indicates that bottom trawl gear contact with the seafloor was at low levels and had no trend from 2014–18 (Figure 57, top). With new spatial closures and openings in the federally managed

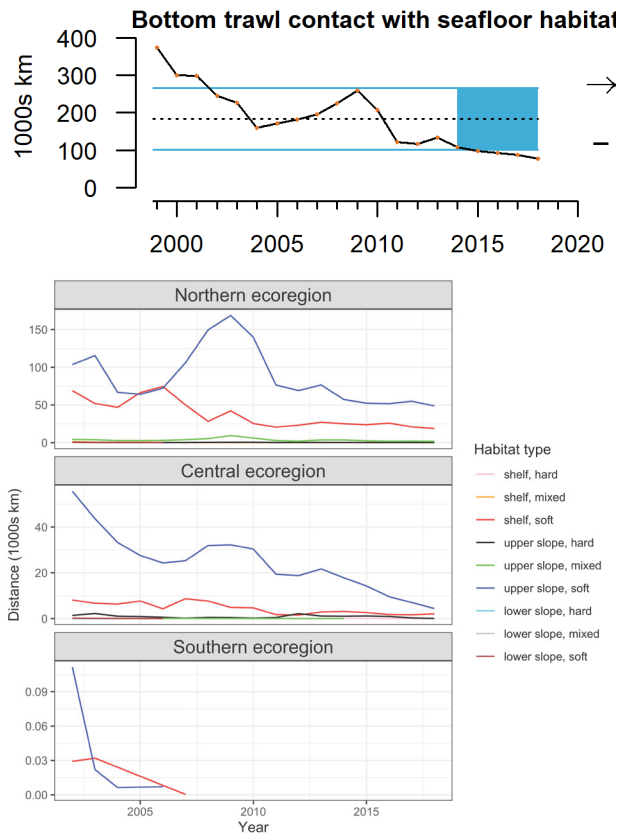


Figure 57. Distance (1,000s km) trawled by federally managed groundfish bottom trawl fisheries across the entire CCE (top; 1999–2018) and within each ecoregion (bottom three panels; 2002–18). Lines, colors, and symbols, top panel, as in Fig 3a. Data for total distance trawled by federally managed bottom trawl fisheries provided by NWFSC West Coast Groundfish Observer Program.

a) 2018 distance trawled

b) 2018 anomaly

c) 2014-2018 trend

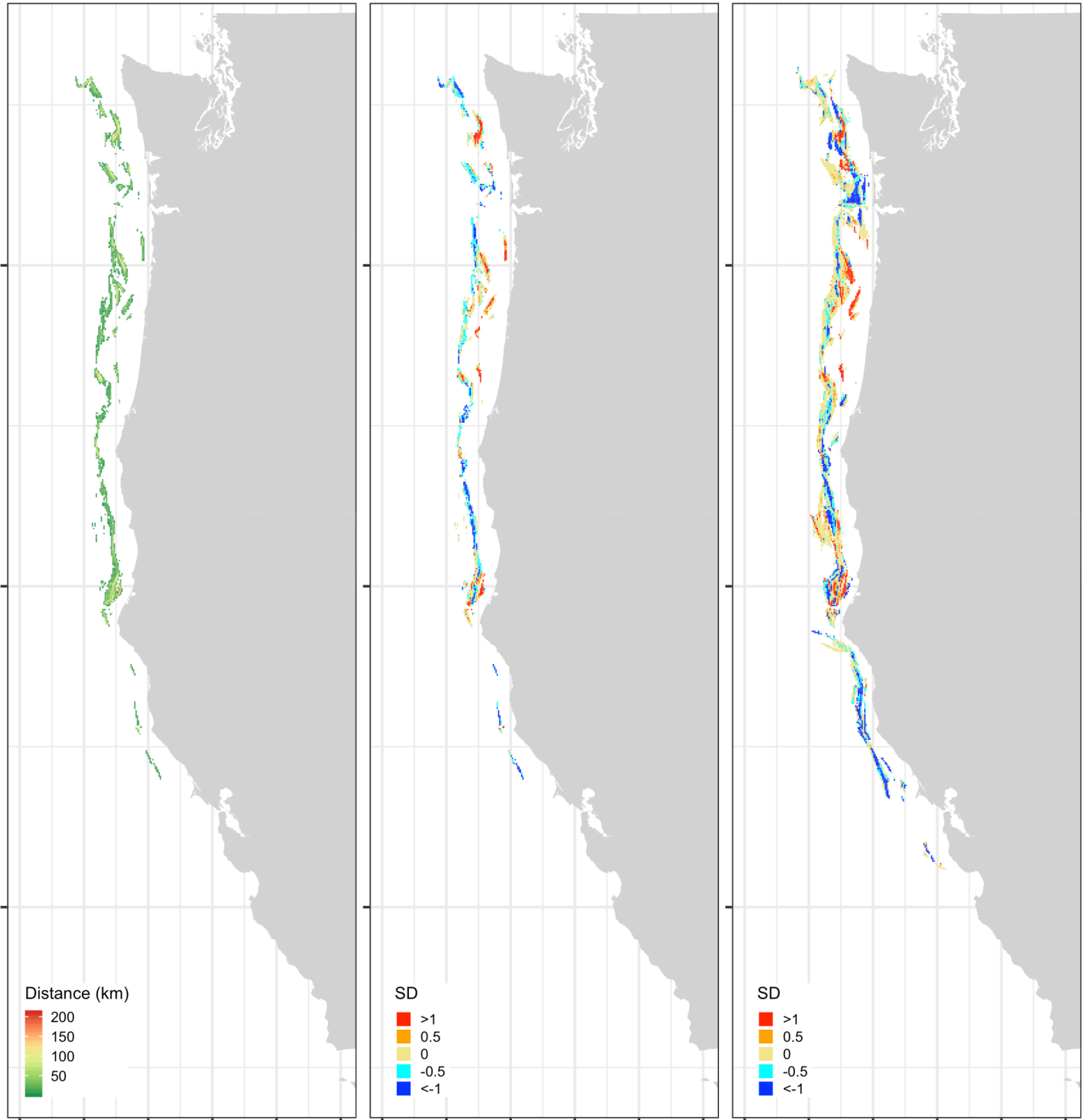


Figure 58. Spatial representation of seafloor contact by bottom trawl gear from federal groundfish fisheries, calculated from annual distances trawled within each 2×2 -km grid cell, 2002–18. (left) Total distances trawled in 2018. (middle) Anomalies in 2018 relative to the long-term mean. (right) Normalized trend values for most-recent 5-yr period (2014–18). Grid cell values >1 (red) or <-1 (blue) represent a cell in which the 2018 anomaly was at least 1 SD away from the long-term mean of that cell or a cell in which the 5-yr trend changed by at least 1 SD of the long-term mean of that cell during the time period. Data for total distance trawled by federally managed bottom trawl fisheries provided by NWFSC West Coast Groundfish Observer Program.

groundfish fishery beginning in 2020,¹¹ this indicator will be of interest over the next several years, as bottom trawl fishing effort is likely to change. Subsequent efforts will incorporate state bottom trawling fisheries effort (e.g., for shrimp), fixed-gear fisheries, and other nonfishing human activities that could affect seafloor habitats. These spatial indicators should provide useful data to understand how fishing behavior might interact with other ocean-use sectors (e.g., offshore renewable energy or aquaculture).

4.3 Aquaculture Production and Seafood Consumption

Aquaculture production is an indicator of seafood demand, and also may be related to some benefits (e.g., water filtration by bivalves, nutrition, or income and employment) or impacts (e.g., habitat conversion, waste discharge, or nonindigenous species introductions). Shellfish (Figure 59, top) and finfish (Figure 59, bottom) aquaculture production in the CCE showed no trends and were within 1 SD of the time series mean from 2014–18, but production for each was near the uppermost limit of time series observations. Patterns for shellfish aquaculture are driven by production in Washington State, which is home to >90% of coastwide shellfish production. Commercial finfish aquaculture in marine waters consists exclusively of Atlantic salmon (*Salmo salar*) raised in net pens. Net-pen rearing of Atlantic salmon in Washington marine waters is scheduled to be phased out by 2022 due to regulatory changes.

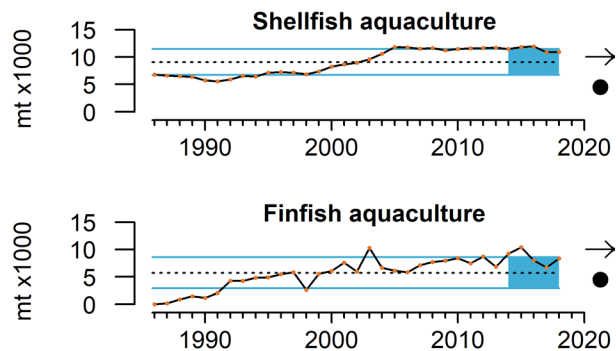


Figure 59. Aquaculture production of shellfish (clams, mussels, oysters) and finfish (Atlantic salmon) in CCE waters from 1986–2018. Lines, colors, and symbols as in Fig 3a. Shellfish production data retrieved and summed together from Washington Department of Fish and Wildlife’s Commercial Harvest Data Team, Oregon Department of Agriculture, and the California Department of Fish and Game; finfish production data from Washington Department of Fish and Wildlife’s Commercial Harvest Data Team.

Total consumption of edible and nonedible fisheries products in the United States was above the long-term average from 2014–18 (Figure 60, top), continuing the overall upward trend generally observed in this indicator’s time series since the early 1970s. Per-capita consumption was stable and remained near the upper end of the time series range from 2014–18 (Figure 60, bottom). With increasing human populations and recommendations in U.S. dietary guidelines¹² to increase seafood intake, total consumption of seafood products might be expected to increase in years to come. However, disruptions in food supply chains and markets caused by the COVID-19 pandemic in 2020 will affect U.S. seafood availability and consumption, and will likely be evident in this indicator time series in the future.

¹¹ See Amendment 28 to the Pacific Fishery Management Council Groundfish Fishery Management Plan; <https://www.pcouncil.org/actions/amendment-28-pacific-coast-groundfish-essential-fish-habitat-rockfish-conservation-area-modifications-and-magnuson-act-discretionary-closures/>

¹² <https://go.usa.gov/xGSb6>

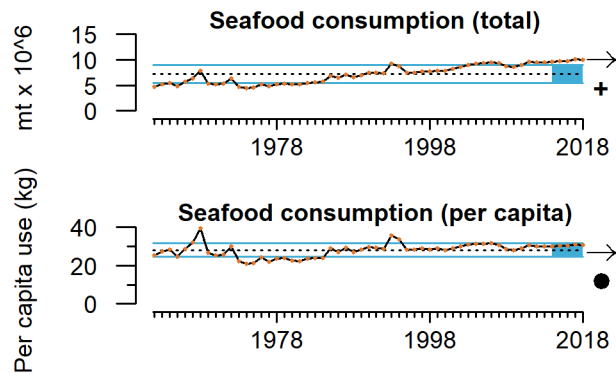


Figure 60. Total (in millions of metric tons) and per-capita (in kg) consumption of edible and nonedible fisheries products in the United States, 1962–2018. Lines, colors, and symbols as in Fig 3a. Data can be found in NOAA’s annual Fisheries of the United States reports (<https://www.fisheries.noaa.gov/resource/document/fisheries-united-states-2018-report>).

4.4 Nonfishing Human Activities

The CCIEA Team compiles and regularly updates indicators of nonfishing human activities in the CCE, some of which may have effects on focal species, ecosystem processes and services, fisheries, and coastal communities. These activities relate to different ocean-use sectors like shipping and energy extraction, or to terrestrial sectors that result in nutrient inputs to coastal waters. We update many of these indicators annually, although some are updated less frequently due to the time required by the source agencies to release their data.

4.4.1 Commercial shipping

Approximately 90% of world trade is carried by the international maritime shipping industry. The volume of cargo moved through U.S. ports increased 3% per year from 2000 to 2017 (U.S. Army Corps of Engineers, Waterborne Commerce Statistics Center¹³), and is expected to continue to increase at that rate through 2030 (Lloyd’s Register et al. 2013). Marine ecosystem impacts associated with commercial shipping include interactions between fishing and shipping vessels; ship strikes of protected species; and underwater noise that affects reproduction, recruitment, migration, behavior, and communication of target and protected species.

Commercial shipping activity is measured by summing the total distances traveled within the CCE by vessels reported under “foreign waterborne” traffic to the U.S. Army Corps of Engineers. “Domestic coastwise” traffic is not included in this calculation because their trips make up only 10% of distances traveled, have no effect on the overall status and trend, and are more difficult to update in a timely manner than the “foreign waterborne” data. Commercial shipping activity in the CCE was stable

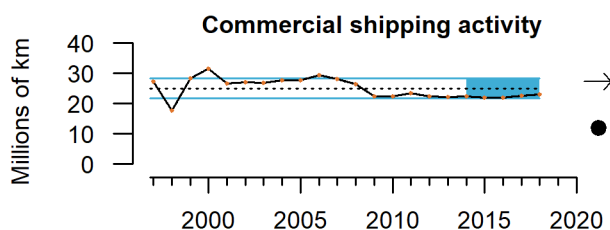


Figure 61. Distance transited by foreign commercial shipping vessels in the CCE, 1997–2018. Lines, colors, and symbols as in Fig 3a. Foreign vessel entrance and clearance data from the U.S. Army Corps of Engineers’ Waterborne Commerce Statistics Center.

¹³ <https://www.iwr.usace.army.mil/About/Technical-Centers/WCSC-Waterborne-Commerce-Statistics-Center/>

and near the lower bounds of the time series from 2014–18 (Figure 61). This contrasts drastically with global estimates of shipping activity, which increased nearly 400% over the last 20 years and are projected to increase nearly 250% between 2010 and 2030 (Lloyd’s Register et al. 2013). Regional differences, lagging economic conditions, and different data sources may be responsible for the observed differences. For example, most maritime shipping activity indicators are based on cargo volume and value of goods, and thus capture different attributes of the industry than we show here (distances traveled). We consider vessel activity as indicated by distance traveled to be more relevant to CCE biota and human activities than the volume or value of the cargo on board. Changes in major trading routes and vessel characteristics (e.g., vessel length and cargo capacity) may also be responsible for the observed differences between global indicators and estimates for the CCE.

4.4.2 Oil and gas activity

Oil and natural gas are extracted in offshore drilling in the CCE, with all active leases located in Southern California in the region of Point Conception and landward of the Channel Islands. Risks posed by offshore oil and gas activities include the release of hydrocarbons, smothering of benthos, sediment anoxia, benthic habitat loss, and the use of explosives. Petroleum products consist of thousands of chemical compounds such as polycyclic aromatic hydrocarbons (PAHs), which may impact marine fish health and reproduction. The effects of the physical presence of oil rigs on fish stocks are less conclusive, as rig structures may provide some habitat benefits.

Offshore oil and gas activity in the CCE has declined steeply and was well below the time series average over 2014–18, the last five years of available data (Figure 62). Offshore oil and gas production in the CCE has been decreasing steadily since the mid-1990s.

4.4.3 Nutrient loading

Nutrient input into coastal waters occurs through natural cycling of materials, as well as through loadings derived from human activities. Nutrient loading is a leading cause of contamination, eutrophication, and related impacts in streams, lakes, wetlands, estuaries, and groundwater throughout the United States. Nutrient input data into all CCE waters have not been updated since 2012, and are thus not presented here.

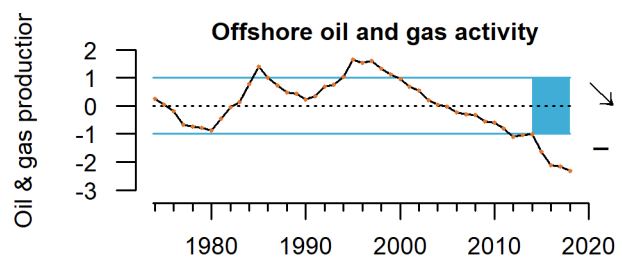


Figure 62. Standardized index of the sum of oil and gas production from offshore wells in California, 1974–2018. Lines, colors, and symbols as in Fig 3a. State oil production data come from annual reports of the [California State Department of Conservation’s Division of Oil, Gas, and Geothermal Resources](https://www.conservation.ca.gov/calgem/pubs_stats/annual_reports/Pages/annual_reports.aspx).^{*} Federal oil production data come from the [Bureau of Safety and Environmental Enforcement](https://www.data.bsee.gov/Main/PacificProduction.aspx).[†] State and federal natural gas production data come from the [U.S. Energy Information Administration](https://www.eia.gov/dnav/ng/ng_prod_sum_dc_rcatf_mmcf_a.htm).[‡]
^{*} https://www.conservation.ca.gov/calgem/pubs_stats/annual_reports/Pages/annual_reports.aspx
[†] <https://www.data.bsee.gov/Main/PacificProduction.aspx>
[‡] https://www.eia.gov/dnav/ng/ng_prod_sum_dc_rcatf_mmcf_a.htm

5 Human Wellbeing

Human wellbeing is inextricably linked to the marine, coastal, and upland environments of the CCE. This relationship depends on qualities of both the biophysical environment and the human social system. The marine ecosystem of the California Current supports human wellbeing through fisheries sustenance and income, aesthetic and recreational opportunities, and a variety of economically and socially discernible contributions. Human wellbeing may be measured at the individual, community, and societal levels, and includes many component elements, some of which have been described and addressed within the output of a CCIEA-originated Social Wellbeing in Marine Management (SWIMM) working group (Breslow et al. 2017).

The subsections below outline several indicators of human wellbeing in the CCE. Community measures of social vulnerability are a way to partially assess human wellbeing at the community level. Social vulnerability measures have been developed and applied to communities where commercial and recreational fishing are important, and the relative salience of marine fishing is likewise available through reliance and engagement indicators that tie communities to marine fishing within the California Current. Economically, the relative fishery diversity within commercial fishing income provides an indicator of wellbeing at both the individual vessel level, as well as the port and community levels.

5.1 Social Vulnerability

Coastal community vulnerability indices are generalized socioeconomic vulnerability metrics for communities. The Community Social Vulnerability Index (CSVI) is derived from social vulnerability data (demographics, personal disruption, poverty, housing characteristics, housing disruption, labor force structure, natural resource labor force, etc.; Jepson and Colburn 2013). The CCIEA Team has been monitoring CSVI in coastal communities that are highly dependent upon fishing. Fishery **dependence** can be expressed by two terms, or by a composite of both: engagement and reliance. **Engagement** refers to the total extent of fishing activity in a community, whereas **reliance** is the per-capita engagement of a community. The commercial fishing engagement index is based on an analysis of variables reflecting commercial fishing engagement in 1,140 communities (e.g., fishery landings, revenues, permits, and processing). The commercial fishing reliance index applies the same factor analysis approach to these variables on a per-capita basis. Thus, in two communities with equal engagement, the community with the smaller population would have a higher reliance on its fisheries activities.

Figure 63 plots CSVI against per-capita commercial fishing reliance for 2017 in the five communities with the highest reliance on commercial fishing in each of five regions: Washington, Oregon, and Northern, Central, and Southern California (five communities per region; states are color-coded in the figures). Of note are communities that are above and to the right of the dashed lines, which indicate above-average levels of social vulnerability (horizontal dashed line) and commercial fishing reliance (vertical dashed line) from among all U.S. West Coast communities. For example, Port Orford and Westport have high fishing reliance (14.3 and 2.1 SD above average, respectively) and high CSVI (3.4 and 6.7 SD above

average) compared to other coastal fishing communities. Coastal fishing communities that are outliers in both indices may be especially socially vulnerable to downturns in commercial fishing due to ecosystem changes, management actions, or market forces.

Figure 64 plots CSVI against total commercial fisheries engagement in 2017 in the five communities with the highest engagement in commercial fishing in each of five regions. Again, communities above and to the right of the dashed lines are at least 1 SD above the coastwide averages of both indices. Of note are fishing-oriented communities like Westport, Crescent City, Coos Bay, Newport, Fort Bragg, Eureka, and Winchester Bay, which have relatively high commercial fishery engagement results and also a high CSVI composite result.

In last year's tech memo (Harvey et al. 2019), we also compared CSVI with recreational fishing reliance, which reflects per-capita recreational fishing engagement (e.g., number of boat launches, number of charter boat and fishing guide license holders, number of charter boat trips, bait and tackle shops, etc.). Unfortunately, the data used last year were available only through 2016 and have not been updated since; we will have to identify alternate indices of recreational engagement for future reports.

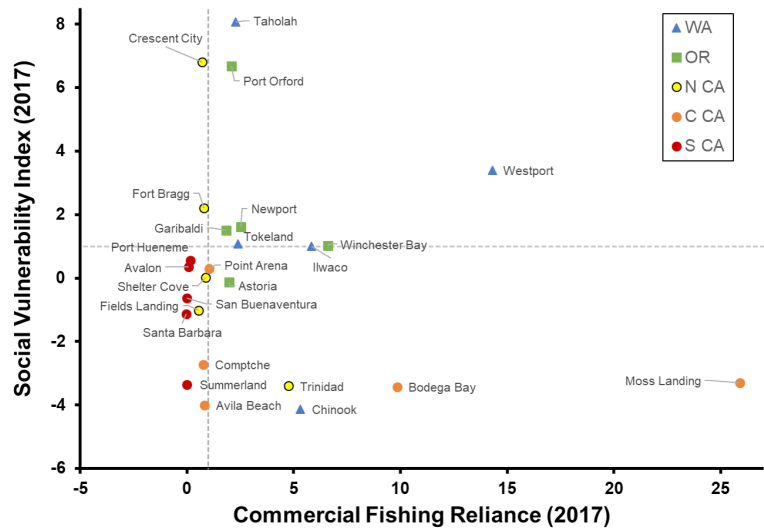


Figure 63. Commercial fishing reliance and social vulnerability scores as of 2017, plotted for 25 communities from each of 5 CCE regions: WA, OR, NCC, CCC, and SCC. Top 5 highest-scoring communities for commercial fishing reliance were selected from each region. CSVI and reliance data provided by K. Norman, NMFS/NWFSC, and A. Phillips, PSMFC, with data derived from the U.S. Census Bureau's American Community Survey (ACS; <https://www.census.gov/programs-surveys/acs/>) and PacFIN (<http://pacfin.psmfc.org>), respectively.

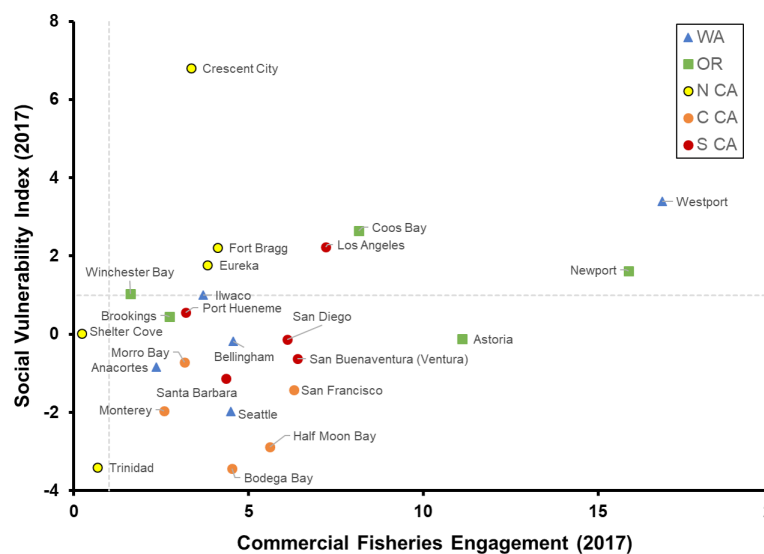


Figure 64. Commercial fisheries engagement and social vulnerability scores as of 2017, plotted for 25 communities from each of 5 CCE regions: WA, OR, NCC, CCC, and SCC. Top 5 highest-scoring communities for commercial fisheries engagement were selected from each region. CSVI and engagement data provided by K. Norman, NMFS/NWFSC, and A. Phillips, PSMFC, with data derived from the ACS and PacFIN.

This is an emerging area of work, and as we have discussed in past reports, these data are difficult to ground-truth and require further study to understand the importance of these relationships. We also lack data for many communities altogether, including many tribal communities. An effort to examine communities that may be particularly affected by ecosystem shifts, with respect to the Magnuson–Stevens Act’s National Standard 8,¹⁴ is ongoing.

5.2 Fishing Revenue Diversification

Catches and prices from many fisheries exhibit high interannual variability leading to high variability in fisher revenue, but variability can be reduced by diversifying fishing activities across multiple fisheries or regions (Kasperski and Holland 2013). It should be noted that there may be good reasons for individuals to specialize, including reduced costs or greater efficiency; thus, while diversification may reduce income variation, it does not necessarily promote higher average profitability. We use the effective Shannon index (ESI) to measure diversification among 28,000 fishing vessels off the U.S. West Coast and Alaska. The index has an intuitive meaning: ESI = 1 when all revenues are from a single species group and region; ESI = 2 if fishery revenues are spread evenly across two fisheries; and so on. It increases both as revenues are spread across *more* fisheries and as revenues are spread *more evenly* across fisheries.

In 2018 (the most recent year analyzed), revenue diversification of the fleet of vessels fishing off the U.S. West Coast and in Alaska was essentially unchanged from 2017 (Figure 65). However, the fleet was less diverse on average than at any time in the preceding 37 years, and this was true for most home states, revenue categories, and size classes (Figures 65b–d). Diversification rates for most categories of vessels fishing on the U.S. West Coast have been trending down for several years, but there was little change over the last year for most vessels. The California fleet had a slight increase in diversification in recent years, while diversification of the Washington and Oregon fleets continued to decline (Figure 65b). Long-term trends for vessels with landings in west coast states are similar to those for the larger fleet of vessels fishing the U.S. West Coast and/or Alaska (Figure 65a), with both showing decreasing diversification over the full 38-year time series. This is due both to entry and exit of vessels, and changes for individual vessels. Over time, less-diversified vessels have been more likely to exit, which would have a positive effect on diversification; however, vessels that remain in the fishery have also become less diversified, at least since the mid-1990s, and newer entrants have generally been less diversified than earlier entrants. The net result is a moderate decline in average diversification since the mid-1990s or earlier. Within the average trends are wide ranges of diversification levels and strategies, within and across vessel classes, and some vessels remain highly diversified. Increased diversification from one year to the next may not always indicate an improvement. For example, if a class of vessels was heavily dependent on a single fishery with highly variable revenues (e.g., Dungeness crab), a decline in that fishery might force vessels into other fisheries, causing average diversification to increase.

As is true with individual vessels, the variability of landed value at the port level is reduced with greater diversification of landings. Diversification of fishing revenue has declined over the last several decades for some ports (Figure 66). Examples of ports where revenue diversification has declined in recent decades include Seattle and many ports in Southern

¹⁴ <https://www.fisheries.noaa.gov/national/laws-and-policies/national-standard-guidelines>

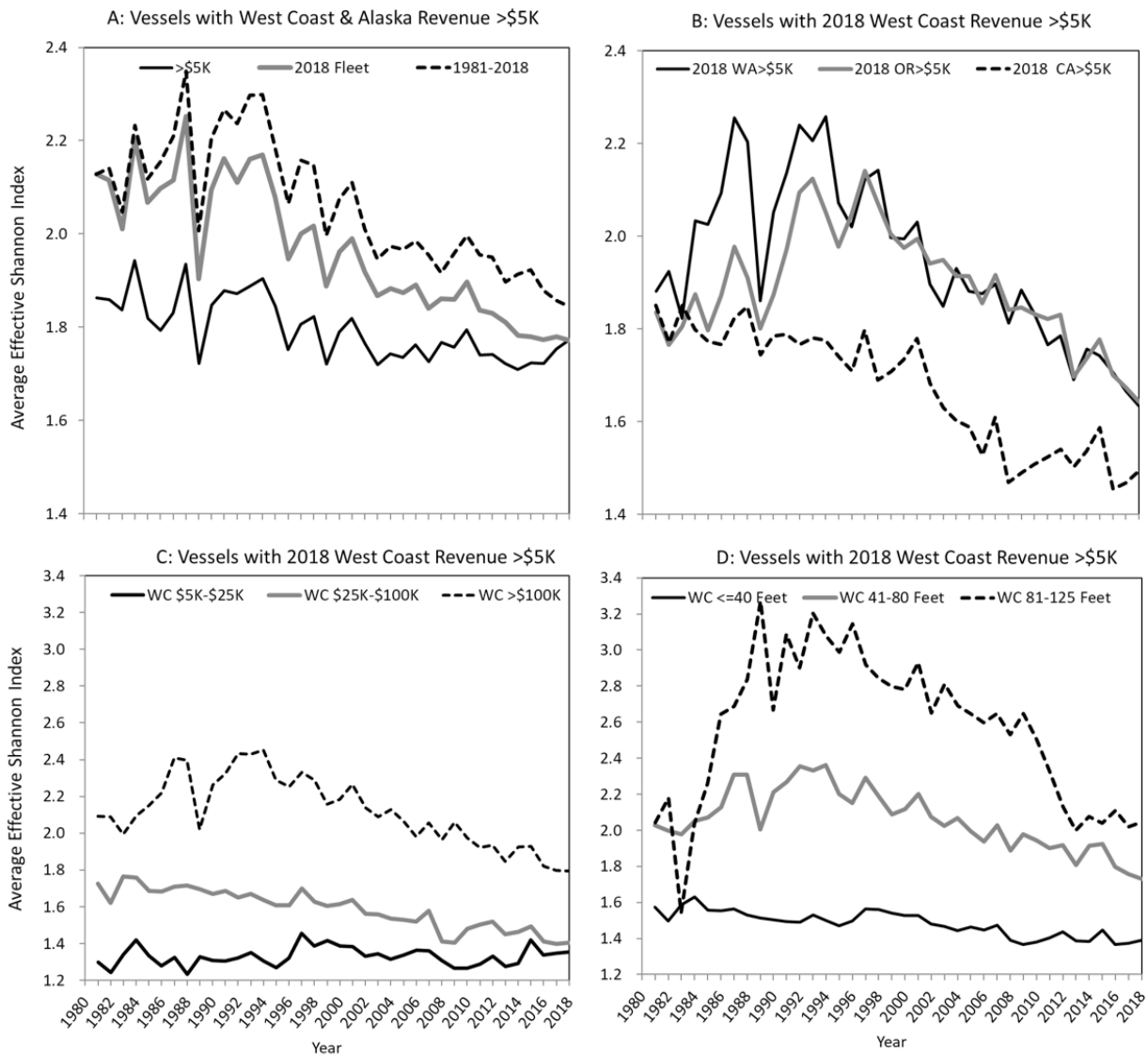


Figure 65. Trends in average diversification for U.S. West Coast and AK fishing vessels with over \$5K in average revenues (top left) and for vessels in the 2018 U.S. West Coast Fleet with over \$5K in average revenues, broken out by state (top right), by average gross revenue class (bottom left), and by vessel length class (bottom right). Fishery diversification estimates provided by D. Holland, NMFS/NWFSC, and S. Kasperski, NMFS/AFSC.

Oregon and California. However, a few ports have become more diversified, including Bellingham and Westport in Washington. Diversification in Astoria, Oregon, has been increasing from 2006–16, but has decreased in recent years, while Brookings, Oregon, has had an erratic increasing trend. Diversification scores are highly variable year-to-year for some ports, particularly those in Southern Oregon (Brookings) and Northern California (Crescent City, Eureka) that depend heavily on the Dungeness crab fishery, which has highly variable landings. Some ports saw a decrease in diversification between 2017 and 2018, but others saw an increase. No clear recent trends are apparent.

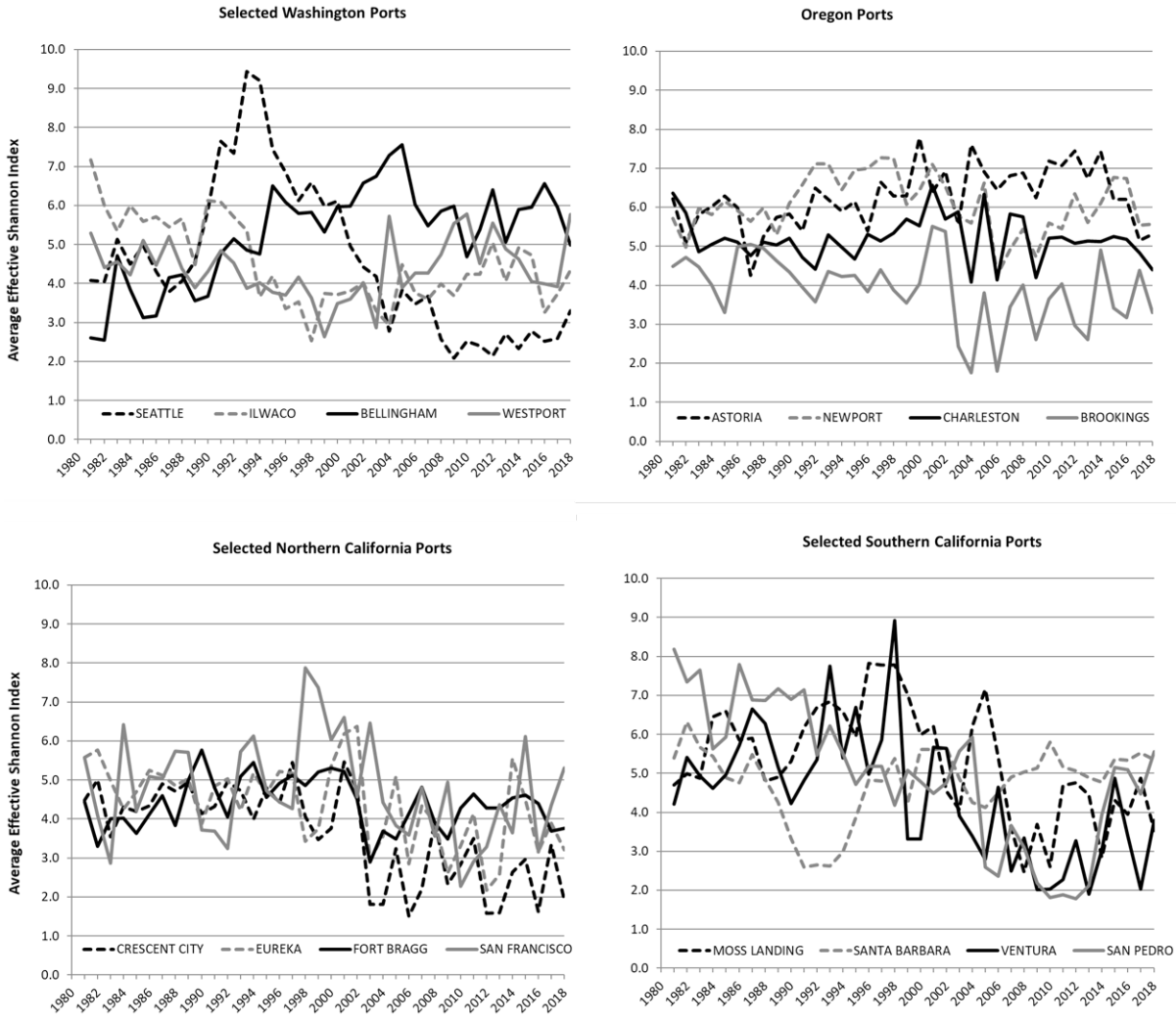


Figure 66. Trends in commercial fishing vessel revenue diversification in major WA, OR, and CA ports, 1981–2018. Fishery diversification estimates provided by D. Holland, NMFS/NWFSC, and S. Kasperski, NMFS/AFSC.

6 Synthesis

As outlined in the [Executive Summary](#), many indicators from the California Current Ecosystem in 2019 pointed toward a natural system that generally experienced average to above-average conditions in the Northern and Southern regions, but a mix of conditions in the Central region, including many indicators of below-average productivity across several trophic levels. Other prevalent signals included some of the highest measurements of anchovy abundance on record, and another large marine heatwave that lasted for much of the latter half of 2019 and intersected with the coast from Washington to Northern California in September. This event likely contributed further to the surplus heat stored in subsurface waters by the series of anomalous warm events that have affected the CCE since 2014. Finally, commercial fishery landings and revenue declined for the second straight year, with landings in 2019 falling close to the long-term average of the last four decades, and roughly 70% of all landings in the form of Pacific hake.

We remain concerned about the amount of stored heat in waters along the U.S. West Coast and throughout the North Pacific. The North Pacific basin has experienced a series of large-scale, intense warming events over the past seven years, beginning with the 2013–16 northeastern Pacific Ocean marine heatwave and followed by a major El Niño in 2016, another large marine heatwave in 2019 (Amaya et al. 2020), and weaker marine heatwaves and El Niño conditions within that time frame as well (e.g., Figures 5 and 8). Effects of these surface-oriented warming events have extended deep into the water column throughout the CCE since 2014 (Figures 7 and 11; see also Harvey et al. 2020, Appendix D). Unless it dissipates, this stored heat may leave the system especially susceptible to development of new marine heatwaves, or maintain anomalously warm conditions that could be suboptimal for species and habitats of value in the system. We are continually monitoring SSTa in the North Pacific and making information on potential new marine heatwaves available on a [dedicated CCIEA webpage](#)¹⁵; as of early May 2020, when this report was being completed, there was a sizeable and intense marine heatwave occupying much of the North Pacific west of long 135°W, and a smaller but intense event in coastal waters off of Southern California.

Many of the ecological surveys of the CCE in 2019 had concluded before the 2019 marine heatwave extended into CCE waters, and we thus have limited information on how it may have affected species or ecological processes. Some field observations co-occurred with the 2019 marine heatwave, including the relatively early truncation of the period in which the northern copepod biomass anomaly was strongly positive off of Newport, Oregon (Figure 30), but it is premature to connect that decline in quality of prey zooplankton to the 2019 marine heatwave.

Furthermore, at the time this report was being completed, many ecological surveys of the CCE in 2020 had been delayed or cancelled in response to the COVID-19 pandemic, which will further limit our ability to measure ecological responses to anomalous warming in 2019 or any similar events that occur in 2020. We can certainly anticipate that the COVID-19 pandemic will cause massive disruption to the human dimensions components of the CCE

¹⁵ <https://www.integratedecosystemassessment.noaa.gov/regions/california-current/cc-projects-blobtracker>

in 2020, due to the many changes caused by social distancing policies and closures of domestic and international markets for west coast seafood. Next year's version of this report will very likely have considerable space dedicated to information on how fishery-dependent coastal communities and fisheries as a whole were affected by the COVID-19 pandemic, though it will likely be years before the impacts on the human system and feedbacks on the ecological system are understood.



References

- Abell, R., M. L. Thieme, C. Revenga, M. Bryer, M. Kottelat, N. Bogutskaya, B. Coad, N. Mandrak, S. C. Balderas, W. Bussing, M. L. J. Stiassny, P. Skelton, G. R. Allen, P. Unmack, A. Naseka, R. Ng, N. Sindorf, J. Robertson, E. Armijo, J. V. Higgins, T. J. Heibel, E. Wikramanayake, D. Olson, H. L. Lopez, R. E. Reis, J. G. Lundberg, M. H. S. Perez, and P. Petry. 2008. Freshwater ecoregions of the world: A new map of biogeographic units for freshwater biodiversity conservation. *BioScience* 58:403–414.
- Alexander, J. D., S. L. Hallett, R. W. Stocking, L. Xue, and J. L. Bartholomew. 2014. Host and parasite populations after a ten year flood: *Manayunkia speciosa* and *Ceratonova* (syn *Ceratomyxa*) *shasta* in the Klamath River. *Northwest Science* 88:219–233.
- Amaya, D. J., A. J. Miller, S. P. Xie, and Y. Kosaka. 2020. Physical drivers of the summer 2019 North Pacific marine heatwave. *Nature Communications* 11:1–9.
- Barton, A., B. Hales, G. G. Waldbusser, C. Langdon, and R. A. Feely. 2012. The Pacific oyster, *Crassostrea gigas*, shows negative correlation to naturally elevated carbon dioxide levels: Implications for near-term ocean acidification effects. *Limnology and Oceanography* 57:698–710.
- Bathwick, R., J. Beck, R. Carle, and M. Hester. 2019. Año Nuevo State Park seabird conservation and habitat restoration report 2019. Unpublished Report to California Department of Parks and Recreation, Año Nuevo State Park.
- Bednarsek, N., R. A. Feely, J. C. P. Reum, B. Peterson, J. Menkel, S. R. Alin, and B. Hales. 2014. *Limacina helicina* shell dissolution as an indicator of declining habitat suitability owing to ocean acidification in the California Current Ecosystem. *Proceedings of the Royal Society B – Biological Sciences* 281:20140123.
- Bradford, M. J., and J. S. Heinonen. 2008. Low flows, instream flow needs and fish ecology in small streams. *Canadian Water Resources Journal* 33:165–180.
- Breslow, S. J., M. Allen, D. Holstein, B. Sojka, R. Barnea, X. Basurto, C. Carothers, S. Charnley, S. Coulthard, N. Dolsak, J. Donatuto, C. Garcia-Quijano, C. C. Hicks, A. Levine, M. B. Mascia, K. Norman, M. Poe, T. Satterfield, K. St. Martin, and P. Levin. 2017. Evaluating indicators of human well-being for ecosystem-based management. *Ecosystem Health and Sustainability* 3:1–18.
- Brodeur, R. D., T. D. Auth, and A. J. Phillips. 2019. Major shifts in pelagic micronekton and macrozooplankton community structure in an upwelling ecosystem related to an unprecedented marine heatwave. *Frontiers in Marine Science* 6:212.
- Brodeur, R. D., J. P. Fisher, R. L. Emmett, C. A. Morgan, and E. Casillas. 2005. Species composition and community structure of pelagic nekton off Oregon and Washington under variable oceanographic conditions. *Marine Ecology Progress Series* 298:41–57.
- Browman, H., P. Cury, R. Hilborn, S. Jennings, H. Lotze, P. Mace, S. Murawski, D. Pauly, M. Sissenwine, K. Stergiou, and D. Zeller. 2004. Perspectives on ecosystem-based approaches to the management of marine resources. *Marine Ecology Progress Series* 274:269–303.
- Burke, B. J., W. T. Peterson, B. R. Beckman, C. Morgan, E. A. Daly, and M. Litz. 2013. Multivariate models of adult Pacific salmon returns. *PLOS One* 8:e54134.
- Chan, F., J. A. Barth, J. Lubchenco, A. Kirincich, H. Weeks, W. T. Peterson, and B. A. Menge. 2008. Emergence of anoxia in the California current large marine ecosystem. *Science* 319(5865):920. DOI: 10.1126/science.1149016
- Demer, D. A., J. P. Zwolinski, K. A. Byers, G. R. Cutter, J. S. Renfree, T. S. Sessions, and B. J. Macewicz. 2012. Prediction and confirmation of seasonal migration of Pacific sardine (*Sardinops sagax*) in the California Current Ecosystem. *Fishery Bulletin* 110:52–70.
- DeVries, P. 1997. Riverine salmonid egg burial depths: Review of published data and implications for scour studies. *Canadian Journal of Fisheries and Aquatic Sciences* 54:1685–1698.

- Dyson, K., and D. D. Huppert. 2010. Regional economic impacts of razor clam beach closures due to harmful algal blooms (HABs) on the Pacific coast of Washington. *Harmful Algae* 9:264–271.
- EPAP (Ecosystem Principles Advisory Panel). 1999. Ecosystem-based fishery management: A report to Congress by the Ecosystem Principles Advisory Panel. National Marine Fisheries Service, Washington, D.C.
- Feely, R. A., R. R. Okazaki, W. J. Cai, N. Bednarsek, S. R. Alin, R. H. Byrne, and A. Fassbender. 2018. The combined effects of acidification and hypoxia on pH and aragonite saturation in the coastal waters of the California Current ecosystem and the northern Gulf of Mexico. *Continental Shelf Research* 152:50–60.
- Feely, R. A., C. L. Sabine, J. M. Hernandez-Ayon, D. Ianson, and B. Hales. 2008. Evidence for upwelling of corrosive “acidified” water onto the continental shelf. *Science* 320:1490–1492.
- Fisher, J. L., W. T. Peterson, and R. R. Rykaczewski. 2015. The impact of El Niño events on the pelagic food chain in the northern California Current. *Global Change Biology* 21:4401–4414.
- Fluharty, D., M. Abbott, R. Davis, M. Donahue, S. Madsen, T. Quinn, J. Rice, and J. Sutinen. 2006. Evolving an ecosystem approach to science and management throughout NOAA and its partners. Final Report of the external review of NOAA’s ecosystem research and science enterprise: A report to the NOAA Science Advisory Board. Silver Spring, Maryland.
- Friedman, W. R., B. T. Martin, B. K. Wells, P. Warzybok, C. J. Michel, E. M. Danner, and S. T. Lindley. 2019. Modeling composite effects of marine and freshwater processes on migratory species. *Ecosphere* 10:e02743.
- Greene, C. M., D. W. Jensen, G. R. Pess, and E. A. Steel. 2005. Effects of environmental conditions during stream, estuary, and ocean residency on Chinook salmon return rates in the Skagit River, Washington. *Transactions of the American Fisheries Society* 134:1562–1581.
- Harvey, C., and N. Garfield, editors. 2017. California Current Integrated Ecosystem Assessment (CCIEA) California Current Ecosystem Status Report, 2017. Report to the Pacific Fishery Management Council, Agenda Item F.1.a, March 2017. Available: www.pccouncil.org/wp-content/uploads/2017/02/F1a_NMFS_Rpt1_2017IEA_Main_Rpt_Final_Mar2017BB.pdf (June 2020).
- Harvey, C., N. Garfield, E. Hazen, and G. Williams, editors. 2014. The California Current Integrated Ecosystem Assessment: Phase III report. Available: www.noaa.gov/iea/CCIEA-Report/index (June 2020).
- Harvey, C., N. Garfield, G. Williams, K. Andrews, C. Barceló, K. Barnas, S. Bograd, R. Brodeur, B. Burke, J. Cope, L. deWitt, J. Field, J. Fisher, C. Greene, T. Good, E. Hazen, D. Holland, M. Jacox, S. Kasperski, S. Kim, A. Leising, S. Melin, C. Morgan, S. Munsch, K. Norman, W. T. Peterson, M. Poe, J. Samhour, I. Schroeder, W. Sydeman, J. Thayer, A. Thompson, N. Tolimieri, A. Varney, B. Wells, T. Williams, and J. Zamon. 2017. Ecosystem status report of the California Current for 2017: A summary of ecosystem indicators compiled by the California Current Integrated Ecosystem Assessment Team (CCIEA). U.S. Department of Commerce, NOAA Technical Memorandum NMFS-NWFSC-139.
- Harvey, C., T. Garfield, G. Williams, and N. Tolimieri, editors. 2020. California Current Integrated Ecosystem Assessment (CCIEA) California Current ecosystem status report, 2020. Report to the Pacific Fishery Management Council. Available: www.integratedecosystemassessment.noaa.gov/regions/california-current/cc-publications-reports (June 2020).
- Harvey, C., N. Garfield, G. Williams, N. Tolimieri, I. Schroeder, K. Andrews, K. Barnas, E. Bjorkstedt, S. Bograd, R. Brodeur, B. Burke, J. Cope, A. Coyne, L. deWitt, J. Dowell, J. Field, J. Fisher, P. Frey, T. Good, C. Greene, E. Hazen, D. Holland, M. Hunter, K. Jacobson, M. Jacox, C. Juhasz, I. Kaplan, S. Kasperski, D. Lawson, A. Leising, A. Manderson, S. Melin, S. Moore, C. Morgan, B. Muhling, S. Munsch, K. Norman, R. Robertson, L. Rogers-Bennett, K. Sakuma, J. Samhour, S. Siedlecki, K. Somers, W. Sydeman, A. Thompson, D. Tommasi, V. Trainer, A. Varney, B. Wells, C. Whitmire, M. Williams, T. Williams, J. Zamon, and S. Zeman. 2019. Ecosystem Status Report of the California Current for 2019: A Summary of Ecosystem Indicators Compiled by the California Current Integrated Ecosystem Assessment Team (CCEIA). U.S. Department of Commerce, NOAA Technical Memorandum NMFS-NWFSC-149.

- Hobday, A. J., L. V. Alexander, S. E. Perkins, D. A. Smale, S. C. Straub, E. C. J. Oliver, J. A. Benthuyzen, M. T. Burrows, M. G. Donat, M. Peng, N. J. Holbrook, P. J. Moore, H. A. Scannell, A. Sen Gupta, and T. Wernberg. 2016. A hierarchical approach to defining marine heatwaves. *Progress in Oceanography* 141:227–238.
- Hodgson, E. E., I. C. Kaplan, K. N. Marshall, J. Leonard, T. E. Essington, D. S. Busch, E. A. Fulton, C. J. Harvey, A. J. Hermann, and P. McElhany. 2018. Consequences of spatially variable ocean acidification in the California Current: Lower pH drives strongest declines in benthic species in southern regions while greatest economic impacts occur in northern regions. *Ecological Modelling* 383:106–117.
- Jacox, M. G., M. A. Alexander, S. J. Bograd, and J. D. Scott. 2020. Thermal displacement by marine heatwaves. *Nature* 584:82–86.
- Jacox, M. G., C. A. Edwards, E. L. Hazen, and S. J. Bograd. 2018. Coastal upwelling revisited: Ekman, Bakun, and improved upwelling indices for the U.S. West Coast. *Journal of Geophysical Research – Oceans* 123:7332–7350.
- Jacox, M. G., E. L. Hazen, and S. J. Bograd. 2016. Optimal environmental conditions and anomalous ecosystem responses: Constraining bottom-up controls of phytoplankton biomass in the California Current System. *Scientific Reports* 6:27612. DOI: 10.1038/srep27612
- Jeffries, K. M., S. G. Hinch, T. Sierocinski, T. D. Clark, E. J. Eliason, M. R. Donaldson, S. R. Li, P. Pavlidis, and K. M. Miller. 2012. Consequences of high temperatures and premature mortality on the transcriptome and blood physiology of wild adult sockeye salmon (*Oncorhynchus nerka*). *Ecology and Evolution* 2:1747–1764.
- Jepson, M., and L. L. Colburn. 2013. Development of social indicators of fishing community vulnerability and resilience in the U.S. Southeast and Northeast regions. U.S. Department of Commerce, NOAA Technical Memorandum NMFS-F/SPO-129.
- Kaplan, I. C., G. D. Williams, N. A. Bond, A. J. Hermann, and S. A. Siedlecki. 2016. Cloudy with a chance of sardines: Forecasting sardine distributions using regional climate models. *Fisheries Oceanography* 25:15–27.
- Kasperski, S., and D. S. Holland. 2013. Income diversification and risk for fishermen. *Proceedings of the National Academy of Sciences of the United States of America* 110:2076–2081.
- Keister, J. E., E. Di Lorenzo, C. A. Morgan, V. Combes, and W. T. Peterson. 2011. Zooplankton species composition is linked to ocean transport in the Northern California Current. *Global Change Biology* 17:2498–2511.
- Keller, A. A., J. R. Wallace, and R. D. Methot. 2017. The Northwest Fisheries Science Center’s West Coast Groundfish Bottom Trawl Survey: History, design and description. U.S. Department of Commerce, NOAA Technical Memorandum NMFS-NWFSC-136.
- Kershner, J., J. F. Samhuri, C. A. James, and P. S. Levin. 2011. Selecting indicator portfolios for marine species and food webs: A Puget Sound case study. *PLOS One* 6(10):e25248.
- Lasker, R. 1978. The relation between oceanographic conditions and larval anchovy food in the California Current: Identification of factors contributing to recruitment failure. *Rapports et Procès-Verbaux des Réunions du Conseil Permanent International pour l’Exploration de la Mer* 173:212–230.
- Lefebvre, K. A., S. Bargu, T. Kieckhefer, and M. W. Silver. 2002. From sanddabs to blue whales: The pervasiveness of domoic acid. *Toxicon* 40:971–977.
- Leising, A. W. In revision. Marine heatwaves of the North East Pacific from 1982–2020: A blobtrospective. *Journal of Geophysical Research: Oceans*.

- Leising, A. W., I. D. Schroeder, S. J. Bograd, J. Abell, R. Durazo, G. Gaxiola-Castro, E. P. Bjorkstedt, J. Field, K. Sakuma, R. R. Robertson, R. Goericke, W. T. Peterson, R. Brodeur, C. Barcelo, T. D. Auth, E. A. Daly, R. M. Suryan, A. J. Gladics, J. M. Porquez, S. McClatchie, E. D. Weber, W. Watson, J. A. Santora, W. J. Sydeman, S. R. Melin, F. P. Chavez, R. T. Golightly, S. R. Schneider, J. Fisher, C. Morgan, R. Bradley, and P. Warybok. 2015. State of the California Current 2014-15: Impacts of the Warm-Water “Blob.” *CalCOFI Reports* 56:31–68.
- Leising, A. W., I. D. Schroeder, S. J. Bograd, E. P. Bjorkstedt, J. Field, K. Sakuma, J. Abell, R. R. Robertson, J. Tyburczy, W. T. Peterson, R. Brodeur, C. Barcelo, T. D. Auth, E. A. Daly, G. S. Campbell, J. A. Hildebrand, R. M. Suryan, A. J. Gladics, C. A. Horton, M. Kahru, M. Manzano-Sarabia, S. McClatchie, E. D. Weber, W. Watson, J. A. Santora, W. J. Sydeman, S. R. Melin, R. L. Delong, J. Largier, S. Y. Kim, F. P. Chavez, R. T. Golightly, S. R. Schneider, P. Warzybok, R. Bradley, J. Jahncke, J. Fisher, and J. Peterson. 2014. State of the California Current 2013-14: El Niño Looming. *CalCOFI Reports* 55:51–87.
- Levin, P. S., S. J. Breslow, C. J. Harvey, K. C. Norman, M. R. Poe, G. D. Williams, and M. L. Plummer. 2016. Conceptualization of social-ecological systems of the California current: An examination of interdisciplinary science supporting ecosystem-based management. *Coastal Management* 44:397–408.
- Levin, P. S., M. J. Fogarty, G. C. Matlock, and M. Ernst. 2008. Integrated Ecosystem Assessments. U.S. Department of Commerce, NOAA Technical Memorandum NMFS-NWFSC-92.
- Levin, P. S., M. J. Fogarty, S. A. Murawski, and D. Fluharty. 2009. Integrated ecosystem assessments: Developing the scientific basis for ecosystem-based management of the ocean. *PLOS Biology* 7:23–28.
- Levin, P. S., and F. B. Schwing, editors. 2011. Technical background for an integrated ecosystem assessment of the California Current: Groundfish, salmon, green sturgeon, and ecosystem health. U.S. Department of Commerce, NOAA Technical Memorandum NMFS-NWFSC-109.
- Levin, P. S., B. K. Wells, and M. B. Sheer, editors. 2013. California Current Integrated Ecosystem Assessment: Phase II Report. Available: www.noaa.gov/iea/CCIEA-Report/pdf/index.html (June 2020).
- Lindgren, F., and H. Rue. 2015. Bayesian spatial modelling with R-INLA. *Journal of Statistical Software* 63:1–25.
- Link, J. 2017. A conversation about NMFS’ Ecosystem-Based Fisheries Management Policy and Road Map. *Fisheries* 42:498–503.
- Lloyd’s Register, QinetiQ, and University of Strathclyde. 2013. Global marine trends 2030. Available: www.lr.org/en-us/insights/global-marine-trends-2030/ (June 2020).
- Long, R., A. Charles, and R. Stephenson. 2015. Key principles of marine ecosystem-based management. *Marine Policy* 57:53–60.
- Marine, K. R., and J. J. Cech. 2004. Effects of high water temperature on growth, smoltification, and predator avoidance in Juvenile Sacramento River Chinook salmon. *North American Journal of Fisheries Management* 24:198–210.
- Marshall, K. N., I. C. Kaplan, E. E. Hodgson, A. Hermann, D. S. Busch, P. McElhany, T. E. Essington, C. J. Harvey, and E. A. Fulton. 2017. Risks of ocean acidification in the California Current food web and fisheries: Ecosystem model projections. *Global Change Biology* 23:1525–1539.
- McCabe, R. M., B. M. Hickey, R. M. Kudela, K. A. Lefebvre, N. G. Adams, B. D. Bill, F. M. D. Gulland, R. E. Thomson, W. P. Cochlan, and V. L. Trainer. 2016. An unprecedented coastwide toxic algal bloom linked to anomalous ocean conditions. *Geophysical Research Letters* 43:10366–10376.
- McClatchie, S. 2014. Regional fisheries oceanography of the California Current system. Springer, Dordrecht, The Netherlands.

- McClatchie, S., R. Goericke, A. Leising, T. Auth, E. Bjorkstedt, R. R. Robertson, R. Brodeur, X. Du, E. A. Daly, C. Morgan, F. Chavez, A. Debich, J. Hildebrand, J. Field, K. Sakuma, M. Jacox, M. Kahru, R. Kudela, C. Anderson, B. E. Lavaniegos, J. Gomez-Valdes, S. Jimenez-Rosenberg, R. McCabe, S. R. Melin, M. D. Ohman, L. Sala, B. Peterson, J. Fisher, I. Schroeder, S. J. Bograd, E. Hazen, S. Schneider, R. T. Golightly, R. M. Suryan, A. J. Gladics, S. Lored, J. M. Porquez, A. Thompson, E. D. Weber, W. Watson, V. Trainer, P. Warzybok, R. Bradley, and J. Jahncke. 2016. State of the California Current 2015-16: Comparisons with the 1997-98 El Niño. *CalCOFI Reports* 57:5-61.
- McFadden, K., and C. Barnes. 2009. The implementation of an ecosystem approach to management within a federal government agency. *Marine Policy* 33:156-163.
- McKibben, S. M., W. Peterson, M. Wood, V. L. Trainer, M. Hunter, and A. E. White. 2017. Climatic regulation of the neurotoxin domoic acid. *Proceedings of the National Academy of Sciences of the United States of America* 114:239-244.
- Melin, S. R., A. J. Orr, J. D. Harris, J. L. Laake, and R. L. DeLong. 2012. California sea lions: An indicator for integrated ecosystem assessment of the California Current system. *CalCOFI Reports* 53:140-152.
- Miller, R. R., J. A. Santora, T. D. Auth, K. M. Sakuma, B. K. Wells, J. C. Field, and R. D. Brodeur. 2019. Distribution of pelagic thaliaceans, *Thetys vagina* and *Pyrosoma atlanticum*, during a period of mass occurrence within the California Current Large Marine Ecosystem. *CalCOFI Reports* 60:94-108.
- Miller, J. A., D. J. Teel, A. Baptista, and C. A. Morgan. 2013. Disentangling bottom-up and top-down effects on survival during early ocean residence in a population of Chinook salmon (*Oncorhynchus tshawytscha*). *Canadian Journal of Fisheries and Aquatic Sciences* 70:617-629.
- Moore, S. K., M. R. Cline, K. Blair, T. Klinger, A. Varney, and K. Norman. 2019. An index of fisheries closures due to harmful algal blooms and a framework for identifying vulnerable fishing communities on the U.S. West Coast. *Marine Policy* 110:103543.
- Morgan, C., B. Beckman, L. Weitkamp, and K. L. Fresh. 2019. Recent ecosystem disturbance in the northern California Current. *Fisheries* 44:465-474.
- Munsch, S., C. Greene, R. Johnson, W. Satterthwaite, H. Imaki, and P. Brandes. 2019. Warm, dry winters truncate timing and size distribution of seaward-migrating salmon across a large, regulated watershed. *Ecological Applications* 29:e01880.
- Neveu, E., A. M. Moore, C. A. Edwards, J. Fiechter, P. Drake, W. J. Crawford, M. G. Jacox, and E. Nuss. 2016. An historical analysis of the California Current circulation using ROMS 4D-Var: System configuration and diagnostics. *Ocean Modelling* 99:133-151.
- NMFS (National Marine Fisheries Service). 2016. Fisheries of the United States, 2015. U.S. Department of Commerce, NOAA Current Fishery Statistics No. 2015. Available: www.st.nmfs.noaa.gov/Assets/commercial/fus/fus15/documents/FUS2015.pdf (June 2020).
- NOAA (National Oceanic and Atmospheric Administration). 2016. Ecosystem-based fisheries management policy of the National Marine Fisheries Service. Available: www.fisheries.noaa.gov/resource/document/ecosystem-based-fisheries-management-policy (June 2020).
- NOAA (National Oceanic and Atmospheric Administration). 2020. 2019 West Coast whale entanglement summary. Available: www.fisheries.noaa.gov/resource/document/2019-west-coast-whale-entanglement-summary-and-infographic (June 2020).
- Peterson, W. T., J. L. Fisher, J. O. Peterson, C. A. Morgan, B. J. Burke, and K. L. Fresh. 2014. Applied fisheries oceanography ecosystem indicators of ocean condition inform fisheries management in the California Current. *Oceanography* 27:80-89.
- PFMC (Pacific Fishery Management Council). 2013. Pacific Coast Fishery Ecosystem Plan for the U.S. portion of the California Current large marine ecosystem. Pacific Fishery Management Council, Portland, Oregon.

- PFMC (Pacific Fishery Management Council). 2019. Status of the Pacific Coast coastal pelagic species fishery and recommended acceptable biological catches. Stock assessment and fishery evaluation for 2018. Pacific Fishery Management Council, Portland, Oregon.
- Phillips, E. M., J. K. Horne, J. Adams, and J. E. Zamon. 2018. Selective occupancy of a persistent yet variable coastal river plume by two seabird species. *Marine Ecology Progress Series* 594:245–261.
- Porquez, J., R. Vargas, C. Turner, J. Dolliver, D. Lyons, and R. Orben. 2019. Yaquina Head seabird colony 2019 season summary. Department of Fisheries and Wildlife, Oregon State University, Newport, Oregon.
- Reynolds, R. W., T. M. Smith, C. Liu, D. B. Chelton, K. S. Casey, and M. G. Schlax. 2007. Daily high-resolution-blended analyses for sea surface temperature. *Journal of Climate* 20:5473–5496.
- Richter, A., and S. A. Kolmes. 2005. Maximum temperature limits for Chinook, coho, and chum salmon, and steelhead trout in the Pacific Northwest. *Reviews in Fisheries Science* 13:23–49.
- Ritzman, J., A. Brodbeck, S. Brostrom, S. McGrew, S. Dreyer, T. Klinger, and S. K. Moore. 2018. Economic and sociocultural impacts of fisheries closures in two fishing-dependent communities following the massive 2015 U.S. West Coast harmful algal bloom. *Harmful Algae* 80:35–45.
- Rudnick, D. L., K. D. Zaba, R. E. Todd, and R. E. Davis. 2017. A climatology of the California Current System from a network of underwater gliders. *Progress in Oceanography* 154:64–106.
- Sainsbury, K., P. Gullestad, and J. Rice. 2014. The use of national frameworks for sustainable development of marine fisheries and conservation, ecosystem-based management and integrated ocean management. *Governance of Marine Fisheries and Biodiversity Conservation: Interaction and Coevolution*:301–316.
- Sakuma, K. M., J. C. Field, N. J. Mantua, S. Ralston, B. B. Marinovic, and C. N. Carrion. 2016. Anomalous epipelagic micronekton assemblage patterns in the neritic waters of the California Current in spring 2015 during a period of extreme ocean conditions. *CalCOFI Reports* 57:163–183.
- Samhuri, J. F., A. J. Haupt, P. S. Levin, J. S. Link, and R. Shuford. 2014. Lessons learned from developing integrated ecosystem assessments to inform marine ecosystem-based management in the USA. *ICES Journal of Marine Science* 71:1205–1215.
- Santora, J. A., N. J. Mantua, I. D. Schroeder, J. C. Field, E. L. Hazen, S. J. Bograd, W. J. Sydeman, B. K. Wells, J. Calambokidis, L. Saez, D. Lawson, and K. A. Forney. 2020. Habitat compression and ecosystem shifts as potential links between marine heatwave and record whale entanglements. *Nature Communications* 11:536.
- Siedlecki, S. A., I. C. Kaplan, A. J. Hermann, T. T. Nguyen, N. A. Bond, J. A. Newton, G. D. Williams, W. T. Peterson, S. R. Alin, and R. A. Feely. 2016. Experiments with seasonal forecasts of ocean conditions for the northern region of the California Current upwelling system. *Scientific Reports* 6:1–18.
- Slater, W., G. DePiper, J. Gove, C. Harvey, E. Hazen, S. Lucey, M. Karnauskas, S. Regan, E. Siddon, E. Yasumiishi, S. Zador, M. Brady, M. Ford, R. Griffis, R. Shuford, H. Townsend, T. O'Brien, J. Peterson, K. Osgood, and J. Link. 2017. Challenges, opportunities and future directions to advance NOAA Fisheries ecosystem status reports (ESRs): Report of the National ESR Workshop. U.S. Department of Commerce, NOAA Technical Memorandum NMFS-F/SPO-174.
- Stierhoff, K. L., J. P. Zwolinski, and D. A. Demer. 2019. Distribution, biomass, and demography of coastal pelagic fishes in the California Current Ecosystem during summer 2018 based on acoustic-trawl sampling. U.S. Department of Commerce, NOAA Technical Memorandum NMFS-SWFSC-613.
- Stierhoff, K. L., J. P. Zwolinski, and D. A. Demer. 2020. Distribution, biomass, and demography of coastal pelagic fishes in the California Current ecosystem during summer 2019 based on acoustic-trawl sampling. U.S. Department of Commerce, NOAA Technical Memorandum NMFS-SWFSC-626. <https://doi.org/10.25923/nghv-7c40>

- Thompson, A., C. Harvey, W. Sydeman, C. Barceló, S. Bograd, R. Brodeur, J. Fiechter, J. Field, N. Garfield, T. Good, E. Hazen, M. Hunsicker, K. Jacobson, M. Jacox, A. Leising, J. Lindsay, S. Melin, J. Santora, I. Schroeder, J. Thayer, B. Wells, and G. Williams. 2019a. Indicators of pelagic forage community shifts in the California Current large marine ecosystem, 1998–2016. *Ecological Indicators* 105:215–228.
- Thompson, A. R., I. D. Schroeder, S. J. Bograd, E. L. Hazen, M. G. Jacox, A. Leising, B. K. Wells, J. L. Largier, J. L. Fisher, K. Jacobson, S. Zeman, E. P. Bjorkstedt, R. R. Robertson, M. Kahru, R. Goericke, C. E. Peabody, T. R. Baumgartner, B. E. Lavaniegos, L.E. Miranda, E. Gomez-Ocampo, J. Gomez-Valdes, T. D. Auth, E. A. Daly, C. A. Morgan, B. J. Burke, J. C. Field, K. M. Sakuma, E. D. Weber, W. Watson, J. M. Porquez, J. Dolliver, D. E. Lyons, R. A. Orben, J. E. Zamon, P. Warzybok, J. Jahncke, J. A. Santora, S. A. Thompson, B. Hoover, W. Sydeman, and S. R. Melin. 2019b. State of the California Current 2018–19: A novel anchovy regime and a new marine heat wave? *CalCOFI Reports* 60:1–65.
- True, K., A. Voss, and J. Foott. 2017. Myxosporean parasite (*Ceratonova shasta* and *Parvicapsula minibicornis*) prevalence of infection in Klamath River basin juvenile Chinook salmon, March–August 2017. U.S. Fish and Wildlife Service, California–Nevada Fish Health Center, Anderson, California.
- Walther, Y. M., and C. Möllmann. 2014. Bringing integrated ecosystem assessments to real life: A scientific framework for ICES. *ICES Journal of Marine Science* 71:1183–1186.
- Waples, R. S. 1995. Evolutionarily significant units and the conservation of biological diversity under the Endangered Species Act. *Evolution and the Aquatic Ecosystem: Defining Unique Units in Population Conservation* 17:8–27.
- Wells, B. K., I. D. Schroeder, J. A. Santora, E. L. Hazen, S. J. Bograd, E. P. Bjorkstedt, V. J. Loeb, S. Mcclatchie, E. D. Weber, W. Watson, A. R. Thompson, W. T. Peterson, R. D. Brodeur, J. Harding, J. Field, K. Sakuma, S. Hayes, N. Mantua, W. J. Sydeman, M. Losekoot, S. A. Thompson, J. Largier, S. Y. Kim, F. P. Chavez, C. Barcelo, P. Warzybok, R. Bradley, J. Jahncke, R. Goericke, G. S. Campbell, J. A. Hildebrand, S. R. Melin, R. L. Delong, J. Gomez-Valdes, B. Lavaniegos, G. Gaxiola-Castro, R. T. Golightly, S. R. Schneider, N. Lo, R. M. Suryan, A. J. Gladics, C. A. Horton, J. Fisher, C. Morgan, J. Peterson, E. A. Daly, T. D. Auth, and J. Abell. 2013. State of the California Current 2012–13: No Such Thing as an “Average” Year. *CalCOFI Reports* 54:37–71.
- Wiens, J. A., and J. T. Scott. 1975. Model estimation of energy flow in Oregon coastal seabird populations. *The Condor* 77:439–452.
- Wilkerson, F. P., A. M. Lassiter, R. C. Dugdale, A. Marchi, and V. E. Hogue. 2006. The phytoplankton bloom response to wind events and upwelled nutrients during the CoOP WEST study. *Deep Sea Research Part II: Topical Studies in Oceanography* 53:3023–3048.
- Zimmerman, M. S., C. Kinsel, E. Beamer, E. J. Connor, and D. E. Pflug. 2015. Abundance, survival, and life history strategies of juvenile Chinook salmon in the Skagit River, Washington. *Transactions of the American Fisheries Society* 144:627–641.
- Zwolinski, J. P., D. A. Demer, K. A. Byers, G. R. Cutter, J. S. Renfree, T. S. Sessions, and B. J. Macewicz. 2012. Distributions and abundances of Pacific sardine (*Sardinops sagax*) and other pelagic fishes in the California Current Ecosystem during spring 2006, 2008, and 2010, estimated from acoustic-trawl surveys. *Fishery Bulletin* 110(1):110–122.
- Zwolinski, J. P., K. L. Stierhoff, and D. A. Demer. 2019. Distribution, biomass, and demography of coastal pelagic fishes in the California Current Ecosystem during summer 2017 based on acoustic-trawl sampling. U.S. Department of Commerce, NOAA Technical Memorandum NMFS-SWFSC-610.

Recently published by the Northwest Fisheries Science Center

NOAA Technical Memorandum NMFS-NWFSC-

- 159 Hartley, M. L., D. M. Schug, K. F. Wellman, B. Lane, W. T. Fairgrieve, and J. A. Luckenbach. 2020.** Sablefish Aquaculture: An Assessment of Recent Developments and Their Potential for Enhancing Profitability. U.S. Department of Commerce, NOAA Technical Memorandum NMFS-NWFSC-159. <https://doi.org/10.25923/cb0y-n468>
- 158 Richerson, K. E., J. E. Jannot, Y.-W. Lee, J. T. McVeigh, K. A. Somers, V. J. Tuttle, and S. Wang. 2020.** Observed and Estimated Bycatch of Green Sturgeon in 2002–17 U.S. West Coast Groundfish Fisheries. U.S. Department of Commerce, NOAA Technical Memorandum NMFS-NWFSC-158. <https://doi.org/10.25923/sn5z-w384>
- 157 Holland, D. S. 2020.** An Analysis of the Pacific Groundfish Trawl Individual Fishing Quota (IFQ) Quota Pound (QP) Market Through 2019. U.S. Department of Commerce, NOAA Technical Memorandum NMFS-NWFSC-157. <https://doi.org/10.25923/sxdw-kb49>
- 156 Zabel, R. W., and C. E. Jordan, editors. 2020.** Life Cycle Models of Interior Columbia River Basin Spring/Summer-run Chinook Salmon Populations. U.S. Department of Commerce, NOAA Technical Memorandum NMFS-NWFSC-156. <https://doi.org/10.25923/phfm-wq72>
- 155 Anderson, L., and J. Hilger. 2020.** A Discrete Choice Experiment Data Collection of U.S. West Coast Saltwater Anglers, 2017: Methodology and Response. U.S. Department of Commerce, NOAA Technical Memorandum NMFS-NWFSC-155. <https://doi.org/10.25923/ge3e-vc58>
- 154 Somers, K. A., J. Jannot, K. Richerson, V. Tuttle, N. B. Riley, and J. T. McVeigh. 2020.** Estimated Discard and Catch of Groundfish Species in the 2018 U.S. West Coast Fisheries. U.S. Department of Commerce, NOAA Technical Memorandum NMFS-NWFSC-154. <https://doi.org/10.25923/z38p-sy40>
- 153 Somers, K. A., C. E. Whitmire, K. Richerson, J. E. Jannot, V. J. Tuttle, and J. T. McVeigh. 2020.** Fishing Effort in the 2002–17 Pacific Coast Groundfish Fisheries. U.S. Department of Commerce, NOAA Technical Memorandum NMFS-NWFSC-153. <https://doi.org/10.25923/8y7r-0g25>
- 152 Jannot, J. E., K. Richerson, K. A. Somers, V. Tuttle, and J. T. McVeigh. 2020.** Pacific Halibut Bycatch in U.S. West Coast Groundfish Fisheries, 2002–18. U.S. Department of Commerce, NOAA Technical Memorandum NMFS-NWFSC-152. <https://doi.org/10.25923/tkr3-b927>
- 151 Pess, G., and C. E. Jordan, editors. 2019.** Characterizing Watershed-Scale Effects of Habitat Restoration Actions to Inform Life Cycle Models: Case Studies Using Data-Rich vs. Data-Poor Approaches. U.S. Department of Commerce, NOAA Technical Memorandum NMFS-NWFSC-151. <https://doi.org/10.25923/vka7-w128>

NOAA Technical Memorandums NMFS-NWFSC are available from the NOAA Institutional Repository, <https://repository.library.noaa.gov>.



U.S. Secretary of Commerce
Wilbur L. Ross, Jr.

Acting Under Secretary of Commerce
for Oceans and Atmosphere
Dr. Neil Jacobs

Assistant Administrator for Fisheries
Chris Oliver

October 2020

www.nmfs.noaa.gov

OFFICIAL BUSINESS

National Marine
Fisheries Service
Northwest Fisheries Science Center
2725 Montlake Boulevard East
Seattle, Washington 98112